RECOVERY OF CRUDE OIL FROM SATURATED POROUS MEDIA AS A FUNCTION OF GEOCHEMISTRY AND WETTING-PHASE DYNAMICS FOR MULTIPLE REMEDIATION FLUSHING STRATEGIES

by

JOE M. BOOTH

GEOFFREY TICK, COMMITTEE CHAIR
RONA DONAHOE
YONG ZHANG
NIHAT AKYOL

A THESIS

Submitted in partial fulfillment of the requirements
for the degree of Master of Science
in the Department for Geological Sciences
in the Graduate School of
The University of Alabama

TUSCALOOSA, ALABAMA

2018

ABSTRACT

A comprehensive study was performed to evaluate the mechanisms controlling mobilization of trapped nonaqueous phase liquid (NAPL) crude oil as a function of wetting phase dynamics and geochemistry during enhanced-flushing conditions. Synchrotron X-ray microtomography (SXM) was used to perform pore-scale examination of NAPL fragmentation and changes in blob morphology, and recovery using three different advective flushing methods: surface-active agent (surfactant) flushing, alkaline flushing, and sequential alkaline-surfactant flushing. This set of experiments was conducted to understand effects on such processes (fragmentation and recovery) as a function of media composition (geochemical/mineralogical) and pH alterations due to calcium-carbonate fraction.

The sequential flushing technique (alkaline→ surfactant) yielded the highest recovery, 32% after 5 pore volumes (PV) of flushing. The crude oil (NAPL) distribution varied due to differences in heterogeneity and type of fluid (i.e. surfactant vs. alkaline) used for flushing. Drop shape analysis was also performed to measure contact angle across the solid-liquid-liquid (S-L-L) junction for a multiphase system for three different API° gravity (or density) crude oils within aqueous solutions of varying pH and in contact with two different types of media including silica (glass plate) and limestone (calcium carbonate plate). Interfacial tension (IFT) was also measured during drop shape analysis for the three different density oils, as a function of pH. Higher pH values showed the greatest change in contact angle (i.e. high to low) and subsequently the lowest IFT measurements.

During alkaline flushing, buoyancy forces predominantly controlled mobilization of NAPL (oil), and during surfactant flushing, viscous forces yielded relative greater control on crude oil (NAPL) mobilization. Calculated capillary force values showed significant variation for the set of experiments due to the changes in interfacial tension between the three crude oils tested and the alkaline aqueous phase (of varying pH). The results from this research can be used to aid in the understanding of physical and chemical parameters/properties that control mobilization of crude in porous saturated media. This can help reduce time and cost during remediation of contaminated sites that contain crude oil or less dense NAPL derivatives consistent with fuel-type petroleum hydrocarbons.

LIST OF ABBREVIATIONS AND SYMBOLS

NAPL	Non- aqueous phase liquid
IFT	Interfacial Tension
SXM	Synchrotron x-ray microtomography
θ	Theta, contact angle
σ	Sigma, interfacial Tension
r	radius
q	Darcy Velocity
μ	dynamic viscosity
Δp	change in density
k_i	Intrinsic Permeability
g	Acceleration dur to gravity
ΔP	Change in capillary pressure
N_C	Capillary Number
N_B	Bond Number
N_T	Trapping Number

ACKNOWLEDGEMENTS

I would like to thank the donors of the Hook's Research Fund for making it possible to travel to Argonne National Laboratory, IL and to the University of Clemson. I would like to thank Dr. Mark Rivers at Argonne National Laboratory, for his help with Synchrotron image collecting. I would like to thank Dr. Christophe Darnault at the University of Clemson for allowing me to use the KRUSS® DSA-1 drop shape analyzer. I would like to thank Dr. Yong Zhang for the use of his computer lab, in which all 3D image conversion was done. I would like to thank my advisor, Dr. Geoffrey Tick for his valuable insight and guidance. I would also like to thank my committee members, Dr. Rona Donahoe, Dr. Yong Zhang, and Dr. Nihat Akyol for suggestions and comment. I would like to thank my research group members, Rebecca Greenberg, Boone Abbott, and Justin Dunaway for helping collect data and perform the experiments. I would also like to say a special thanks to Dr. Fred Andrus for making sure I was able to finish this research. I would like to thank my parent for their support and encouragement. Last but not least, I would like to thank my wife, Alise Booth for the love and support throughout this research. She has been my foundation and I would have not been able to complete this project without her support.

CONTENTS

ABSTRACT..... ii

LIST OF ABBREVIATIONS AND SYMBOLS.....iv

ACKNOWLEDGEMENTS.....v

LIST OF TABLES.....viii

LIST OF FIGURES.....ix

INTRODUCTION.....1

BACKGROUND.....4

Surfactant Flushing 4

Alkaline Flushing.....5

Objectives of the Research 10

MATERIALS AND METHODS 12

Synchrotron X-ray Microtomography 12

Drop Shape and Interfacial Tension Analyses 15

Oil (NAPL) Trapping and Mobilization Analysis 17

RESULTS AND DISCUSSION 21

Crude Oil (NAPL) Distribution 21

Crude Oil Removal/ Recovery 28

Changes in Oil Morphology on Recovery 33

Distribution of Oil Blobs per Oil Blob Volume 36

Drop Shape Analysis 41

Oil Mobilization and Trapping Potential Analyses – N_C, N_B, N_T, ΔP 45

CONCLUSIONS.....50

Future Works 52

REFERENCES.....54

TABLES AND FIGURES..... 58

Tables 58

Figures 63

APPENDIX A- 3D IMAGES OF COLUMNS FROM SXM.....76

APPENDIX B – BLOB DISTRIBUTION AND HISTOGRAMS FOR COLUMNS DURING SXM.....83

APPENDIX C – CALCULATIONS OF BOND, CAPILLARY AND TRAPPING NUMBERS FOR HETEROGENOUS COLUMNS.....90

LIST OF TABLES

1. List of experimental conditions for each enhanced-flushing experiment.....58

2. List of parameters for NAPL residual saturation, alkaline and surfactant flushing..... 58

3. Oil (NAPL) recovery pre- and post- flushing events..... 59

4. List of measured contact angle in varying pH solutions in contact with varying media..... 60

5. List of measured Interfacial tension between NAPL varying pH solutions and 3 different oil densities..... 61

6.1 Calculations of capillary, bond, and trapping number for residual saturation, and surfactant flushing along with parameters used 61

6.2 Calculations of capillary, bond, and trapping number for varying pH alkaline solutions along with parameters used..... 62

7. Calculated change in capillary pressure for different density crude oil in contact with varying pH alkaline solutions..... 63

LIST OF FIGURES

1. Schematic of Light NAPL source distributed through the subsurface to groundwater and residual saturation of trapped NAPL..... 63

2.1-2.5 Representative 3D images of crude oil blobs for each column. The first image is residual saturation, the second is after 2 PV flush, and the third after 5 PV flush 64-65

3.1-3.5 Comparison of Blob Volume to Normalized Surface Area. Each chart compares blobs to perfect spherical shape. Figure 2.1 is for Exp-1, Alkaline Flush in homogeneous sand. Figure 2.2 is for Exp-2, Surfactant Flush in homogeneous sand. Figure 2.3 is for Exp-3 Sequential Flush in homogeneous sand. Figure 2.4 is for Exp-4, Surfactant in slight heterogeneous sand (25% karst sand, 75% 40/50 Accusand). Figure 2.5 is for Exp-5, Surfactant flush with moderate heterogeneous sand (50% karst sand, 50% 40/50 Accusand) 66-67

4.1-4.5 Comparison of Blob Volume to Normalized Surface Area. Figure 3.1 is for Exp-1, Alkaline Flush in homogeneous sand. Figure 3.2 is for Exp-2, Surfactant Flush in homogeneous sand. Figure 3.3 is for Exp-3, Sequential Flush in homogeneous sand. Figure 3.4 is for Exp-4, Surfactant in slight heterogeneous sand (25% karst sand, 75% 40/50 Accusand). Figure 3.5 is for Exp-5, Surfactant flush with moderate heterogeneous sand (50% karst sand, 50% 40/50 Accusand) 68-69

5.1-5.5 Comparison of Blob Volume to the fraction of Blobs smaller. Figure 4.1 is for Exp-1, Alkaline Flush in homogeneous sand. Figure 4.2 is for Exp-2, Surfactant Flush in homogeneous sand. Figure 4.3 is for Exp-3, Sequential Flush in homogeneous sand. Figure 4.4 is for Exp-4, Surfactant in slight heterogeneous sand (25% karst sand, 75% 40/50 Accusand). Figure 4.5 is for Exp-5, Surfactant flush with moderate heterogeneous sand (50% karst sand, 50% 40/50 Accusand) 70-71

6. Images taken by the KRUSS® DSA-1 drop shape analyzer. The images show the three different density oils in contact with a silica plate for varying pH NaOH solutions 72

7. Images taken by the KRUSS® DSA-1 drop shape analyzer. The images show the three different density oils in contact with a limestone plate for varying pH NaOH solutions.....73

8. A comparison of pH of the NaOH solution vs contact angle along the S-L-L junction. The top is for silica media, and the bottom calcium carbonate media 74

9. A comparison of Interfacial Tension to different solutions with increasing pH values 75

INTRODUCTION

The presence of petroleum hydrocarbons in soil and groundwater pose significant risks to human health and the environment. Hydrocarbons and other fuel derivatives are one of the most common contaminants present at hazardous waste and Superfund sites across the U.S. (USEPA, 2000; 2003; 2007). Nonaqueous phase liquids (NAPL) are generally classified by their fluid densities relative to that of water whereby light NAPL (LNAPL) is less dense than water and dense NAPL (DNAPL) is denser than water. Most fuel derivatives and petroleum hydrocarbons exist as LNAPL and solvents and solvent stabilizers predominantly exist as DNAPL. Oil spills and/or unintentional releases (i.e. underground storage tanks), either small or large scale, can migrate downward through the subsurface reaching groundwater whereby pure-phase (NAPL) oil can be retained in pore spaces of consolidated or unconsolidated rocks (aquifers), and act as a long-term sources of continuous groundwater contamination (Connor, 1988; Pennell et al., 1996). Figure 1 shows an example of NAPL acting as a source for contamination in ground water, and shows how residual oil can be trapped in small capillary spaces. It has been well documented that the presence to NAPL in the subsurface is generally considered to be the primary factor limiting remediation of sites contaminated by organic compounds (NRC, 1994; 1997; 1999; 2005). Although significant progress has been made for the removal or remediation of NAPL (i.e. chloroethenes, crude oils, diesels, etc.) from the subsurface over the past few decades, significant challenges and limitations still remain for complete source

removal (Ghosh and Tick, 2013). In fact, it has been shown that significant limitations with currently available remedial technologies persist, making it unlikely to reach cleanup goals for complex contaminated groundwater sites in a time period of 50-100 years (NRC, 2013). Typical pump-and-treat technologies have been used for the remediation of groundwater, although they are generally not effective for the removal of NAPL sources to reach maximum contaminant levels in groundwater (McCray et al., 2011). Permeability distribution of the aquifer media, such as highly heterogeneous aquifers, the presence of NAPL sources, and the viscosity of the flushing solution can also be factors influencing contaminant recovery. Du et al. (2013) shows that high viscosity crude oil in a highly heterogeneous permeability system generally exhibited lower oil recovery effectiveness than that of lower viscosity oils. Hence, in a more homogeneous system with lower permeabilities, higher viscosity oil showed greater recovery due to increased pressure gradients produced when pumping additional fluid into the system. The removal of trapped NAPL (oil) via flushing processes is controlled by viscous, buoyancy, and capillary forces as a function of the interfacial tension and density differences between the NAPL and aqueous flushing phase (Ghosh and Tick, 2013). A significant percentage of residual NAPL (oil) may remain in groundwater after a conventional pump-and-treat technique, and as mentioned prior, significant mass can still remain in the subsurface even after more aggressive source-zone removal methods have been implemented. The residual NAPL may be trapped in smaller capillaries or adsorbed to the grains of the surrounding rocks or soil. Enhanced flushing techniques (i.e. surfactant flushing, etc.) can aid in the removal of residual NAPL (Mulligan et al., 2001). Previous research has shown that a combination of alkaline and surfactant flushing used by the petroleum industry (enhanced oil recovery, EOR) can be a viable

method for more efficient oil extraction (Al-Rossies et al., 2010; Du et al., 2013; Mulligan et al., 2001; Zhao et al., 2013). An understanding of how these enhanced flushing techniques can change the NAPL distribution and blob morphology, along with particular relevant chemical reactions that may occur in the subsurface or with the NAPL itself can help when designing and implementing removal strategies for residual NAPL (or oil) trapped in groundwater systems.

BACKGROUND

Surfactant Flushing

Surfactant flushing technologies were developed by the oil industry as a soil washing technique for the recovery of petroleum products (Mulligan et al., 2001). Surfactants have two functional groups (or moieties), a polar or hydrophilic (water-soluble) group, and a non-polar or hydrophobic (oil-soluble) group (Kanicky et al., 2001). The hydrophilic (head) group can be present as an anionic (i.e. sulfates, and carboxylates), non-ionic (i.e. alcohols), and cationic (i.e. aluminum salts) moiety of the surfactant monomer molecule (Kanicky et al., 2001; Schramm, 2000). Crude oil contains organic acids, salts and alcohols, which when brought in contact with a surfactant can form an adsorbed film which reduces the interfacial tension between the oil and water phases (Wilson and Conrad, 1984).

The concentration of the surfactant determines whether NAPL (oil) removal from soil or groundwater will be predominantly influenced (and/or controlled) by solubilization or mobilization processes. As surfactant concentrations increase, the individual monomers will aggregate into spherical polymers called micelles (Kanicky et al., 2001). When this happens the concentration of the surfactant has reached (or exceeded) the critical micelle concentration (CMC). At concentrations above the CMC solubilization (polymer induced solubilization) of the oil begins to take place and is generally responsible for the removal of crude oil (NAPL). For reservoir extraction of crude oil, relying on solubilization removal can prove to be costly and

inefficient due to the slow (rate-limited mass-transfer) removal of hydrocarbon resource per time (or per volume of flush). Below the CMC, mobilization and removal of crude oil is induced via monomer aggregation and corresponding reduction of interfacial tension (solid-oil-solution) during the hydraulic solution flushing process. Mobilization recovery based processes have proven to be more cost and time effective than relying on solubilization mechanisms of removal (Mulligan et al., 2001).

Cationic surfactants have been shown to lower permeability by adsorption to the aquifer media thereby "clogging" pore space and hindering flow processes in the subsurface (Mulligan et al., 2001). Anionic and nonionic surfactants are less likely to be adsorbed to the media. There are several other factors to consider when using a surfactant for such enhanced-flushing strategies. Surfactants can adsorb to clays and organic carbon-rich sediments, they can biodegrade reducing desired concentration and effectiveness, and they can be difficult to recover requiring high removal rates (or volumes) of groundwater (Mulligan et al., 2001; Hunky et al., 2010). Other considerations are the density of the oil (LNAPL vs. DNAPL), permeability and heterogeneity of the subsurface system, and the viscosity of the trapped oil (NAPL). Higher viscosity NAPL (oil) will require longer remediation times in lower permeability environments resulting in higher overall costs (Wu et al., 2005).

Alkaline Flushing

Alkaline flushing techniques have also been widely used by the petroleum industry for crude oil recovery due to its ability to reduce interfacial tension between the oil and aqueous phases (Schramm, 2000). For oil recovery purposes, alkaline flushing techniques work by introducing a hydroxide anion to hydrolyze the hydrogen cation in naturally acidic crude oil.

The alkaline flush hydroxide anions react with the saponifiable components in the crude oil. The components are described as petroleum acids (naphthenic acids) (Sheng, 2015). These acids are highly oil soluble and are a combination of several carboxylic acids present in crude oil. Sheng (2015) describes the complete hydrolysis reaction of such an acid when in contact with an alkaline flush. This reaction will produce a soluble in-situ soap (anionic surfactant). The reaction of such an acid with sodium hydroxide is given as:

$$HA_o + OH^- \leftrightarrow A^- + H_2O \qquad (1)$$

where, HA_o is a single naphthenic acid species, OH^- is the hydroxyl anion from sodium hydroxide, and A^- is the soluble anionic surfactant. The sodium will act conservatively in this reaction and is completely soluble in solution. The reaction is strongly dependent on pH of the solution. The interaction of the ionized acid with neutral acids can lead to the formation of an acidic soap. The equilibrium constant of the reaction can be written as:

$$K = \frac{[A^-]}{[HA_o][OH^-]} = \frac{K_A K_D}{K_W} \qquad (2)$$

where, $[A^-]$ is the concentration of the surfactant, $[HA_o]$ is the concentration of naphthenic acid, $[OH^-]$ is the concentration of hydroxyl anion, K_A is the acid dissociation constant in the aqueous phase, K_D is the acid partitioning coefficient describing the ratio of acid in the aqueous phase to the acid in oil phase, and K_w is the dissociation constant for water.

We can rewrite the above equation (2) to solve for the concentration of the surfactant as:

$$[A^-] = \frac{K_A K_D [HA_o][OH^-]}{K_W} \qquad (3)$$

If more sodium hydroxide is added, and pH increases there will be a higher concentration of the in-situ surfactant produced. This surfactant will reduce the interfacial tension between the oil and aqueous phase with the effect of potentially increasing the mobility of the oil. For complete solubility of the surfactant in the aqueous phase, a solution with pH near 14 (which is not practical in real world cases) must be used (Sheng, 2015).

Another benefit of alkaline flushing is the ability to change the contact angle at the solid-liquid-liquid or grain-oil-solution (S-L-L) junction, changing the system from oil wet to water wet (Al-Rossies et al., 2010). In an oil-wet system, the oil will have a greater contact area with the media. This makes mobilization of the oil more difficult due to the high interfacial and surface tension between the solid and oil phases. In a water-wet system, the oil phase will have smaller contact area with the solid and interfacial and surficial tensions are reduced. We can use Young's equation derived for a S-L-L system to express this change in contact angle. Young's equation (S-L-L) is defined as (Al-Rossies et al., 2010):

$$\cos q = \frac{s_{sw} - s_{so}}{s_{ow}} \qquad (4)$$

where, θ is the contact angle across the S-L-L junction, σ_{sw} is the interfacial tension between the solid and aqueous phases, σ_{so} is the interfacial tension between the solid and oil phases, and σ_{ow} is the interfacial tension between the oil and aqueous phase. If the contact angle between the three phases were 90 degrees, the interfacial tension of the solid-aqueous phases is equal to the interfacial tension of the solid-oil phases, producing a zero value. Hence, the greater the contact angle, then the interfacial tension of the solid-oil phases is greater than the interfacial tension of the solid-aqueous phases, producing a negative ($cos\theta$) value. The closer

the angle gets to 180 degrees, the closer the interfacial tension of the solid-oil phases and the interfacial tension of the oil-aqueous phases are equal, producing a "-1" value. In contrast, the lower the contact angle, then the interfacial tension of the solid-aqueous phases are greater than the interfacial tension of the solid-oil phases, producing a net positive $(cos\theta)$ value. The closer the angle gets to 0 the closer the interfacial tension of the solid-aqueous phases and the interfacial tension of the oil-aqueous phases are equal, yielding a value of "1". The properties of the oil, especially viscosity can have a major effect on this value calculated from equation (4). The higher the viscosity of the oil, the greater the interfacial tension between the solid and oil phases. In comparison, the interfacial tension between the solid and aqueous phases is typically quite low. For mobility to take place, a reduction of contact angle and a reduction of the interfacial tensions between the NAPL and aqueous phases must take place. One benefit of using alkaline solutions for oil (NAPL) removal is that they can act to influence both the reduction of contact angle and interfacial tension.

The use of an alkaline flush is much cheaper, in terms of material cost, compared to the cost of commercial surfactants. However, the disadvantages related to use of alkaline solutions must be considered before this can be a viable remediation flushing strategy. Higher pH concentrations must be maintained for alkaline flushing to be effective (Kanicky et al., 2001). A pH value of 9.5 or greater must be used to effectively reduce the interfacial tensions and contact angle (Sheng, 2015). At higher pH values, there are particular concerns for the precipitation of metals, dissolution of silicates (above pH 10) must be considered, which can lead to structural failure of the media, impact clays that may be in the system causing potentially higher *D*-spacing shifts in the clays as well as enhancing the precipitation and or

diffusion of other contaminants or species in the clay. Other disadvantages of alkalinity flushing, at higher pH, are the resulting impacts on the microbiology whereby beneficial hydrocarbon-degrading bacteria can be killed and redox conditions may be altered adversely to that desired.

The limitations of alkaline flushing are directly related to the pH of the solution being flushed. Silica (quartz) type aquifer media is relatively stable at low pH ranges. The solubility of quartz starts to increase above pH of 9.5, becoming more soluble as pH further increases. The solubility of silica will dramatically increase as pH goes above 10. This will cause any silica sands in the subsurface to become unstable possibly leading to structural failure in the aquifer. As pH increases precipitation of metal hydroxides also becomes an issue. For example, if iron were present in the subsurface the addition of a high pH solution could cause goethite (FeOOH) to precipitate which would coat the media grains in the system causing clogging of the pore spaces. This would cause higher capillary pressures and cause the NAPL to remain immobile or trapped in the pores of the media. This would cause the remediation efforts to take longer and cost more money. In order for alkaline flushing to be considered a viable remediation strategy, the pH of the solution should take these factors into account so that NAPL can mobilize and not structural failure will not occur during flushing.

Objectives of the Research

The overall purpose of this study is to evaluate the effectiveness of a combination of alkaline- and surfactant-based enhanced-flushing techniques for the removal of hydrocarbon NAPL (crude oil) from groundwater. This research aims to improve our understanding of the pore-scale processes that influence NAPL (crude oil) during enhanced-flushing conditions using

novel synchrotron X-ray microtomography (SXM) imaging and Drop Shape Analysis (DSA) techniques. Specifically, the objectives include: 1) assessing the impact of crude oil (NAPL) mobilization by quantifying the changes in oil distribution and morphology during independent surfactant and alkaline flushing, and combination sequential alkaline-surfactant flushing; 2) quantifying oil recovery as a function of changes in oil blob distribution and morphology for various enhanced flushing scenarios; 3) relating changes in oil wettability and recovery (mobilization) by quantifying changes in solid-oil-solution contact angle and interfacial tension as a function of the flushing solution pH; 4) determining the primary trapping mechanisms controlling the mobilization potential of oil (NAPL) during various enhanced flushing scenarios via Capillary, Bond, and Trapping Number analyses; and 5) quantifying oil-phase (NAPL) recovery due to calcium carbonate sand fraction in porous media and related effects on system pH and oil wettability.

A series of small-scale column experiments including both independent alkaline and surfactant flushing and sequential alkaline-surfactant flushing scenarios (within homogeneous porous media) was conducted to address several of the objectives above. As mentioned previously, synchrotron X-ray microtomography (SXM) was implemented to characterize and quantify changes in crude oil distribution and morphology during mobilization-induced surfactant (polymer-induced mobilization, C<CMC), alkaline (wetting-phase alteration and reduction of interfacial tension), and sequential-surfactant-alkaline flushing scenarios. In addition, this research will provide an improved understanding of processes controlling oil recovery as a function of increasing media heterogeneity (calcium-carbonate sand fraction) and related effects of pH change due to the presence of calcium-carbonate mixture within the

porous media. Lastly, the Drop Shape Analysis (DSA) for solid-fluid-fluid dynamics (contact angle and interfacial tension) will provide a basis for determining how changes in flushing solution pH in contact with different density and viscosity crude oils will influence mobilization and recovery potential in terms of shifts in oil wettability and changes in resulting capillary pressure. Such measurements will be used to calculate trapping and mobilization parameters (Capillary, Bond, and Trapping Numbers) for determination of oil mobilization and recovery potential under the alkaline flushing conditions. The results from the combination of experiments conducted herein will provide enhanced understanding for oil (NAPL) removal potential during various surfactant, alkaline, and sequential-alkaline-surfactant enhanced-flushing based technologies. Thus, implications from this work may be valuable for the development of more accurate risk assessments and improved selection of a remediation strategy when implementing enhanced-flushing techniques for sites contaminated with petroleum hydrocarbons (oil and/or NAPL).

MATERIALS AND METHODS

Synchrotron X-ray Microtomography

A lighter-than-water crude oil was chosen as the model nonaqueous phase liquid (NAPL) and is characterized as a "medium" gravity (29.6 API°) oil also known as Poseidon crude (BP, Houston, TX). The surfactant used for flushing was a 0.1% (by volume) anionic surfactant branched alcohol propoxy sulfate (commercially named, Petrostep S-1) solution. The alkaline solution used for flushing was prepared using NaOH (ACS grade, BDH Chemicals) diluted in NANOpure water (18 MΩ-cm) and adjusted to a pH of 12.

A series of five small-scale enhanced-flushing column experiments were performed using thin-walled aluminum porous medium packed columns. The columns ranged in length (4.5 - 5.0 cm) with an inner diameter (i.e.) of 0.5 cm. Both ends of the columns were outfitted with Swagelok® end-fittings. A polypropylene frit was inserted between the porous medium and end-caps to reduce preferential flow and to keep the porous medium contained within the system during saturation and flushing. The first three columns (Exp-1, Exp-2, and Exp-3) were dry packed with a homogeneous 40/50-mesh Accusand. The fourth column (Exp-4) was dry packed with 25%-75% (by weight) mixture of "karst" calcium-carbonate sand and 40/50-mesh Accusand. The fifth column (Exp-5) was dry packed with a 50%-50% (by weight) mixture of the "karst" sand and 40/50-mesh Accusand. The sand-packed columns were then saturated vertically upward with NANOpure water using a single piston pump (Acuflow, Series II) for a

period of 48 hours, at a pumping rate (linear pore velocity, v_p) of 6-8 cm/hr. The columns were weighed over the saturation period until the weight stabilized to ensure that fully saturated conditions were maintained prior to oil (NAPL) emplacement. Once the columns were fully saturated they were independently injected using a syringe pump (KD Scientific model: 780100, Holliston, MA) vertically downward with 4 pore volumes (PV) of the medium crude oil, to maintain stable displacement of the water from the column by the less-dense-than water crude oil fraction. Prior to this injection step, the oil was first doped with 10% (by volume) iodobenzene to improve imaging contrast for the oil (NAPL) via optimizing (maximizing) X-ray absorption energy above and below the iodine-edge. The columns were then flushed vertically upwards with a NANOpure water doped with 60 g/L cesium chloride (cesium chloride, CsCl, is added to improve imaging contrast for the aqueous phase by maximizing X-ray absorption below the cesium K-edge) (see methods Ghosh and Tick, 2013). The flushing of CsCl solution was performed in two sequential steps at varying velocities (2-PV at v_p of 6-10 cm/hr. and 10 PV at 20-30 cm/hr.) to establish residual oil saturation conditions prior to the enhanced-flushing experiments. The addition of CsCl has negligible effect on interfacial tension in the aqueous phase (Schnaar and Brusseau, 2006a). However, oil phase doping with iodobenzene showed minor changes in interfacial tension for the bulk oil (Ghosh and Tick, 2013). These dopants also showed negligible partitioning to non-target fluids in other studies (Schnaar and Brusseau, 2006a). The methods used to attain residual saturation are similar to those from previous work (Ghosh and Tick, 2013; Schnaar and Brusseau, 2006a; Schnaar and Brusseau 2006b).

After residual saturation was attained, each column was sealed and imaged using synchrotron X-ray microtomography (SXM). SXM was used to specifically quantify oil

distribution and blob morphology for a series of surfactant, alkaline, and sequential alkaline-surfactant column flushing experiments. All imaging was performed at GeoSoilEnviroCARS (GSECARS) BM-13D beamline sector, at Advanced Photon Source, Argonne National Laboratory, IL. After each complete initial scan (residual saturation condition), columns were then subsequently flushed vertically downward at a linear pore-velocity of 20 cm/hr. using CsCl-doped flushing solution in two steps, first a 2-PV flushing period and then a 3-PV flushing period whereby after each respective flush the column was scanned using SXM. Column 1 (Exp-1) was flushed with the alkaline solution (NaOH) and columns 2 (Exp-2), 4 (Exp-4), and 5 (Exp-5) were flushed with the surfactant solution. Column 3 (Exp-3) was flushed sequentially with the alkaline solution (2 PV) followed immediately by the surfactant solution (2 PV). Again, it should be noted that all aqueous flushing solutions were doped with CsCl (60 g/L) prior to being flushed through each column experiment for reasons described previously. Table 1 lists each column with the media used and type of flushing experiment performed. Each SXM scan generated files that could be used to resolve images for the aqueous and NAPL phases; whereby the above iodine K-edge energy was used to resolve the oil phase and the below cesium K-edge was used to resolve the aqueous phase (i.e. CsCl-surfactant, alkaline solution).

All SXM generated volume image files were pre-processed at Argonne National Laboratory, and converted into stacks to be turned into a 3D image arrays. The images were then processed with ImageJ Software, and iodine K-edge generated volume files were subtracted from the cesium K-edge generated volume files to produce image files of only the crude oil (NAPL) distribution with the column system. Blob3D Software (Ketcham, 2005) was then used to convert the stack of 2D images to 3D images. Blob3D was also used to extract

quantitative parameters such as oil volume and surface area of the oil and aqueous phases. The data were used to quantify blob volume distribution, blob radius and diameter, blob morphology (blob deviation from spheres), equivalent surface-area to volume, and volume recovered. Conditions and parameters associated with each of the flushing experiments are reported in Table 2. Further details about SXM imaging collection for geologic media and fluid phases as well as 2D and 3D image processing methods can be found in related literature (Sutton et al., 2002; Wildenschild et al., 2002; Schnaar and Brusseau, 2005, 2006a; Brusseau et al., 2007; Ghosh and Tick, 2013).

Drop Shape and Interfacial Tension Analyses

Drop shape analysis (DSA) was performed using a KRUSS® Drop Shape Analyzer DSA1 Instrument (FM40Mk2, Kruss® GmbH, Germany) housed within the Department of Environmental Engineering and Earth Sciences at Clemson University. The experiments were performed using three crude oils as the model fluid, light oil (41.4 API^{o}) known as Western Texas Intermediate crude (BP, Houston, TX), medium oil (29.6 API^{o}) known as Poseidon crude (BP, Houston, TX), and heavy oil (14.0 API^{o}) known as San Joaquin Valley crude (Chevron, Richmond, CA). Each crude oil was then placed in the KRUSS® drop shape analyzer under varying pH solutions, pH 4 (HCl), pH 7 (deionized water), and pH 10, 12, and 13.5 of NaOH. More specifically, the respective API^{o} oil was loaded into the instrument reservoir and drawn into a syringe system and the injection of an oil drop was released while submerged in the presence of particular pH solution. While in solution, the released LNAPL oil blob was allowed to collect beneath a solid plate and images were obtained to determine contact angle and phase wettability, as well as interfacial tension between the two-fluid-phase systems. Two sets

of experiments were conducted for each oil under each pH condition (level). The first set of experiments used a silica (glass) plate and the second used a calcium carbonate (limestone) plate. As described above, a small blob of each oil was emplaced under the plate in each varying pH solution and contact angle was measured along the solid-liquid-liquid (S-L-L) junction. Drop shape analysis software (Kruss® GmbH, Germany) was used to measure contact angle with circle fitting parameters and sessile drop type boundary analysis. Images were taken of the oil blobs at a 79.827 (pixels/mm) magnification factor and oil contact angle and interfacial tension values were quantified. It should be noted that some of the oil/plate contact images were extremely blurry likely due to dynamic changes of the oil morphology during the camera image collection analysis.

As mentioned above, interfacial tension (IFT) was also measured simultaneously using the KRUSS® Drop Shape Analyzer Instrument. Each oil type (light, medium, and heavy) was collected into a syringe. A J-hook was placed into the syringe and submersed into the various pH solutions (pH 4, 7, 10, 12, and 13.5) for each respective experiment. A small drop of oil was displaced through the end of the 0.2-mm J-hook end diameter. The KRUSS® drop shape analysis software (Kruss® GmbH, Germany) was used to quantify IFT using two independent settings which included both tear-drop and pendant-drop type configurations. Once the oil drop was stable on the end of the J-hook (i.e. maintained for 30 seconds), IFT was measured every 10 seconds for a period of 5 minutes. The values were then collected and averaged, and descriptive statistics generated for the values including the mean value and the associated 95% confidence interval (C.I., 1.96σ) was calculated (about the mean) for each set of experiments. More information about the KRUSS® drop shape analyzer can be found in Pales et al. (2017).

Oil (NAPL) Trapping and Mobilization Analysis

Trapping and mobilization mechanisms of crude oil are controlled by capillary processes due to porous media geometry, wettability of the media, crude oil viscosity, oil-solution densities, and capillary pressures. The data collected from both the SXM and KRUSS® Drop Shape Analyzer instruments were used to determine the potential of oil mobilization and/or trapping for the various experiments. Quantitative results such as oil (NAPL) blob size distribution, normalized oil surface-to-volume ratios, oil volume recovered for column flushing experiments, as well as capillary number (N_C), Bond number (N_B), trapping number (N_T), and change in capillary pressure (ΔP) for the drop shape and interfacial tension experiments were integrated to assess oil mobilization/trapping behavior or potential. N_C, N_B, and N_T are dimensionless numbers used to describe the potential for oil mobilization. Capillary pressure is the difference of pressure across the interface of two immiscible liquids (i.e. oil and aqueous solution). These parameters are described in further detail in the following section.

The capillary number describes the ratio of viscous forces to interfacial tension forces. Higher values indicate a greater potential for oil to be mobilized. Mercer and Cohen (1990) have observed that in order initiate oil mobilization, capillary numbers should be on the order of 10^{-5} or greater. For complete removal of oil, capillary numbers should be on the order of 10^{-3} or greater, depending on specifics of the S-L-L system. Capillary number is defined as (Morrow and Songkran, 1981; Mercer and Cohen, 1990; Boving and Brusseau, 2000; Pennell et al., 1994, 1996; Ghosh and Tick, 2013):

$$N_C = \frac{q\mu}{\sigma_{ow}} \quad (5)$$

where, q is the Darcy velocity of the flushing fluid (cm/s), μ is the dynamic viscosity of the flushing fluid (dyn s/cm^2) and σ_{ow} is the interfacial tension between the oil and aqueous phases (dyn/cm). To increase the capillary number, the injection (flushing) rate of the aqueous solution can be increased (increase viscous force) but this can adversely induce high pressure regimes and alter the rock structure, and relies on higher viscosity solutions which is often impractical or infeasible (Kanicky et al., 2001). Therefore, to increase the capillary number, a more viable and well-accepted parameter-modification technique relies on using a solution that acts to reduce of interfacial tension between the oil and aqueous phases.

Bond number is a dimensionless parameter describing the potential for mobilization of oil (NAPL) by a ratio of the buoyancy to interfacial tension forces between the oil and aqueous phases. Bond number is defined as (Morrow and Songkran, 1981; Boving and Brusseau, 2000; Pennell et al., 1994, 1996; Ghosh and Tick, 2013):

$$N_B = \frac{k_i \Delta\rho g}{\sigma_{ow}} \quad (6)$$

where, k_i is the intrinsic permeability of the porous media (cm^2), $\Delta\rho$ is the density difference between the aqueous flushing solution and the oil (g/cm^3), g is the acceleration due to gravity (cm/s^2), and σ_{ow} is the interfacial tension between the oil and water phases (dyn/cm). The effect of buoyancy and viscous force must be considered under vertical flow conditions, whereby the trapping number is described as the sum of the buoyancy and viscous forces (Pennell et al., 1996; Ghosh and Tick, 2013):

$$N_T = \left| N_C + N_B \right| \quad (7)$$

Pennell et al. (1996) show that under vertical flow, NAPL cannot generally be mobilized or displaced in porous media if N_T is less than 2×10^{-5}.

The change in capillary pressure describes the difference between the pressures of the two liquid phases (i.e. oil and water). This value is dependent on which fluid phase is considered to be the wetting fluid. Mercer and Cohen (1990) describe the contact angle at the S-L-L junction as the controlling factor of wettability, with contact angles above 110° being oil-wet conditions, contact angles below 70° being water-wet conditions, and neutral conditions in between 70° and 110°. The equation for the change in capillary pressures is described as (Mercer and Cohen, 1990; Al-Rossies et al., 2010):

$$\Delta P = P_{nw} - P_w \tag{8}$$

where, ΔP is the change in capillary pressure, P_{nw} is the pressure of the non-wetting fluid, and P_w is the pressure of the wetting fluid. The contact angle, interfacial tension, and the radius of the pores in the porous media are used in the form of the Young's-Laplace equation to show the same change in capillary pressure (eq. 8) as follows (Mercer and Cohen, 1990; Al-Rossies et al., 2010):

$$\Delta P = \frac{2\sigma_{ow}\cos\theta}{r} \tag{9}$$

where, σ_{ow} is the interfacial tension between the oil water interface, θ is the contact angle at the S-L-L junction, and *r* is the average pore radius in the porous media. Using the Young's-Laplace equation, the wetting agent is defined by the contact angle at the S-L-L junction. A contact angle above 90° defines oil as the wetting fluid, while an angle below 90° defines the aqueous phase as the wetting fluid. Negative capillary pressure values indicate that oil is the wetting fluid and that

there is a higher net pressure exerted on the oil. Positive changes in capillary pressure indicate that the aqueous phase is the wetting fluid with higher net pressures exerted on the oil phase. Larger capillary pressure (i.e. changes in pressure, ΔP) values indicate that a higher overall threshold value (capillary force) is required to overcome the capillary pressure that holds the oil phase within the pore space for mobilization to occur.

RESULTS AND DISCUSSION

Crude Oil (NAPL) Distribution

3D imaged sections show a random distribution of crude oil under residual saturation conditions in both the homogeneous porous media (Accusand) and increasingly heterogeneous calcium carbonate (karst) sand packed columns (i.e. increasing karst sand content). Oil (NAPL) distribution patterns show a variety of blob morphology and configuration. Disconnected individual blobs known as “singlets” and “doublets” can be seen throughout the residual saturation conditions (initial SXM scans). Regions where higher concentrations of oil blobs are present tend to be aggregated in “ganglia” that are connected within the interconnected pore space. The images in Figures 2.1, 2.2, 2.3, 2.4, and 2.5 show a representative imaged section of each of the five columns at residual oil saturation, after a 2 PV flush, and after a subsequent 3 PV flush (total of 5 PV) (a complete catalog of all 3D images for all columns is provided in Appendix A).

Figure 2.1 shows converted 3D images for Exp-1 (Column 1 – alkaline flush in homogeneous sand). The first column image scan shows a random distribution of oil blobs for residual saturation. The random (variable) oil distribution shows more singlet and doublet blobs towards the center of the column, and more interconnected ganglia towards the edges (walls) of the column whereby preferential flow can be observed to have occurred. The second column image scan, after the 2 PV flush, shows (and quantified) that the oil blobs become

smaller in terms of volume and radii, and there that is a greater number of blobs present compared to the initial saturation condition. This is due to the larger oil blobs being fragmented ("dispersed"), likely from the reduction of interfacial tension between the oil and aqueous phases. The third column image scan, after the subsequent 3-PV (5 PV total) flush is shown in Figure 2.1. A greater number of oil blobs can be observed (and quantified) after this final flushing step (i.e. image after 5 PV total), compared to after only the first 2-PV flushing step (i.e. image after 2 PV flush). Again, there are some preferential flow paths toward the edge of the column walls that can be observed whereby oil ganglia are distributed. Progressively smaller blob sizes (volume, radii) are observed (quantified) after the final 3-PV (5 PV total) flushing step (i.e. observed in the final scanned image). However, some oil ganglia are also observed toward the center of the column in between the sand grains, indicating a variable distribution of oil (i.e. singlets, doublets, and ganglia) within the column after a total of 5 PV of flushing.

Figure 2.2 shows converted 3D images for Exp-2 (Column 2 – surfactant flush in homogeneous sand). The first column image scan of the initial residual oil saturation condition, (like that for Exp-1), shows a random distribution of oil blobs with the formation of ganglia near the column walls due to preferential flow paths. The second column image scan (after 2 PV of flushing), shows a greater number of observed (and quantified) oil blobs with smaller size and volume compared to that observed (quantified) in the initial residual saturation condition (i.e. first image). Some oil ganglia are observed along the column walls (i.e. preferential flow via wall effects), as well as distributed within the center of the column in the pore space between the sand grains. For the third column image scan (subsequent 3-PV of flushing, i.e. 5 PV total)

an even greater distribution (number) of oil blobs (i.e. singlets and doublets) can be observed (quantified) relative to ganglia distribution. This image (after the final flushing step) shows relatively small oil blobs filling the pore spaces between the sand grains, with preferential flow of oil distributed (i.e. as ganglia) along the column walls.

Figure 2.3 shows converted 3D images for Exp-3 (Column 3 – sequential alkaline/surfactant flush in homogeneous sand). The first column image scan (similar to Exp-1 and Exp-2) for the initial residual oil saturation condition shows a random (variable) distribution of oil blobs with preferential flow of oil distributed (i.e. as ganglia) along the column walls. For the second column image scan (after 2 PV of alkaline flushing), the distribution of oil blobs is present (quantified) predominantly as interconnected blobs in the form of ganglia throughout the column. Under such conditions it is expected that this oil ganglia-type distribution may require greater viscous forces (pressure differential) across the oil-body to mobilize and remove from the column; thereby providing limited to no benefit over either independent enhanced-flushing scenario (alkaline or surfactant). For the third column image scan (subsequent 3-PV of surfactant flushing, i.e. 5 PV total), the number of oil ganglia are observed (quantified) to decrease in size (volume), with a greater concentration of oil ganglia in the pore space between the sand grains. Such conditions may be induced via emulsification processes whereby the oil phase droplets coalesce with the bulk aqueous solution (disperse mixture) that can be associated with increases of pH (Sheng, 2015).

Figure 2.4 shows converted 3D images for Exp-4 (Column 4 – surfactant flush with mildly heterogeneous sand; 25% calcium carbonate (karst) sand and 75% Accusand). These set of experiments, Exp-4 and Exp-5, were conducted to evaluate the impacts of increasing physical

heterogeneity and calcium-carbon (karst sand) content on oil distribution and recovery during surfactant flushing. Overall, the initial residual oil saturation condition exhibits a random (variable) distribution of oil blobs and relatively larger ganglia distributed within the porous medium of the column, with larger ganglia observed nearest the column walls (i.e. indication of preferential flow). As mentioned prior, the presence of the oi ganglia-type distribution may require greater viscous forces (pressure differential) across the oil-body to mobilize and remove from the column; thereby providing limited to no benefit prior to flushing with a particular enhanced-flushing agent. The second column image scan (after 2 PV of surfactant flushing) shows that some of the large ganglia are being dispersed (fragmented) into smaller singlet and doublet oil blobs. Additionally, there is a notable decrease in the size (volume) of the larger oil ganglia throughout the column, via visual observation and Blob-3D quantified results. The third column image scan (subsequent 3-PV of surfactant flushing, i.e. 5 PV total) shows further fragmentation of the larger ganglia into smaller oil blobs (observed and quantified) within the center region of the column. However, the larger oil ganglia nearest the column walls show negligible (observed and quantified) change in volume and morphology after the second (final) surfactant flushing event (i.e. results from second image) compared to after the first 2-PV flushing event (after 2 PV and after 5 PV flushing).

Figure 2.5 shows converted 3D images for Exp-5 (Column 5 – surfactant flush with moderately heterogeneous sand; 50% karst sand and 50% Accusand). The initial residual oil saturation condition exhibits a random (variable) distribution of oil blobs and ganglia distributed within the column, however, the oil blobs and ganglia are generally larger in size (volume) than that in the previous experiments (via visual image observation and Blob3D

quantification). The first column image scan (residual oil saturation) exhibits the relatively largest oil-blob volume fraction compared to the results (distribution) after subsequent surfactant flushing; however, the oil blobs are not as evenly distributed throughout the column due to the relative greater degree of heterogeneity associated with this system. Interestingly, a notably higher residual oil volume was also observed (quantified via Blob3D) in this system compared to the other column experiments. This condition may be due to the greater relative heterogeneity and/or due to potential interfacial dynamics (transition of wettability) and related chemical interaction between the oil and media from the calcium-carbonate (karst sand) content. The second column image scan (after 2 PV of surfactant flushing) shows minimal change in oil distribution from the initial residual condition except for a slight decrease in the volume of the larger oil blobs in the system. It can be observed that some extremely small size oil blobs are present (visual observation and quantified), volumes on the order of 10^{-9} mm^3, but fragmentation of the oil blobs is not as noticeable compared to that in the other columns after flushing. The third column image scan (subsequent 3-PV of surfactant flushing, i.e. 5 PV total) exhibits an overall further decrease in size (volume) of the larger oil blobs (observed and quantified), however, with relatively lower distribution of very small oil blobs present in the system (similar to the image results after the 2-PV flush). This indicates that the smallest oil blobs may have been effectively removed from the system during the final flushing step.

Evaluation of the series of homogeneous sand column experiments (Exp-1-alkaline, Exp-2-surfactant, and Exp-3-sequential alkaline/surfactant) show that the fragmentation of oil blobs into smaller blobs occurs progressively after each flushing step, particularly for Exp-1 and Exp-2. Hence, these two column experiments show a similar general trend whereby a greater number

of oil blobs with progressively smaller blob volumes result through each flushing step. More specifically, there was a greater increase in the number of oil blobs in produced (via fragmentation) after both the 2 PV and 5 PV flushing events (quantified via Blob3D) for Exp-2 in comparison to that for Exp-1. This could be due the surfactant's (Exp-1) ability to yield a greater reduction of IFT between the oil and aqueous phases, compared to the alkaline solution (Exp-2). The results for Exp-3 show that the oil blobs within the column include a greater number of interconnected ganglia compared to the oil blob distribution within the columns for Exp-1 and Exp-2. As previously stated, this could negatively affect the recovery of oil volume due to greater viscous forces needed to overcome capillary forces needed to mobilize the entire ganglia body. The formation of the interconnected ganglia may also be attributed to the emulsion of the oil into the aqueous phase whereby the oil-water exists as a quasi-single phase within particular regions of the pore system (Thomas and Ali, 1989). The progressive reduction in size (volume) of the oil ganglia over flushing steps (i.e. 2-PV surfactant flush, subsequent 3-PV alkaline flush; 5 PV total), via image analysis and Blob3D quantification, indicates that ganglia fragmentation occurs as flushing continues.

Evaluation of the series of surfactant flushing experiments within increasing porous medium heterogeneity (Exp-2, Exp-4, and Exp-5) shows that there are notable differences in oil distribution/configurations for the initial residual oil condition. In general, visual observations and quantitative analyses (Blob3D results) show that smaller, more spherical (rounder) oil blobs are present in Exp-2 (homogeneous media), larger interconnected-ganglia are present in Exp-4 (mildly heterogeneous media), and skewed (uneven) distribution of oil blobs with relatively large volumes are present in Exp-5 (moderately heterogeneous media). Differences in

observed and quantified oil distributions between Exp-2 to Exp-4 may be due to increased solution pH (carbonate dissolution, Exp-4) and associated impacts from reductions in IFT and/or transition in system wettability (i.e. oil-water to water-wet). Such conditions may cause the oil to distribute more widely as ganglia within the intergranular pore spaces. For the most heterogeneous system, Exp-5, the larger volume oil blobs (ganglia) may be attributed to the greater heterogeneity (permeability) distribution, whereby smaller pore spaces restrict oil movement causing "pooling" of the oil in larger pore spaces. The effects of the surfactant flushing on oil distribution are relatively similar for each of these column systems, wherein the oil blob or ganglia volume continues to decrease (via fragmentation) as flushing progresses. This particular fragmentation (blob/ganglia reduction with flushing) trend is more noticeable in the homogeneous medium (Exp-2) and less distinct with the increasing heterogeneity (i.e. Exp-4 and Exp-5, respectively).

In general, the results of SXM image analyses and Blob3D oil quantification show that enhanced flushing (alkaline and surfactant) can induce changes in oil blob distribution associated with decreases in oil blob volume and increases in the number of oil blobs, and, in some cases, evolution to an interconnected ganglia oil network or quasi-single-phase emulsion state as flushing progresses (Walstra, 1993). The SXM-generated column images show that at the pore scale level these oil distribution changes can be quite dramatic. The reduction of IFT, due to the effects of the surfactant or alkaline flushing solution, allows expansion of the interfacial surface between the oil and aqueous phases. One mechanism by which this increase in surface occurs is by breaking (fragmenting) the blobs into smaller blobs and dispersing them into the aqueous phase as smaller fragments (Levorsen, 2001). It should be noted that a general

trend in the change from more spherical oil blobs to more flattened blobs was observed and quantified after each progressive enhanced flushing event (time-series). This effect contributes to an overall increase in the total oil surface area that is in contact with the aqueous flushing solution. Although the overall oil blob volumes decrease in this manner, the change in morphology (to less spherical, i.e. flattened) allows greater surface area of the oil to be in contact with the solid and/or aqueous boundary. This change in morphology can be attributed to the reduction of IFT at the oil-water interface and is expected to affect oil recovery as discussed in later sections.

Crude Oil Removal/Recovery

Changes in oil or NAPL distribution, particularly changes in oil body (blob or ganglia) volume and surface area due to enhanced-flushing processes, can influence the overall rate (or percent) of oil recovery. Oil body (blob and ganglia) volumes and surface areas were quantified using the Blob3D software (Ketcham, 2005) before and after sequential enhanced-flushing events. Extraction of these parameters, and others, from 3D images constructed from SXM were used to relate oil recovery processes to changes in oil morphology and distribution over a range of flushing intervals. The total oil blob/ganglia volumes for each column experiment (Exp-1 through Exp-5) after initial residual saturation conditions and after each sequential flushing event (2-PV and 3-PV (5-PV total)) are presented in Table 3. For Exp-1 (alkaline flush – homogeneous media) and Exp-2 (surfactant flush – homogeneous media) the calculated oil (NAPL) recoveries were comparable after each respective flushing event. Exp-1 shows an initial oil recovery of 3.14% after 2 PV of flushing. After another subsequent 3 PV flush (a total of 5 PV of flushing), the total recovery of oil increased to 6.71% with respect to the initial total oil

volume present in the column prior to enhanced-flushing. The step-wise oil recovery for the 3 PV flushing period (3.68%) was consistent to that after the initial 2 PV flushing step (3.14%), indicating that removal processes via alkaline flushing were relatively consistent with a slight decrease in efficiency (oil % removed per PV) as flushing progressed. Exp-2 shows an initial oil recovery of 4.95% after 2 PV of surfactant flushing and 7.74% after a total of 5 PV of flushing. The step-wise oil recovery for the second 3-PV flushing period if 2.93% showed a notable decrease (~2 times) compared to that quantified after the initial 2 PV flushing step (4.95%), indicating that removal processes via surfactant flushing were less efficient (oil % removed per PV) as flushing progressed. These results also indicate that the alkaline flushing may be slightly more efficient over longer periods of flushing compared to surfactant flushing. Exp-3 focused on evaluating oil recovery (homogeneous medium) via a combined sequential alkaline-surfactant flushing technique whereby alkaline solution was introduced first and then directly followed by surfactant flushing for equal time periods for each flushing step (step-1: 2 PV; step-2: 2 PV; 4 PV total for the first flush; step-3: 3PV; step-4: 3PV; 10 total PV for all flushes). This alkaline-surfactant flush yielded the greatest overall oil recovery when compared to the independent alkaline and surfactant flushing experiments (Exp-1 and Exp-2). Exp-2 shows an initial oil recovery of 21.11% after 2 PV of surfactant flushing and 34.02% after a total of 5 PV of flushing. The step-wise oil recovery for the 3-PV flushing period (16.37%) was relatively consistent to that after the initial 2 PV flushing step (21.11%), showing only a slight decrease (1.3 times) in removal efficiency compared to that quantified after the initial 2 PV flushing step. However, this condition may indicate that that removal processes associated with dual sequential alkaline-surfactant flushing techniques may be slightly less efficient (oil % removed

per PV) as flushing progresses. More importantly, the sequential alkaline-surfactant flush demonstrated a significant increase in oil recovery (4.4–5.1 times greater) compared to the other two independent enhanced-flushing experiments which may hold promise for remediation at larger scales (flow cells to pilot-scale field tests). Of course, it should be noted that more laboratory and pilot field tests are needed to understand both the recovery and environmental impacts before implementing such aggressive techniques for field scale remediation.

Another series of independent surfactant-flushing experiments (Exp-4 and Exp-5) were conducted to evaluate the effects of increasing physical heterogeneity and calcium-carbonate (karst sand) content on oil (NAPL) removal and recovery as a function of oil morphology and distribution during flushing. Addition of the karst sand not only introduces finer grain sediments increasing heterogeneity, it also introduces carbonate dissolution processes that can alter system pH (solution and grain boundaries) potentially influencing oil (NAPL) distribution and recovery processes. Previous literature and experiments conducted as part of this study confirm that the relatively higher pH associated (solution and grain surface) in these sand-karst mixed systems tend to alter solid-liquid wettability from more oil-wet to more water-wet condition. Under this dynamic trend, oil (NAPL) will generally become more mobile under such water-wet conditions and thereby be extracted more easily from the subsurface during flushing. Exp-4 (25%-75% karst-Accusand, mildly heterogeneous) shows an oil recovery of 9.16% and 14.16% after 2 PV and 5 PV of flushing, respectively. The step-wise oil recovery for the 3-PV flushing period (5.61%) showed a decrease (~1.6 times) compared to that quantified after the first 2-PV flushing step (9.16%), indicating that removal processes may be slightly less efficient (oil %

removed per PV) as flushing progresses. Compared to the most homogeneous conditions of EXP-2 (40/50 Accusand, homogeneous) this surfactant flushing experiment showed significant improvement in oil recovery for both initial flushing and later flushing stages even though this system was more heterogeneous. Most notable was the nearly 2-fold increase in oil removal effectiveness for the complete 5 PV of flushing (Exp-4: 14.2% vs. Exp-2: 7.7%). The higher overall oil recovery may have been related to increased solution pH (carbonate dissolution) grain boundary charge (net negative charge) and reactions with the oil to initiate more water-wet conditions and associated higher oil removal rates. The effect of the increased pH and potential to alter the system to more water-wet may help offset expected reductions in oil recovery due to the associated increased heterogeneity (i.e. lower permeability). Exp-5 (50%-50% karst-Accusand, moderately heterogeneous) shows an oil recovery of 4.10% and 21.33% after 2 PV and 5 PV of flushing, respectively. The step-wise oil recovery for the 3-PV flushing period (17.97%) showed a notable (largest) increase (~4.4 times) compared to that quantified after the first 2-PV flushing step (4.10%), indicating that removal processes may be much more efficient (oil % removed per PV) as flushing progresses when calcium carbonate sediments are present. Compared to the most homogeneous conditions of EXP-2 (40/50 Accusand, homogeneous) this surfactant flushing experiment showed significant improvement in oil recovery, predominantly during the later stages of flushing, even though this system was significantly more heterogeneous. Most notable was the nearly 3.2-fold increase in oil removal effectiveness after the complete 5 PV of flushing (Exp-5: 21.3% vs. Exp-2: 7.7%). Similar to EXP-4, the higher overall oil recovery may have been related to increased solution pH (carbonate dissolution) grain boundary charge (net negative charge) and reactions with the oil to initiate

more water-wet conditions and associated higher oil removal rates. Since oil recovery rates are relatively consistent for both systems during the early stages of surfactant flushing, it may be that the dissolution and reaction processes altering the wettability of the system (to more water-wet) exhibited greater kinetic limitations. Such an effect may be related to the greater heterogeneity (lower permeability) condition of the porous medium, whereby permeability had greater control on early-time oil removal (less recovery initially) and then subsequent increases in pH with more time (carbonate dissolution) imposed greater control on removal processes, countering the reduced permeability effects, and yielding greater oil recovery. As described above, the higher overall oil recovery (later-time) may have been related to increased solution pH (carbonate dissolution) grain boundary charge (net negative charge) and reactions (more kinetically controlled) with the oil to initiate more water-wet conditions and associated higher oil removal rates. The effect of the increased pH and potential to alter the system to more water-wet may help offset expected reductions in oil recovery due to the associated increased heterogeneity (i.e. lower permeability).

In general, overall oil recovery was higher for the heterogeneous columns (Exp-4 and Exp-5) under surfactant flushing conditions compared to all homogeneous column flushing experiments (alkaline and surfactant) with the exception of the sequential alkaline-surfactant flushing experiment. As mentioned previously, these greater quantified oil recoveries are likely attributed to an increase of pH due to the presence of the karst sand and associated dissolution of calcium carbonate (karst). The greatest overall oil recovery was observed for the sequential alkaline-surfactant flushing experiment. The initial reduction of interfacial tension (i.e. via a decrease contact angle) by the alkaline flushing solution was followed by further reduction of

IFT during the surfactant flush leading to the increase in oil volume recovery. The removal process was relatively consistent for each of the flushing steps (after 2 PV and after 3 PV (5 PV total)), indicating that relatively higher associated removal conditions may be maintained as flushing progresses. Also, the emulsion of the oil into the aqueous phase may have also contributed to greater oil recovery. Although surfactant and alkaline flushing can affect the multiphase systems beyond the reduction of interfacial tension (i.e. unstable/stable emulsion phases, polarity of the solution, etc.) this study assumes that oil recovery is due primarily to the reduction of IFT between the oil and water phases (Ghosh and Tick, 2013). Because of this IFT reduction, less capillary pressure is required to displace "mobilize" the crude oil through the pore network.

Changes in Oil Morphology on Recovery

A comparison of the change in oil body (blob and ganglia) morphology may provide further insight into the recovery processes of crude oil or NAPL. As noted previously, oil blob (and ganglia) morphology was observed to flatten (deviate more from spherical) after progressive enhanced flushing as shown in 2D and 3D image analyses. This flattening effect causes greater oil surface area to be in contact with the flushing fluid thereby reducing the IFT of the oil body over a greater surface. Figures 3 and 4 show comparisons of the normalized oil-blob surface-area (surface-area/volume), also termed specific-surface area (a^o), to oil blob volume for each of the enhanced-flushing column experiments. Figure 3 specifically compares the conditions at residual oil saturation, prior to flushing, and after 2 PV of enhanced flushing; while Figure 4 compares the conditions at residual oil saturation and after 5 PV of flushing. A particular blob volume possesses a minimum surface area as a spherical shape, and any

deviation from a sphere will result in a greater surface area. It should be noted that the graphical representation of blob deviations from a sphere is more robust for distributions of disconnected blobs. Therefore, these analyses and associated graphical plots cannot be successfully applied when the majority of the oil (NAPL) phase is connected as ganglia. The surface-area-to-volume ratio of a perfect sphere is represented by the black curved model lines (Figures 3 and 4), and denotes the minimum specific surface area (a^o) as represented by a perfect (oil blob) sphere. The oil blobs below the line (smaller blob volumes, i.e. $<10^{-8}$ mm^3) can be attributed to the limitations of the Blob3D software and/or the parameters assigned during the grayscale thresholding and partitioning of the 2D images, before 3D conversion. Oil bodies (blobs or ganglia) deviating above the black (model) line exhibit relative higher surface areas compared to that of a perfect sphere geometry (i.e. become more flattened, or deviate more from spherical). Under such conditions, it would be expected that the flushing fluid would be more effective as it contacts greater relative oil (NAPL) surface area by reducing IFT at this boundary. For Exp-1 (Figures 3.1 and 4.1) and Exp-2 (Figures 3.2 and 4.2) in homogeneous media, the oil blobs and ganglia generally become more spherical in shape as flushing progresses (i.e. after 2 PV and 5 PV of flushing), especially for lower oil volumes ranges ($<10^{-7}$ mm^3). This may be enhanced by the solution contacting larger blobs and ganglia, allowing for fragmentation into smaller more spherical oil blob morphologies as flushing progresses. The larger oil blob (ganglia) volume sizes ($>10^{-6}$ mm^3) tend to deviate more from a sphere than the smaller blob volumes (i.e. after 2 PV and 5 PV flushing), and although the larger oil blobs tend to remain less spherical overall, the blobs tend to become slightly more spherical in shape after 5 PV of flushing. For Exp-3 (Figures 3.3 and 4.3), the oil blobs and ganglia show a more

noticeable change in blob morphology from less spherical to more spherical as flushing progresses. The oil blobs in the initial residual oil saturation condition exhibited the greatest deviations from spherical shape but became increasingly spherical with each respective flush event (after 2 PV and 5 PV flushing events). However, similar to Exp-1 and Exp-2, the larger oil blob (ganglia) volume sizes (>10^{-6} mm^3) tended to deviate more from a sphere for the later flushing event (after 5 PV event). In contrast to the independent alkaline and surfactant flushing experiments (Exp-1 and Exp-2), overall blob morphology tended to deviate more as flushing progressed for the larger oil blob volume size ranges (>10^{-6} mm^3).

The heterogeneous experiments (Exp-4 and Exp-5) show a different blob distribution than what can be observed from the homogeneous columns described above. For Exp-4 (Figures 3.4 and 4.4), blob variations do not deviate much from that of the initial residual oil distribution, as flushing progresses. At smaller volumes (<10^{-8} mm^3) oil blobs become slightly more spherical. Oil blob volumes between 10^{-8} and 10^{-6} mm^3 show slight deviation from spherical shape, and the larger ganglia volumes (>10^{-6} mm^3) show virtually no deviation from the residual oil blobs (which all generally plot above the spherical model line). This trend continues as flushing progresses (2 PV to 5 PV). For Exp-5 (Figures 3.5 and 4.5), the oil blobs show the greatest deviation from spherical shape (flattening of the oil blobs) compared to Exp-4 (and Exp-2). This notable increase in oil blob flattening (deviation from spherical) generally occurs for volumes as large as ~10^{-6} mm^3 and continues to the smallest volumes of oil, with even more deviation from spherical shape as flushing progress (from 2 PV to 5PV; Figure 4.5). With respect to oil volume recovery, Exp-4 shows minimal change in the blob shape (morphology) from that of the initial residual saturation condition. Thus, the oil volume

recovered from this experiment is strictly from the fragmentation of the large ganglia due to reduction of IFT between the oil and aqueous phases due to surfactant flushing encountering the relatively larger surface area of the oil blobs and ganglia. For Exp-5, as flushing progresses, surface area is increased which when in contact with the surfactant causes fragmentation of the larger oil blobs to smaller resulting blobs. Thus, it is presumed that due to the relatively larger surface areas of the oil present in Exp-4 and Exp-5, the surfactant was in contact with more of the oil. This greater surfactant-oil contact is likely causing fragmentation of the oil into smaller blobs which are better able to be mobilized within the pore space of the heterogeneous sand. Thus, the fragmentation of the oil can be attributed to the higher overall recovery volumes as compared to mobilization of the oil from the homogeneous experiments (with exception to Exp-3).

The greater the surface area to volume ratio, the greater potential for reduction of IFT between the oil-aqueous-solid interface, and thereby would be expected to yield greater oil recovery. Similarly, for equivalent blob volumes, the more spherical the oil blobs are during flushing (i.e. closer to black spherical model line) the less oil area would be available to solution, having lower impact via a reduction of IFT. Under such conditions, contact angle is reduced (or lower), and therefore, only at smaller oil volumes will the crude oil be mobilized. As oil particle size gets smaller, spherical shape is preferred for recovery. Hence, the singlet oil blobs tend to exist predominantly as the smallest blob sizes (volumes), which allow for greater mobilization and recovery with the aqueous phase. Large volume oil spheres and large ganglia will require greater pressure to move through tiny pore spaces, which can make recovery less efficient and less cost effective.

Distribution of Oil Blobs per Oil Blob Volume

Evaluation of the distribution of oil blob size throughout the column also aids in understanding the potential for oil recovery in the various systems. As volumes of the oil blobs are reduced during flushing, mobilization potential should increase throughout the pore networks. However, it should be noted that the distribution of larger blobs will account for most of the total oil volume within the system at any given time of flushing. Figure 5 show the cumulative distribution of oil blobs over a range of oil blob volumes whereby the distribution denotes the percentage of blobs finer than a corresponding volume size. These cumulative distribution plots provide a means to assess overall heterogeneity of oil blobs within the column as well as the dominant oil blob size (volume) fraction within the column before and after each respective flushing episode. As can be observed, most oil blob sizes occur within volume ranges between the smallest and largest blob volume extremes (Figure 5). An oil distribution with an extremely high slope (over the range of cumulative fraction %) indicates a relatively homogeneous (uniform) oil blob distribution whereby most of the oil blobs within the column are all about the same volume size. Conversely, if the slope of the oil distribution curve is relatively low (over the cumulative fraction %), the oil distribution is relatively heterogeneous whereby a large variation of oil blob sizes (volumes) are present in the column. Furthermore, such plots provide an effective way to evaluate how mean oil blob size (volume at or 50% fraction finer than) for the distribution changes (evolves) during flushing (i.e. after each enhanced flushing episode).

Exp-1 (alkaline-homogeneous medium) and Exp-2 (surfactant-homogeneous medium) (Figures 5.1 and 5.2) show similar trends in oil blob distribution over the various flushing

episodes. The oil blob distributions for the initial residual saturation conditions show relatively homogeneous (uniform) distribution of oil blobs with mean blob sizes corresponding to ~10^{-6} mm^3. After 2-PV of flushing (alkaline and surfactant) the oil blob distributions remain relatively uniform but the volume size of the distribution significantly decreases with mean blob sizes corresponding to ~10^{-8} and 10^{-7} mm^3 for Exp-1 and Exp-2, respectively. Similarly, after 5-PV of flushing the oil blob distributions remain relatively uniform, however, the volume size of the distribution is fairly consistent to that after the 2-PV flushing events, with mean blob sizes of 5×10^{-8} and 10^{-7} mm^3 for Exp1 and Exp-2, respectively. The cumulative distribution plots, after 2-PV of flushing, demonstrate the pronounced reduction in oil blob volumes (for the distributions) from the initial residual saturation conditions. The results show that greater oil recovery was directly related to the reduction of oil blob volume distribution resulting after each respective flushing episode. For example, the larger the gap between the cumulative distribution curves prior to and after progressive flushing events (i.e. residual saturation, 2-PV flush, 5-PV flush) indicated generally greater oil recoveries for that system and particular flushing episode. Although fairly consistent to that after the 2-PV flushes, the cumulative oil distributions after 5 PV of flushing yield slightly larger oil blob volume distributions. This effect may be attributed to interconnection (or recoalescing) of oil blobs along preferential flow paths or within the pores spaces as the oil is mobilized. For Exp-3 (sequential alkaline-surfactant, homogeneous medium) (Figure 5.3), the oil blob distribution for the initial residual saturation condition shows a relatively heterogeneous (wide variation of volume size) distribution of oil blobs (compared to Exp-1 and Exp-2), with a mean blob size corresponding to ~10^{-6} mm^3. After 2-PV of flushing (alkaline) the oil blob distribution remains consistently heterogeneous (i.e.

initial saturation condition) and the volume size of the distribution increases slightly primarily for the lowest and highest oil blob volume ranges. However, the mean oil blob size for the cumulative distribution remains consistent to the initial residual saturation condition of ~10^{-6} mm^3. This blob size distribution increase may be due the interconnection (or recoalescing) of oil blobs within the pores spaces and/or to the formation of oil-in-water emulsions as the oil is mobilized during flushing. Such formation of emulsions could explain the slight differences in the cumulative oil distribution curves as a result of enhanced flushing, compared to the initial residual oil saturation distribution. Although fairly consistent to that after the 2-PV alkaline flush, the cumulative oil distribution after 3 PV of subsequent surfactant flushing (5 PV total) remained consistently heterogeneous, however, the blob volume size of the distribution slightly decreases as a result of this final flushing step. However, similar to the prior alkaline flushing step, the mean oil blob size of the cumulative distribution remained approximately the same at 10^{-6} mm^3 over the sequential flushing episodes. For Exp-4 (surfactant-mildly heterogeneous medium) (Figure 5.4), the oil blob distribution for the initial residual saturation condition shows a relatively homogeneous condition, however, a significant majority of the oil blobs range in volume sizes between 10^{-7} and 10^{-5} mm^3 which does demonstrate some variation and heterogeneity (non-uniformity) of the oil distribution. The mean oil blob size of this distribution (i.e. residual saturation) is consistent with the other experiments at approximately 10^{-6} mm^3. Overall, the oil blob distributions after both the 2-PV and subsequent 3-PV (5 PV total) surfactant flushes are nearly identical to the residual saturation oil distribution condition, in terms of both blob heterogeneity and mean blob size. However, although the blob distribution after both 2 PV and a total of 5 PV of flushing are nearly identical (overlap), both distributions

exhibit slightly larger blob volume size distributions as a result of flushing (curves shifted slightly), compared to the initial residual distribution condition (Figure 5.4). The slightly larger oil blob distribution that ensues after the two flushing episodes (in combination with the image analysis) show that slightly larger ganglia are present which may in part be due to emulsification effects during flushing as a result of dissolution of the carbonate sand and associated higher pH values. Again, however, it should be noted that there were minimal differences in the oil blob distribution before (residual saturation) and after respective (2 PV and 5 PV total) flushing events. Over the complete duration of surfactant flushing, there was more oil volume recovered (in terms of % recovery) from the mildly-heterogeneous medium experiment (Exp-4) compared to that from the homogeneous medium experiment (Exp-2), whereby reduction in the size (volume) of the oil blobs and ganglia was greater in Exp-4 than that of the oil in Exp-2. Unlike that for Exp-4, for Exp-5 (surfactant-moderately heterogeneous medium) (Figure 5.5) the oil blob distribution of the initial residual saturation condition shows a relatively heterogeneous condition with a wide range of oil blob volume (size) variation (10^{-9} – 10^{-4} mm^3). Although the mean oil blob size for the distribution is consistent (10^{-6} mm^3) with the other experiments (i.e. Exp-4 and Exp-2), the oil blob distribution is significantly different than for Exp-4 (and others), in which the distribution profile is notable concave upward compared to the results of all other experiments. Also of notable interest is the fact that both successive surfactant flushing episodes (i.e. 2 PV and 3 PV (5 PV total) had a dramatic effect on reducing the size (volume) distribution of the oil blobs. In fact, an overall progressive reduction in oil blob size (volume) distribution resulted after each successive surfactant flushing episode (2 PV and 3 PV (5 PV total)), with mean oil blob sizes of approximately 10^{-8} and 5×10^{-9} mm^3, respectively.

Furthermore, a slight increase in oil blob uniformity (homogeneity) resulted after each progressive flushing event, whereby the oil blob distribution curves (over the range of most blob volume sizes) sharpened (increased slope) with as flushing continued (Figure 5.5). The overall oil volume recovered in Exp-5 is more likely due to the reduction of oil blob rather than the mobilization of larger blobs through the porous network. The medium is moderately heterogeneous and larger oil blobs will generally be more difficult to mobilize and remove due to smaller pore networks (Appendix B has figures and histograms further describing the distribution on blob size and blob volumes).

The results above describe the trends in oil distribution of blob volume (size) and changes in relative surface area (morphology) after enhanced flushing and provides an improved understanding of the conditions controlling (i.e. limiting or enhancing) oil removal of oil in various porous media systems (physical heterogeneity, chemical composition (CaCO3), etc.). Additionally, the pore network structure (i.e. permeability) plays a large role in oil recovery. Larger pore networks will aid in the mobilization of oil, even for larger volume oil blobs. In general, it can be observed that an increase in the preferential flow (mobilization) of oil occurred in systems with increasing heterogeneity. Even though more oil was recovered in Exp-5 than that of Exp-2, as a result of the overall significant reduction of oil blob size distribution with flushing, it is expected that the largest blobs and ganglia remaining in the system will be difficult to remove via enough volume reduction and corresponding mobilization and removal from the pore network. Under such conditions, the largest oil blobs and ganglia trapped within heterogeneous porous media and/or “blocked” by the smallest pore-size distribution will be difficult to remove leading to less cost effective (inefficient) recovery.

Drop Shape Analysis

Drop shape analysis is another useful tool to further help understand the mobilization and remediation of crude oil. Images were taken during contact angle measurements along the S-L-L junction from the KRUSS® DSA-1 drop shape analyzer, with Figure 6 showing the images for three different weight crude oils (light oil - 41.0° API, medium oil - 29.6° API and heavy oil - 14.1° API) in contact with silica glass (blurry images were excluded from this paper) while in solution with increasing pH (pH 4 – HCl solution, pH 7 – distilled water, pH 10, 12, and 13.5 – NaOH solution). Figure 7 shows images taken with the three model oils (listed above) in contact with limestone plate (calcium carbonate) with increasing pH solutions (also listed above). Recorded contact angle measurements are reported in Table 4. Contact angle measurements for light oil in contact with glass (silica) are 77.9°, 95.5°, 17.5°, 13.9°, and 11.1° for increasing pH of the solution (pH 4, 7, 10, 12, and 13.5, respectively). Contact angle measurements for the medium oil in contact with glass (silica) are 78.2°, 108.3°, 75.6°, 47.1°, and 13.3° for increasing pH of the solution (pH 4, 7, 10, 12, and 13.5, respectively). Contact angle measurements for the heavy oil in contact with glass (silica) are 102.7°, 133.4°, 60.8°, 55.1°, and 48.8° for increasing solution pH of 4, 7, 10, 12, and 13.5, respectively. For all three model oils, there is an increase in contact angle from pH 4 to pH 7, and a subsequent decrease in contact angle as pH is increased (10 to 12 to 13.5). This behavior can be observed from the images in Figure 6, where a change in oil volume is also observed. At higher pH values of the solution, a much smaller oil volume is observed due to the decrease of IFT between the oil and aqueous phases, where the solution causes larger oil particles to fragment into smaller drops. Figure 8.1 is a plot showing changes in contact angle as a function of aqueous solution pH when

the oil blob (droplet) is in contact with a silica plate. This figure also shows the particular wetting fluid phase (according to the definition given in Mercer and Cohen (1990); water wet $\theta < 90^o$, oil wet $\theta > 90^o$). Figure 8.1 shows that the light oil becomes water wet ($\theta < 90^o$) at a solution pH of 8 and the medium and heavy oils (all in contact with the silica plate) reach water wet conditions close to a solution pH of 10.

Figure 7 shows images of the three model oils in contact with limestone (calcium carbonate, $CaCO_3$)) while in increasing pH solutions (listed above). Contact angle measurements (Table 4) for light oil in contact with limestone ($CaCO_3$) are 94^o, 118^o, 79.5^o, 50.5^o, and 49.4^o for increasing solution pH of 4, 7, 10, 12, and 13.5, respectively. Contact angle measurements for the medium oil in contact with limestone ($CaCO_3$) are 93.7^o, 117.7^o, 108.1^o, 99^o, and 72.1^o for increasing solution pH of 4, 7, 10, 12, and 13.5, respectively. Contact angle measurements for the heavy oil in contact with limestone ($CaCO_3$) are 92.4^o, 93.3^o, 96.6^o, 129.1^o, and 119.5^o for increasing solution pH of 4, 7, 10, 12, and 13.5, respectively. The larger contact angles for all oils in contact with the limestone media ($CaCO_3$), as compared to the contact angles observed for oils in contact with silica, can be explained by the presence of carbonic acid via saturation of CO_2 (atmosphere) in solution. The addition of carbonic acid (a weak acid) in contact with an alkaline (NaOH) solution will create the addition of water, causing a decrease in solution pH. This reduction in pH changes how the oil reacts with the pH-varying solutions, causing an increase in contact angle for the higher pH range. This addition of carbonic acid has the greatest effect on the contact angle changes for the heavy oil, whereby oil-phase contact angle increases as pH increases (from pH 4 to pH 12), and contact angle is reduced for the oil droplet in contact with the limestone ($CaCO_3$) within in the pH 13.5 solution.

Figure 8.2 shows the measured contact angle values for the three model oils in contact with limestone as a function of increasing solution pH (pH 4 to 13.5). In the presence of limestone, the light oil attains a water wet condition at a higher solution pH (~10) compared to that in contact with silica (pH~8). The medium oil becomes water wet at a pH of approximately 13 and the heavy oil never attains a water wet condition. Such contact angle experiments (i.e. Figure 8.2) provide direct evidence that limestone in the presence of higher pH solutions (pH 10-13.5) can act to decrease solution pH (via carbonic acid reaction) and thereby not impose as great of an oil wettability change as preferred (for better oil removal). Thus, for the alkaline (NaOH) column flushing experiments with karst ($CaCO_3$) sand fractions, crude oil mobilization and recovery may be significantly hindered from this competing pH/oil-wettability process (as described above).

IFT was also measured for each of the three model oils in each of the five pH solutions (pH 4, 7, 10, 12, and 13.5) (Table 5). For these measurements the respective oil was only in contact with the particular pH solution. For light oil, IFT values were 18.03, 22.61, 8.28, 5.62 and 2.82 $dyn \cdot cm^{-1}$ for solution pH values of 4, 7, 10, 12, 13.5, respectively. For the medium oil, IFT values were 17.35, 20.9, 9.43, 7.29, 6.98 $dyn \cdot cm^{-1}$ for pH values of 4, 7, 10, 12, 13.5, respectively. For the heavy oil, IFT values were 15.5, 36.36, 27.96, 25.8, 11.52 $dyn \cdot cm^{-1}$ for pH values of 4, 7, 10, 12, 13.5, respectively. Figure 9 is a plot showing solution pH as a function of IFT for each crude oil type (light, medium, and heavy), whereby values are measured averages of IFT, with the corresponding 95% confidence intervals (2σ) presented, for the range of solution pH. The IFT values show similar trends to that for contact angle (in contact with glass), with IFT increasing from pH 4 to 7, and then decreasing from pH 7 to 13.5. The higher overall

IFT values of the heavy oil (in solution), over the range of varying solution pH, demonstrate that the heavy oil is more resistant to IFT reduction due to changes (increases) in solution pH. The values measured for both contact angle and IFT (i.e. oil/pH-solution) will be used in the next section for oil mobilization potential and trapping potential analyses.

Oil Mobilization and Trapping Potential Analyses – N_C, N_B, N_T, ΔP

For the analysis of oil trapping and/or oil displacement, a system that has a higher capillary and bond number will have the potential to yield higher recoveries of oil. The mobility of trapped oil in porous media is, in part, controlled by imposed viscous forces of the flushing fluid, the interfacial tension between the oil-aqueous-solid interface, the density differences between oil and flushing solution, porous-medium permeability, and a combination of these factors. The capillary number (N_C) describes the ratio of viscous forces to interfacial tension forces, the Bond number (N_B) describes the ratio of buoyancy forces to interfacial tension, and the trapping number (N_T) describes the effect of both buoyancy and viscous forces relative to interfacial forces (Boving and Brusseau, 2000; Morrow and Chatzis, 1982; Pennell et al., 1994, 1996; Ghosh and Tick, 2013). Interfacial tension values measured during drop shape analysis were used for calculations with respect to increasing solution pH values due to alkaline flushing. For surfactant flushing, the interfacial tension values reported in Ghosh and Tick (2013) were used for calculations. Table 6.1 reports the values calculated for capillary number, Bond number, and trapping number for residual saturation and during surfactant flushing. Table 6.2 reports these values for the alkaline flushing under increasing solution pH values. Under residual saturation conditions, Bond numbers were much higher than capillary numbers, meaning that buoyancy forces were responsible for the trapping and mobilization of crude oil.

For all conditions (light, medium and heavy oil) buoyancy forces had a greater effect on trapping and mobilization (Bond number is an order of magnitude higher than capillary number) compared to viscous forces (i.e. N_C) and this effect was more prominent with decreasing oil density (i.e. increasing ^{o}API) (light vs. medium vs. heavy oil). The values for Bond number compared to capillary number under residual saturation were 14, 10, and 4 times greater for light, medium and heavy oils, respectively. Compared to the capillary numbers (N_C) under residual saturation conditions, the effects of surfactant flushing cause significant increases in N_C (+461% for light oil, +366% for medium oil, and +288% for heavy oil). The effects of surfactant flushing also increased Bond number (N_B) but not nearly to the extent as that observed by the change in N_C values. Calculated changes in Bond number (N_B), as a result of surfactant flushing, showed comparatively smaller increases in N_B (+146% for light oil, +88% for medium oil, and +71% for heavy oil). The greater increase for capillary number is likely due to the reduction of IFT due to surfactant flushing and corresponding greater impact on the viscous forces as compared to buoyancy forces. The impacts of surfactant flushing also caused an increase change of trapping numbers (N_T) (+146% for light oil, +114% for medium oil, and +117% for heavy oil), however, oil the potential for oil mobilization is controlled by buoyancy forces over viscous forces when considering the combined effects of both factors.

For the alkaline flush, the impact of reducing IFT for calculated values of Bond and capillary numbers changes as pH of the solution increases. For NaOH solutions of pH 10, capillary numbers (N_C) increase by 255%, 189%, and 69% for light, medium, and heavy oil, respectively. Although not to the extent of the N_C value changes, the effect of alkaline solution (reduced IFT) also increased the Bond numbers (N_B) yielding changes of 172%, 122% and 29%

for light, medium, and heavy oil, respectively. A greater calculated increase in capillary numbers (N_C) with respect to Bond numbers (N_B) demonstrate that the reduction of IFT and corresponding greater relative increase in viscous forces (via N_C) play a greater role on potential of oil mobilization than buoyancy forces (N_B). However, Bond number magnitudes are still an order of magnitude higher than the capillary number for the alkaline flushes (with the exception of the heavy oil in pH 13.5 solution). These higher N_B values indicate that alkaline flushing may have a greater impact on oil mobilization via buoyancy forces compared to surfactant flushing. The impacts of alkaline flushing also caused an increase change of trapping numbers (N_T) for a solution pH of 10 with changes in values of 179%, 127%, and 38% for light, medium, and heavy oils, respectively. For the oils in the presence of the higher 13.5 NaOH solution, trapping numbers (N_T) increase by 735%, 218%, and 266% for light, medium, and heavy oil, respectively. While capillary numbers increase as pH of the solution increases (an increase of almost 1200% for light oil in pH 13.5 solution), the relative increase in trapping number (N_T) is primarily due to the increase in the buoyancy forces, as Bond numbers are generally a magnitude greater than capillary numbers. Hence, buoyancy forces are generally controlling trapping and mobilization of oil during alkaline flushing, while viscous forces have a greater impact on trapping and mobilization during surfactant flushing.

Change in capillary pressure (P_C) can also contribute to trapping and mobilization of oil in porous saturated media. The change in pressure between the wetting and non-wetting fluids is can be described as a ratio of interfacial tension between the oil and aqueous phases to pore radius in the porous medium. Data collected from the drop shape analysis were used to calculate changes in capillary pressure and are presented in Table 7. These values are

representative of the change in pressure between the two fluid phases in the system, and not the overall pressure exerted on the oil in the pore spaces of the medium. Values were calculated for oil-aqueous systems with solution pH values of 7 or higher. Capillary pressure values (P_C) were calculated using the Young-Laplace equation with an average pore radius of 0.009 cm (reported by Unimin Corporation for 40/50-mesh sands) and contact angles of the oil measured in contact with silica (glass) plate. Negative P_C values indicate that greater pressure is added to the system due to a higher interfacial tension between the oil and aqueous phases, whereby pressure exerted on the oil phase (considered the wetting fluid) is higher than the pressure exerted on the aqueous phase (considered the non-wetting fluid). A change in the system, from oil wet to water wet occurs when contact angles are less than 90^o, which will yield positive capillary pressure values (P_C). The larger the absolute value of the change in pressure (P_C) means that more energy is required to remove the oil. Negative P_C values are shown for all three oils at a solution pH value of 7, with the largest negative value shown for the heavy oil (-555.17 N/m^2). Light oil shows the highest change in P_C in the presence of the pH 10 solution (175.48 N/m^2), and the lowest change in P_C (for water-wet conditions) in the pH 13.5 solution (61.49 N/m^2). The medium oil shows just the opposite, with the lowest change in P_C in the presence of the pH 10 solution (52.11 N/m^2), and the highest change in P_C in the pH 13.5 solution (150.95 N/m^2). The heavy oil shows the greatest changes in P_C in the presence of both the pH 12 and pH10 solutions (328.03 N/m^2; and 303.12 N/m^2, respectively), with the smallest change in P_C in the pH 13.5 solution (168.62 N/m^2). The P_C values calculated provide an enhanced understanding of the energy requirements (i.e. higher pumping velocity of the flushing fluid, larger viscous forces, etc.) for the removal of crude oil in saturated porous media.

For all of the oil-aqueous-solid systems tested in Table 7, the lowest changes in capillary pressure (P_C) calculated was for the medium oil within the pH 10 solution. This indicates that less energy is required to remove the oil from the pore spaces, as the pressures (P_C) between the two fluids are closest under this pH range, and therefore requiring less pressure (force) needed to overcome the capillary forces (trapping oil) for oil to be mobilized. The P_C values shown will change throughout the system based on the radius of the pores in the medium. For comparison purposes the porous medium average pore size was used, with the understanding that smaller pore sizes will yield larger P_C values and larger pore sizes will yield smaller P_C values. Hence, more pressure (force) will need to be applied to mobilize both flushing and NAPL fluids in smaller pores, as compared to the pressure needed to mobilize the fluids in larger pores. As previously mentioned, the use of a pH 13.5 solution is primarily for comparing pressure and interfacial effects on the oil-aqueous-solid systems under the most extreme pH scenarios, as it is recognized that this high pH condition could have severe adverse or unintended impacts on the subsurface microbiology, soil and clay chemistry, and release or retention of other metals or contaminants in groundwater under real world application.

CONCLUSIONS

The success of enhanced-flushing remediation relies upon the removal of NAPL form saturated porous media and the knowledge of the mechanisms responsible tor NAPL mobilization and trapping. Understanding specific site characteristics, such as pore space in the media, the composition of the media, heterogeneity of the system etc., is also important to the success of remediation. The mechanisms responsible for mobilization include NAPL blob morphology, capillary forces, chemistry of the system, viscous and buoyancy forces, available NAPL surface area, and interfacial tension and surface tensions along the NAPL surface. Understanding how to best manipulate these parameters is paramount in the removal of NAPL from contaminated sites. This comprehensive study for the mechanisms responsible for mobilization of NAPL will give a better understanding to aid in future research and remediation efforts. The pore scale studies using SXM have shown that the fractioning of NAPL under different fluids flushes can reduce the volume of oil for both surfactant and alkaline flushing. Buoyancy forces control mobilization for alkaline flushing and viscous forces control mobilization for surfactant flushing. The sequential flush (Exp-3) was most effective in the recovery of oil in the column experiments, by utilizing both buoyancy and viscous forces. The reduction of interfacial tension along the NAPL- aqueous phase boundaries is the most responsible for the mobilization of the NAPL. Further testing will need to be conducted on the potential of a sequential alkaline-surfactant flushing strategy as a viable remediation option.

The addition of carbonate karst sand has also been shown in this study to increase the recovery of the NAPL during surfactant flushing, due to the increase in pH of the system as a function of the dissolution of karst sand, and due to the increase in the surface area of the oil blobs and ganglia. The SXM 3D imaging methods were critical in showing the distribution of oil blobs as well as the change in morphology during flushing experiments. The data show an increase in in fractionation of large blobs to smaller spherical blobs, and an increase of surface area for larger blobs and ganglia which can allow the flushing fluid greater contact with the NAPL casing further fractionation. The drop shape analysis was key for the understanding of the chemical reaction of NAPL in an alkaline solution. Contact angle and IFT were both measured with the KRUSS® DSA-1 drop shape analyzer. The values measured show a change in the wettability of the system as a function of pH. Higher pH solutions have smaller contact angles and making the aqueous phase the wetting agent, as opposed to larger contact angles were the NAPL is the wetting agent. Through drop shape analysis, the reduction of interfacial tension between the NAPL and aqueous phases was also shown to be a function of pH. The addition of a carbonate in contact with atmospheric carbonic acid in solution will negatively impact pH, thus impacting both contact angle and interfacial tension. Values for contact angle and IFT were used for change in capillary pressure, showing that energy required for NAPL mobilization to occur in saturated porous media.

The cost of the remediation is dependent on the effectiveness of the solution, the time needed to remove the contaminant and the initial cost of the solutions. Comparing the cost of alkaline flushing, surfactant flushing and the sequential flush, and based off the results from this research, alkaline flushing would be very cost effective in the short term. The initial cost

compared to the surfactant and sequential flush would be lower, however the long-term cost of using an alkaline flush could be substantially higher depending the time of remediation, as alkaline flushing alone could take longer to remove the NAPL, and the ability to recycle the solution would be more difficult. The surfactant flushing has a higher initial cost, but surfactants can be recovered and recycled causing long term cost to be lowered. The sequential flush has the potential to be the most cost-effective method. The initial cost would be less than surfactant flushing alone. Long-term cost would also be lower due to the effectiveness of the solution to mobilize the NAPL and reduce the time needed for remediation.

Future Work

Future work of this research needs to be conducted to make the sequential flush and alkaline flush viable remediation techniques for removing NAPL from contaminated groundwater. In order to compare the alkaline flush to surfactant flushing drop shape analysis needs to be conducted with the surfactant to show how contact angle is affected when in contact with both silica and limestone media. Also, the measurement of IFT should be evaluated for each of the three oils in the study using the KRUSS® DSA-1 drop shape analyzer so the measurements can be compared to that of the alkaline solution. Other surfactants besides the Petrostep-1 can be analyzed and compared to each other to see which has a greater effect of OFT and contact angle. Different concentrations of the Petrostep-1 should also be evaluated to find the optimum concentration by weight for removal of NAPL.

Future work should also include SXM experiments using alkaline solutions with pH ranges between 8 and 10. This would eliminate some of the adverse limitations of alkaline flushing. Sequential flushing experiments should also be conducted with alkaline solution with

pH ranges between 8 and 10. If this can be shown to have the same effectiveness as the solution with pH 12 performed in this research than further testing can be done to expand on the potential for a sequential flushing remediation technique. This could lead to field testing and may prove to reduce the time required to remove residual NAPL trapped in the subsurface.

REFERENCES

Al-Rossies, A.A.S, Al-Anazi, B.D., Palaman, A.M., 2010, Effects on pH values on the Contact angle and Interfacial Tension, *NAFTA, v.61, p. 181-186.*

Boving, T.B., Brusseau, M.L., 2000. Solubilization and removal of residual trichloroethene from porous media: comparison of several solubilization agents. *J. Contam. Hydrol. 42 (1), 51–67.*

Brusseau, M.L., Peng, S., Schnaar, G., Murao, A., 2007. Measuring air-water interfacial areas with X-ray microtomography and interfacial partitioning tracer tests. *Environ. Sci. Technol. 41 (6), 1956–1961.*

Connor, J.R., 1988. Case study of soil venting. *Pollution Eng., 20(7), 74-78*.

Du, Y., Zhang, G., Ge, J., Li, G., Feng, A., 2013, Influence of Oil Viscosity on Alkaline Flooding for Enhanced Heavy Oil Recovery, *Journal of Chemistry, v. 2013, p. 1-8.*

Ghosh, J., Tick, G., 2013, A pore scale investigation of crude oil distribution and removal from homogeneous porous media during surfactant-induced remediation, *Journal of Contaminant Hydrology, v. 155, p. 20-30.*

Hunky, R.M., Wu, Y., Bai, B., Dunn-Norman, S., 2010. An experimental study of alkaline surfactant flushing for ultra-shallow heavy oil reservoirs. Soc. Petrol. Eng., Western Regional Meeting, 27-29 May 2010, Anaheim, California, doi:10.2118/132537-MS.

Kanicky, J. R., Lopez-Montilla, J. C., Pandey, S., & Shah, D. O. (2001). Surface chemistry in the petroleum industry. *Handbook of applied surface and colloid chemistry, 1, 251-267.*

Ketcham, R.A., 2005. Computational methods for quantitative analysis of three dimensional features in geological specimens. *Geosphere 1 (1), 32–41.*

de Laplace, P. S. (1814). *Théorie analytique des probabilités. Courcier.*

Levorsen, A.I., 2001. Geology of Petroleum, 2nd ed. The AAPG Foundation, Tulsa, Oklahoma.

McCray, J.E., Tick, G.R., Jawitz, J.W., Gierke, J.S., Brusseau, M.L., Falta, R.W., Knox, R.C., Sabatini, D.A., Annable, M.D., Harwell, J.H., Wood, A.L., 2011. Remediation of NAPL source zones: lessons learned from field studies at Hill and Dover AFB. *Groundwater 49 (5), 727–744.*

Mercer, J. W., & Cohen, R. M. (1990). A review of immiscible fluids in the subsurface: properties, models, characterization and remediation. *Journal of Contaminant Hydrology, 6(2), 107-163*

Morrow, N.R., Chatzis, I., 1982. Measurement and correlation of conditions for entrapment and mobilization of residual oil. Dep.Energy (DOE) Rep. 10310–20, 59.

Morrow, N.R., Songkran, B., 1981. Effect of trapping and buoyancy forces on non-wetting phase trapping in porousmedia. In: O Shah, Do. (Ed.), *Surface Phenomena in Enhanced Oil Recovery*. Plenum Publishing Corporation.

Mulligan, C.N., Yong, R.N. and Gibbs, B.F., 2001. Surfactant-enhanced remediation of contaminated soil: a review. *Engineering Geology, 60(1), pp.371-380.*

National Research Council (NRC) (U.S.). 1994. Alternatives for Ground Water Cleanup. Washington, DC, National Research Council (NRC).

National Research Council (NRC) (U.S.). 1997. Innovation in Groundwater and Soil Cleanup, Washington, DC: National Academy Press.

National Research Council (NRC) (U.S.). 1999. Groundwater and Soil Cleanup: Improving Management of Persistent Contaminants. Washington, DC: National Academy of Sciences.

National Research Council (NRC) (U.S.). 2005. Contaminants in the Subsurface: Source Zone Assessment and Remediation. Washington, DC: National Academy of Sciences.

National Research Council (NRC). 2013. Alternatives for Managing the Nation's Complex Contaminated Groundwater Sites. Washington D.C.

Pennell, K.D., Jin, M., Abriola, L.M., Pope, G.A., 1994. Surfactant enhanced remediation of soil columns contaminated by residual tetrachloroethylene. *J. Contam. Hydrol. 16, 35–53.*

Pennell, K.D., Pope, G.A., Abriola, L.M., 1996. Influence of viscous and buoyancy forces on the mobilization of residual tetrachloroethylene during surfactant flushing. *Environ. Sci. Technol. 30 (4), 1328–1335*.

Schnaar, G., Brusseau, M.L., 2005. Pore-scale characterization of organic immiscible-liquid morphology in natural porous media using synchrotron X-ray microtomography. *Environ. Sci. Technol. 39 (21), 8403–8410.*

Schnaar, G., Brusseau, M.L., 2006a. Characterizing pore-scale dissolution of organic immiscible liquid in natural porous media using synchrotron Xray microtomography. *Environ. Sci. Technol. 40 (21), 6622–6629.*

Schnaar, G., Brusseau,M.L., 2006b. Characterizing pore scale configuration of organic liquid in multiphase systems with synchrotron X-ray microtomography. *Vadose Zone J. 5 (2), 641–648*.

Schramm, L.L., 2000. Surfactants: Fundamentals and applications in the petroleum industry. Cambridge University Press, N.Y., USA.

Sheng, J. J. (2015). Investigation of alkaline–crude oil reaction. *Petroleum, 1(1), 31-39.*

Sutton, S.R., Bertsch, P.M., Newville,M., Rivers, M.L., Lanzirotti, A., Eng, P., 2002. Micro fluorescence and microtomography analyses of heterogeneous earth and environmental materials. Applications of synchrotron radiation in low temperature geochemistry and environmental sciences. In: Fenter, P.A., et al. (Ed.), *Book Series: Reviews in Mineralogy an Geochemistry, The Mineralogical Society of America., vol. 49, pp. 429–483*.

Thomas, S., Ali, S.M.F., 1989. Flow of emulsions in porous media and potential for enhanced oil recovery. J. Pet. Sci. Eng. 3 (1-2), 121-136, doi: 10.1016/0920-4105(89)90038-7.

U.S. Environmental Protection Agency (U.S. EPA). 2000. Innovative Remediation Technologies: Field-scale Demonstration Projects in North America, 2nd Edition. Year 200 Report. EPA 542-B-00-004, June 2000, www.epa.gov.

U.S. Environmental Protection Agency (U.S. EPA). 2003. The DNAPL remediation challenge: Is there a case for source depletion? Expert panel on DNAPL remediation, Kavanaugh, MC. And PSC Rao, Co-chairs, EPA/600/R- 03/143. Office of Research and Development, Washington, DC.

U.S. Environmental Protection Agency (U.S. EPA). 2007. Research provides remediation tools to manage dense non-aqueous phase liquids.

Walstra, P., 1993. Principles of emulsion formation. Chem. Eng. Sci. 48 (2), 333-349, doi: 10.1016/0009-2509(93)80021-H.

Wildenschild, D., Hopmans, J.W., Vaz, C.M.P., Rivers, M.L., Rikard, D., Christensen, B.S.B., 2002. Using X-ray computed tomography in hydrology: systems, resolutions, and limitations. *J. Hydrol. 267 (3–4), 285–297.*

Wilson, J.L., Conrad, S.H., 1984. Is physical displacement of residual hydrocarbons a realistic possibility in aquifer restoration? In: Proceedings of the national water well association. API conference on petroleum hydrocarbons and organic chemicals in ground water. National Water Well Assoc., Worthington, Ohio, pp. 274-298.

Wu, Y., Shuler, P., Blanco, M., Tang, Y., Goddard, W.A., 2005. A study of branched alcohol propoxylate sulfate surfactants for improved oil recovery. SPE Annual Technical Conference and Exhibition, October 9-12, 2005, Dallas, TX, doi: 10.2118/95404-MS

Zhao, L., Li, A., Wu, X., Xie, H., Wang, J., Wang, Q., 2013, Oil-water Interfacial Tension Effects on Relative Permeability Curves in Low-permeability Reservoirs, Journal of Petroleum Science Research, v. 2, I. 2, p. 78-81.

TABLES AND FIGURES

Tables

Table 1. List of experimental conditions for each enhanced-flushing experiment.

Experiment # (Column)	Oil Gravity [APIº]	Porous Medium	Flushing fluid
Exp-1 (Col 1)	29.6	40/50 Accusand	Alkaline (NaOH, pH 12)
Exp-2 (Col 2)	29.6	40/50 Accusand	Surfactant (0.1 vol.%)
Exp-3 (Col 3)	29.6	40/50 Accusand	Sequential Alkaline-Surfactant
Exp-4 (Col 4)	29.6	25%-75% Karst Sand-Accusand Mix	Surfactant (0.1 vol.%)
Exp-5 (Col 5)	29.6	50%-50% Karst Sand-Accusand Mix	Surfactant (0.1 vol.%)

Table 2. List of parameters for NAPL residual saturation, alkaline and surfactant flushing.

Properties	Residual Saturation	Surfactant Flushing	Alkaline Flushing		
	CsCl solution	0.1 vol.% Surfactant solution	pH 10 NaOH solution	pH 12 NaOH solution	pH 13.5 NaOH solution
Dynamic Viscosity (μ) [dyn*s/cm2]	0.0084	0.0221	0.0109	0.0116	0.0134
Solution Density (ρ) [g/cm3]	1.03	1.04	1.03	1.03	1.03
Linear Pore Velocity (v_p) [cm/hr]	20	20	20	20	20
Darcy Velocity (cm/min)	0.1	0.10	0.10	0.10	0.10
40/50 sand porosity [-]	0.33	0.33	0.33	0.33	0.33
40/50 Accusand Permeability (cm^2)	9.00E-07	9.00E-07	9.00E-07	9.00E-07	9.00E-07
Carbonate Karst Sand Permeability (cm^2)	8.00E-09	8.00E-09	8.00E-09	8.00E-09	8.00E-09

Table 3. Oil (NAPL) recovery pre- and post- flushing events.

Experiment (flush type)	PV Flushed	Oil Volume [cm^3]	#Oil Volume Recovered [cm^3]	Recovery [%]
Exp-1 (alkaline)	0	0.008332	-	-
Exp-1 (alkaline)	2	0.008070	0.000261	3.14
Exp-1 (alkaline)	5	0.007773	(0.000297) 0.000559	(3.68) 6.71
Exp-2 (surfactant)	0	0.009479	-	-
Exp-2 (surfactant)	2	0.009010	0.000469	4.95
Exp-2 (surfactant)	5	0.008746	(0.000264) 0.000733	(2.93) 7.74
Exp-3 (alkaline-surfactant)	0	0.009949	-	-
Exp-3 (alkaline-surfactant)	2/2	0.007849	0.0021	21.11
Exp-3 (alkaline-surfactant)	5/5	0.006564	(0.00126) 0.003385	(16.37) 34.02
Exp-4 (surfactant, 25% karst)	0	0.009283	-	-
Exp-4 (surfactant, 25% karst)	2	0.008433	0.00085	9.16%
Exp-4 (surfactant, 25% karst)	5	0.007969	(0.000473) 0.001314	(5.61) 14.16
Exp-5 (surfactant, 50% karst)	0	0.021991	-	-
Exp-5 (surfactant, 50% karst)	2	0.021089	0.000903	4.10
Exp-5 (surfactant, 50% karst)	5	0.0173	(0.00379) 0.004692	(17.97) 21.33

#: values in parentheses indicate removal or recovery between the 5 PV and 2 PV of flushing; values otherwise indicated total removal or recovery relative to initial volume present.

Table 4. List of measured contact angle in varying pH solutions in contact with varying media.

Oil Gravity [APIº]	pH $\{H^+\}$	Media	Contact Angle θ [deg.˚]	Oil Gravity [APIº]	pH $\{H^+\}$	Media	Contact Angle θ [deg.˚]*
41.4	4	Glass	77.9	41.4	4	Limestone	94 (+21.3%)
41.4	7	Glass	95.5	41.4	7	Limestone	118 (+23.6)
41.4	10	Glass	17.5	41.4	10	Limestone	79.5 (+354.3%)
41.4	12	Glass	13.9	41.4	12	Limestone	50.5 (+263.3%)
41.4	13.5	Glass	11.1	41.4	13.5	Limestone	49.4 (+345.0%)
29.6	4	Glass	78.2	29.6	4	Limestone	93.7 (+19.8%)
29.6	7	Glass	108.3	29.6	7	Limestone	117.7 (+8.7%)
29.6	10	Glass	75.6	29.6	10	Limestone	108.1 (+43.0%)
29.6	12	Glass	47.1	29.6	12	Limestone	99 (+110.2%)
29.6	13.5	Glass	13.3	29.6	13.5	Limestone	72.1 (+44.1%)
14	4	Glass	102.7	14	4	Limestone	92.4 (-11.2%)
14	7	Glass	133.4	14	7	Limestone	93.3 (-30.1%)
14	10	Glass	60.8	14	10	Limestone	96.6 (+58.9%)
14	12	Glass	55.1	14	12	Limestone	129.1 (+134.3%)
14	13.5	Glass	48.8	14	13.5	Limestone	119.5 (+144.9%)

* - values in parenthesis are calculated percent increase of the contact angle of oil in contact with limestone vs contact angle of the oil in contact with glass.

Table 5. List of measured Interfacial tension between NAPL varying pH solutions and 3 different oil densities

pH $\{H^+\}$	Oil Gravity [APIº]	IFT (dyn/s)		pH $\{H^+\}$	Oil Gravity [APIº]	IFT (dyn/s)		pH $\{H^+\}$	Oil Gravity [APIº]	IFT (dyn/s)
4	41.4	18.03		4	29.6	17.35		4	14	15.15
7	41.4	22.61		7	29.6	20.9		7	14	36.36
10	41.4	8.28		10	29.6	9.43		10	14	27.96
12	41.4	5.62		12	29.6	7.29		12	14	25.8
13.5	41.4	2.82		13.5	29.6	6.98		13.5	14	11.52

Table 6.1 Calculations of capillary, bond, and trapping number for residual saturation, and surfactant flushing along with parameters used.

Properties	Residual Saturation			Surfactant Flushing		
Oil	Light	Medium	Heavy	Light	Medium	Heavy
Interfacial Tension [dyn/cm]	22.61	20.9	36.36	10.6	11.8	24.7
Oil Gravity [APIº]	41.4	29.6	14	41.4	29.6	14
Oil Density [g/cm^3]	0.81	0.87	0.97	0.81	0.87	0.97
Flushing Fluid Density [g/cm^3]	1.03	1.03	1.03	1.04	1.04	1.04
Δρ – Change in Density [g/cm^3]	0.22	0.16	0.06	0.23	0.17	0.07
Capillary Number- N_C	6.31E-07	6.82E-07	3.92E-07	3.54E-06 (+461%)	3.18E-06 (+366%)	1.52E-06 (+288%)
Bond Number - N_B	8.58E-06	6.75E-06	1.46E-06	1.91E-05 (+123%)	1.27E-05 (+88%)	2.5E-06 (+71%)
Trapping Number - N_T	9.21E-06	7.43E-06	1.85E-06	2.27E-05 (+146%)	1.59E-05 (+114%)	4.02E-06 (+117%)

Table 6.2 Calculations of capillary, bond, and trapping number for varying pH alkaline solutions along with parameters used.

Properties	Alkaline Flushing								
	pH 10 solution			pH 12 Solution			pH 13.5 Solution		
Oil	Light	Medium	Heavy	Light	Medium	Heavy	Light	Medium	Heavy
Interfacial Tension [dyn/cm]	8.28	9.43	27.96	5.62	7.29	25.8	2.82	6.98	11.52
Oil Gravity [APIº]	41.4	29.6	14	41.4	29.6	14	41.4	29.6	14
Oil Density $[g/cm^3]$	0.81	0.87	0.97	0.81	0.87	0.97	0.81	0.87	0.97
Flushing Fluid Density $[g/cm^3]$	1.03	1.03	1.03	1.03	1.03	1.03	1.03	1.03	1.03
Δρ – Change in Density $[g/cm^3]$	0.22	0.16	0.06	0.22	0.16	0.06	0.22	0.16	0.06
Capillary Number- N_C	2.24E-06 +255 %	1.97E-06 +189%	6.64E-07 +69%	3.5E-06 +455%	2.7E-06 +295%	7.63E-07 +95	8.07E-06 +1179%	3.26E-06 +378%	1.98E-06 +404%
Bond Number - N_B	2.34E-05 +172 %	1.5E-05 +122%	1.89E-06 +29%	3.45E-05 +302%	1.94E-05 +187%	2.05E-06 +41%	6.88E-05 +702%	2.02E-05 +200%	4.59E-06 +214%
Trapping Number - N_T	2.57E-05 +179 %	1.69E-05 +127%	2.56E-06 +38%	3.8E-05 +313%	2.21E-05 +197%	2.81E-06 +51%	7.69E-05 +735%	2.35E-05 +216%	6.57E-06 +255%

Table 7. Calculated change in capillary pressure for different density crude oil in contact with varying pH alkaline solutions

Oil	pH $\{H^+\}$	Angle θ[deg]	IFT [dyn/cm]	ΔP [m/L^2], N/m^2
Light Oil	7	95.5	22.61	-48.16
	10	17.5	8.28	175.48
	12	13.9	5.62	121.23
	13.5	11.1	2.82	61.49
Medium Oil	7	108.3	20.9	-145.83
	10	75.6	9.43	52.11
	12	47.1	7.29	110.28
	13.5	13.3	6.98	150.95
Heavy Oil	7	133.4	36.36	-555.17
	10	60.8	27.96	303.12
	12	55.1	25.8	328.03
	13.5	48.8	11.52	168.62

Figures

Figure 1 - Ami Adini & Associates, Inc. Environmental Consultants, 2008 – Schematic of Light NAPL source distributed through the subsurface to groundwater and residual saturation of trapped NAPL.

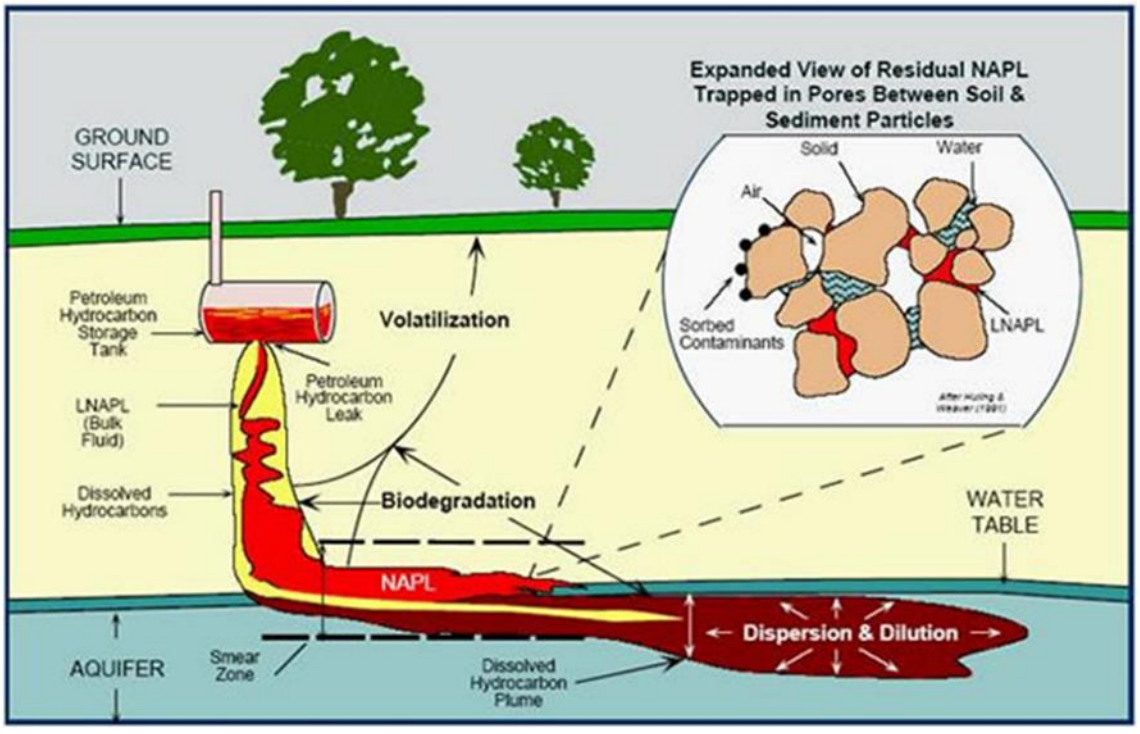

Figure 2.1-2.5 Representative 3D images of crude oil blobs for each column. The first image is residual saturation, the second is after 2 PV flush, and the third after 5 PV flush

Figure 2.1 Exp-1-Column 1 (alkaline flush)

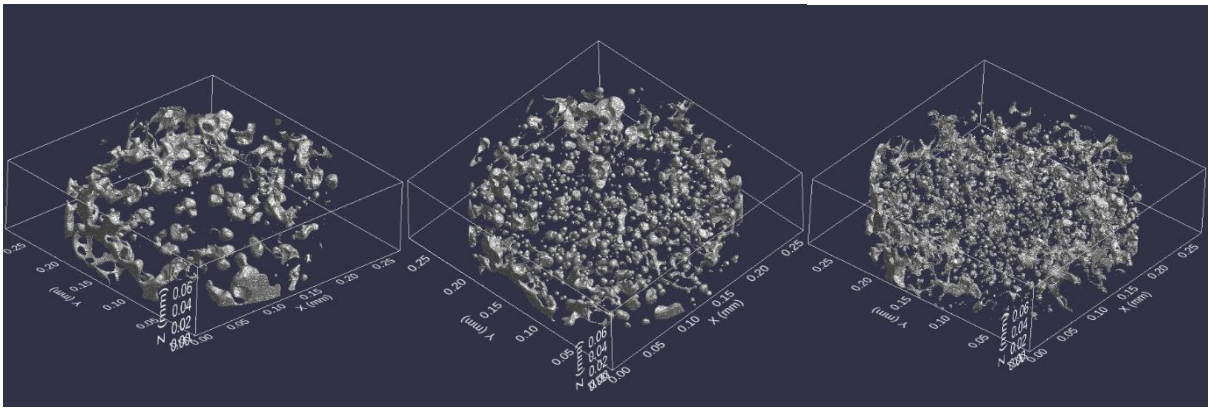

Figure 2.2 Exp-2-Column 2 (surfactant flush)

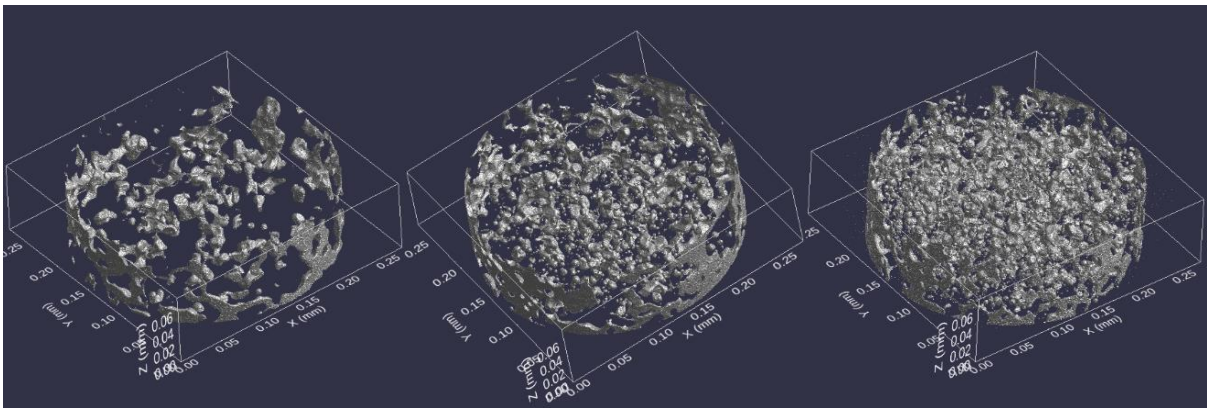

Figure 2.3 Exp-3-Column 3 (sequential flush)

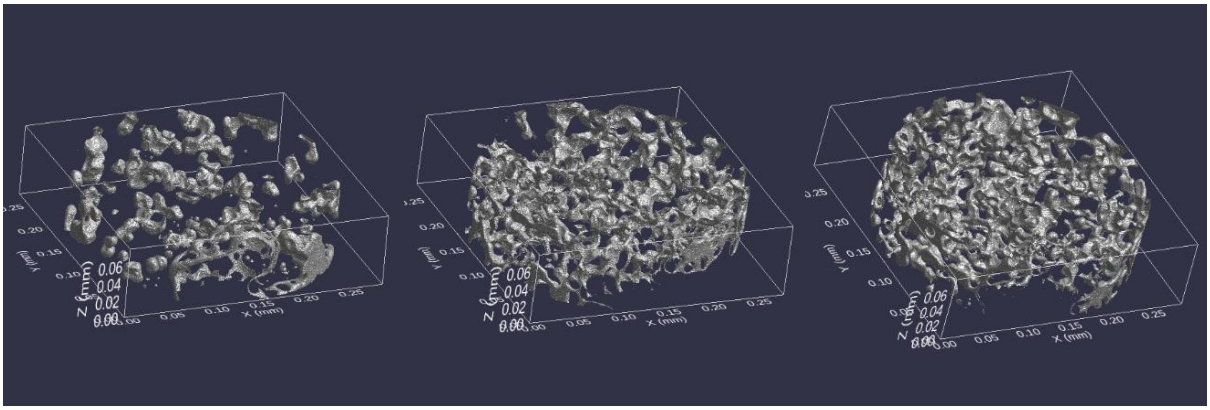

Figure 2.4 Exp-4-Column 4 (surfactant flush) 75% Accusand, 25% Carbonate Karst Sand

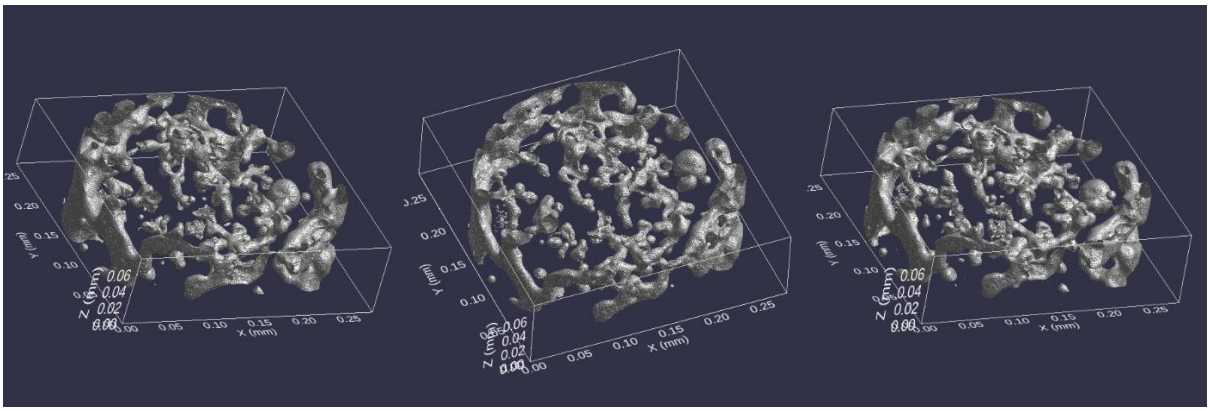

Figure 2.5 Exp-5-Column 5 (surfactant flush) 50% Accusand, 50% Carbonate Karst Sand

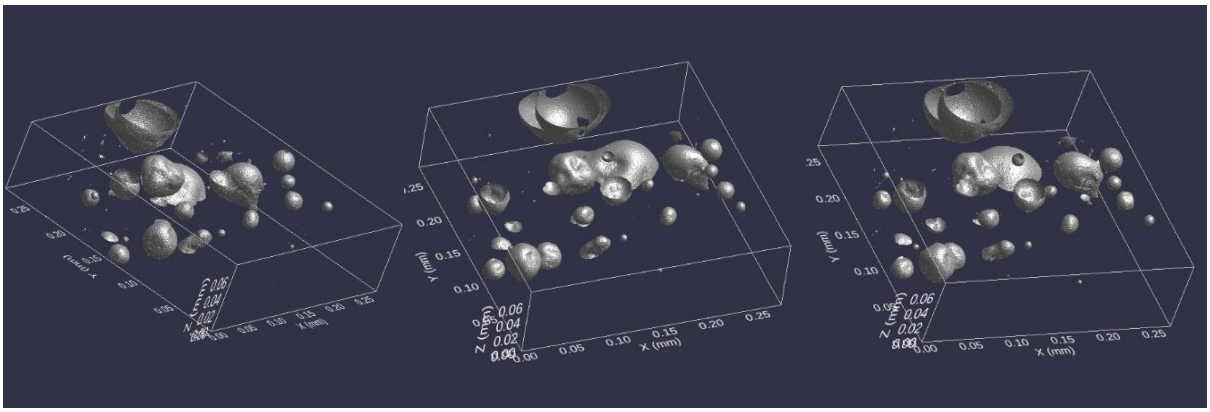

Figure 3.1-3.5 – Comparison of Blob Volume to Normalized Surface Area. Each chart compares blobs to perfect spherical shape. Above the perfect sphere line is greater surface area. The figures also compare residual blobs to those after 2 PV flush. Figure 2.1 is for Exp-1, Alkaline Flush in homogeneous sand. Figure 2.2 is for Exp-2, Surfactant Flush in homogeneous sand. Figure 2.3 is for Exp-3, Sequential Flush in homogeneous sand. Figure 2.4 is for Exp-4, Surfactant in slight heterogeneous sand (25% karst sand, 75% 40/50 Accusand). Figure 2.5 is for Exp-5, Surfactant flush with moderate heterogeneous sand (50% karst sand, 50% 40/50 Accusand).

Figure 3.1

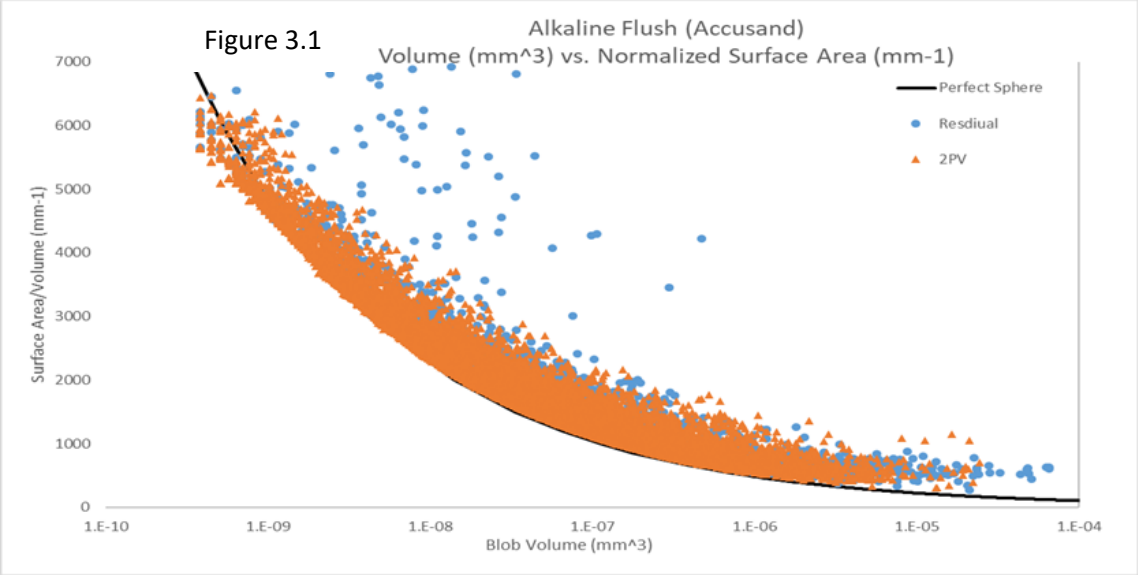

Figure 3.2

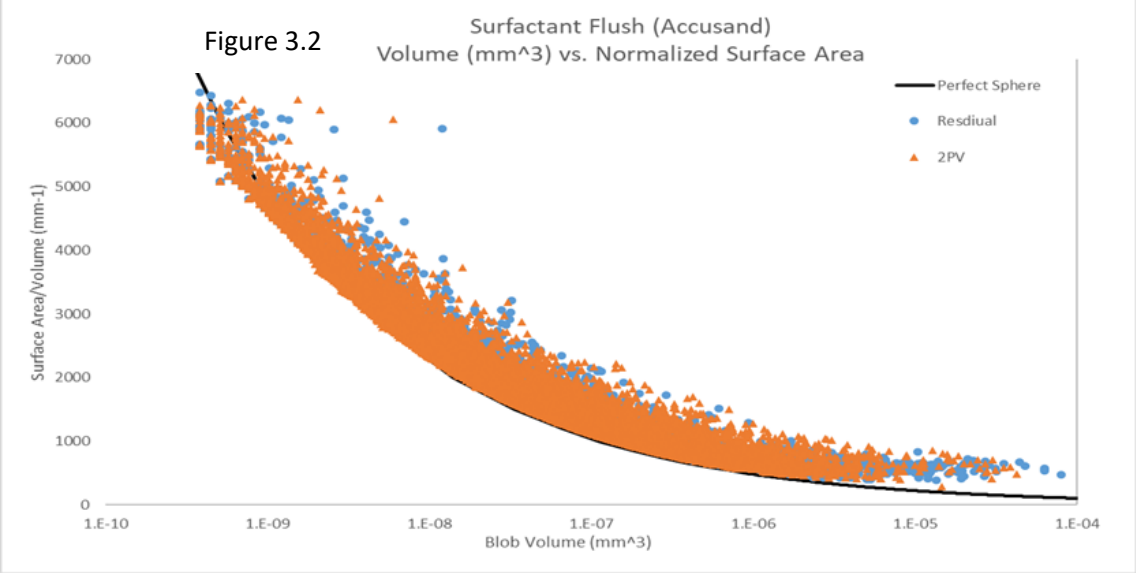

Figure 3.3

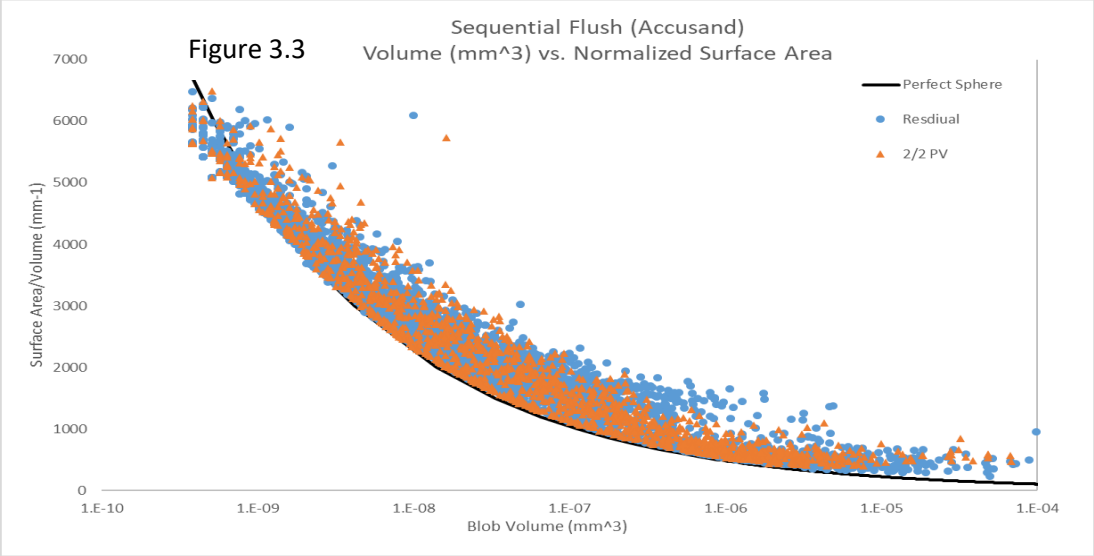

Figure 3.4

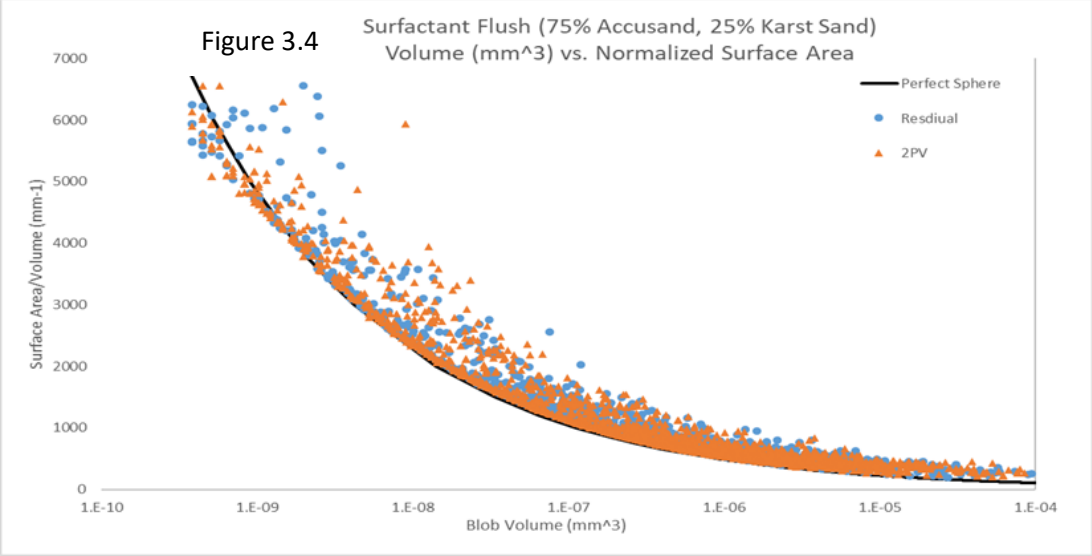

Figure 3.5

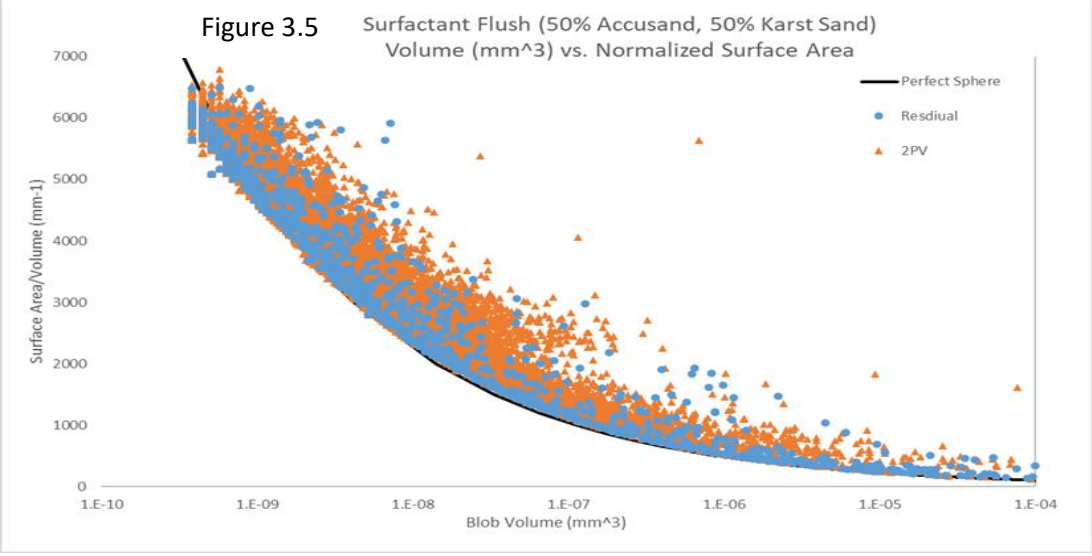

Figure 4.1-4.5 – Comparison of Blob Volume to Normalized Surface Area. Each chart compares blobs to perfect spherical shape. Above the perfect sphere line is greater surface area. The figures also compare residual blobs to those after 5 PV flush. Figure 3.1 is for Exp-1, Alkaline Flush in homogeneous sand. Figure 3.2 is for Exp-2, Surfactant Flush in homogeneous sand. Figure 3.3 is for Exp-3, Sequential Flush in homogeneous sand. Figure 3.4 is for Exp-4, Surfactant in slight heterogeneous sand (25% karst sand, 75% 40/50 Accusand). Figure 3.5 is for Exp-5, Surfactant flush with moderate heterogeneous sand (50% karst sand, 50% 40/50 Accusand).

Figure 4.1

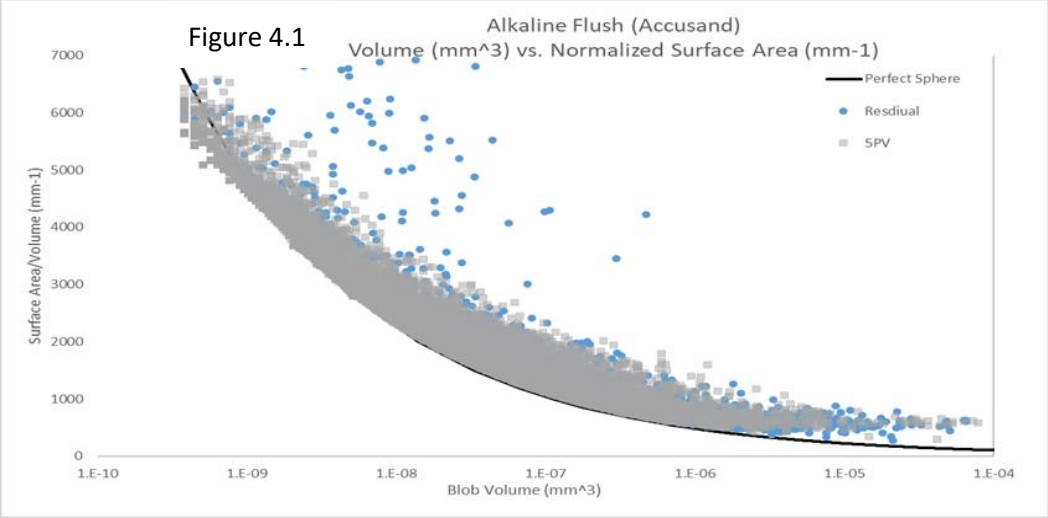

Figure 4.2

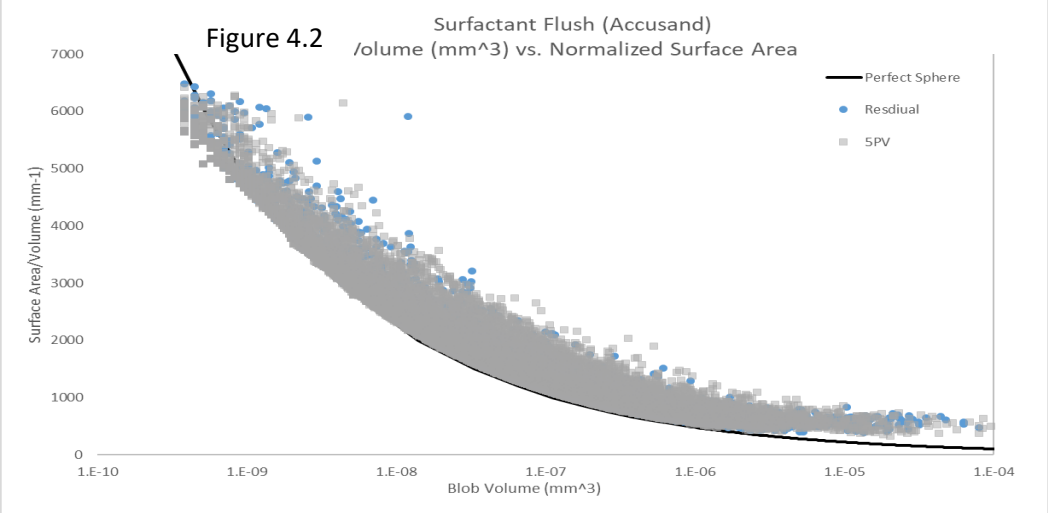

Figure 4.3

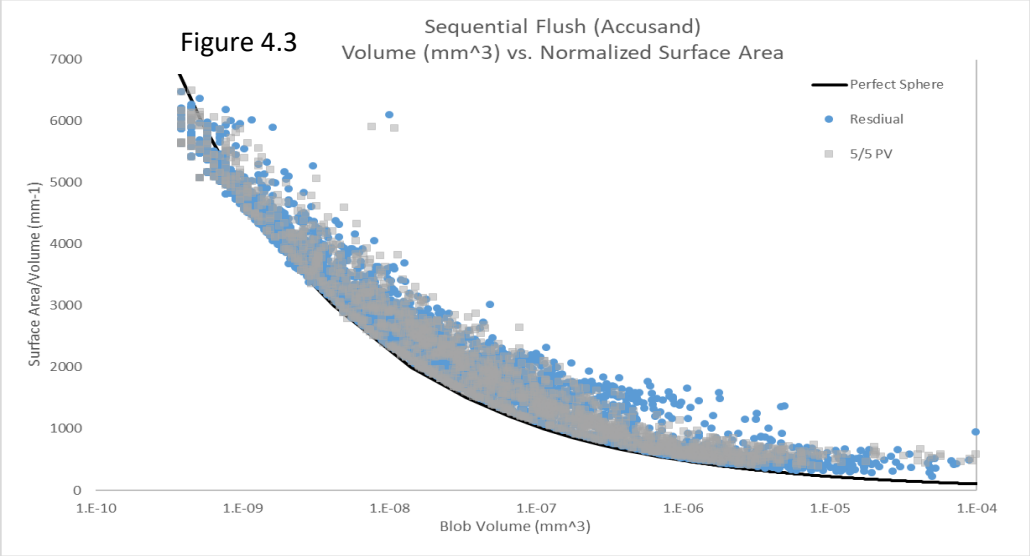

Figure 4.4

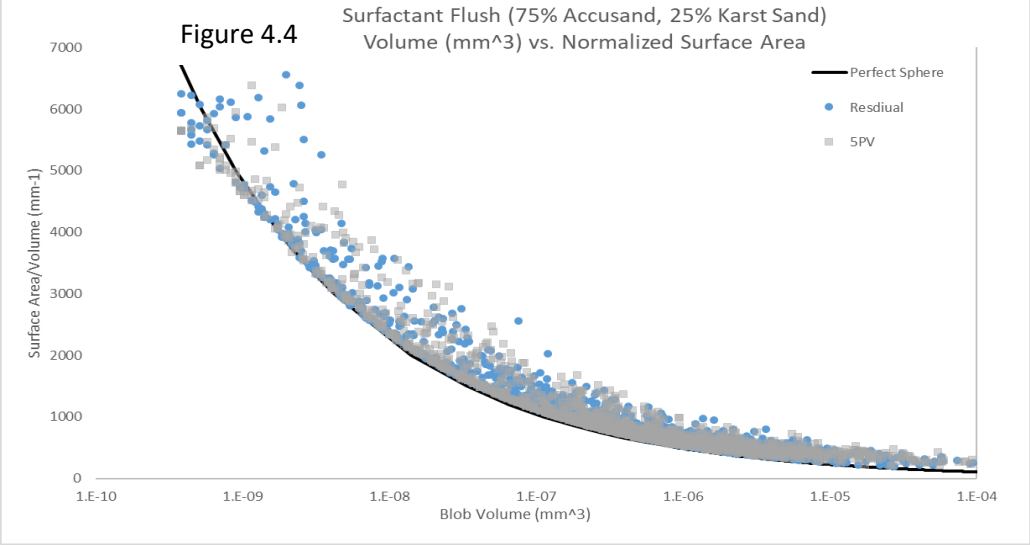

Figure 4.5

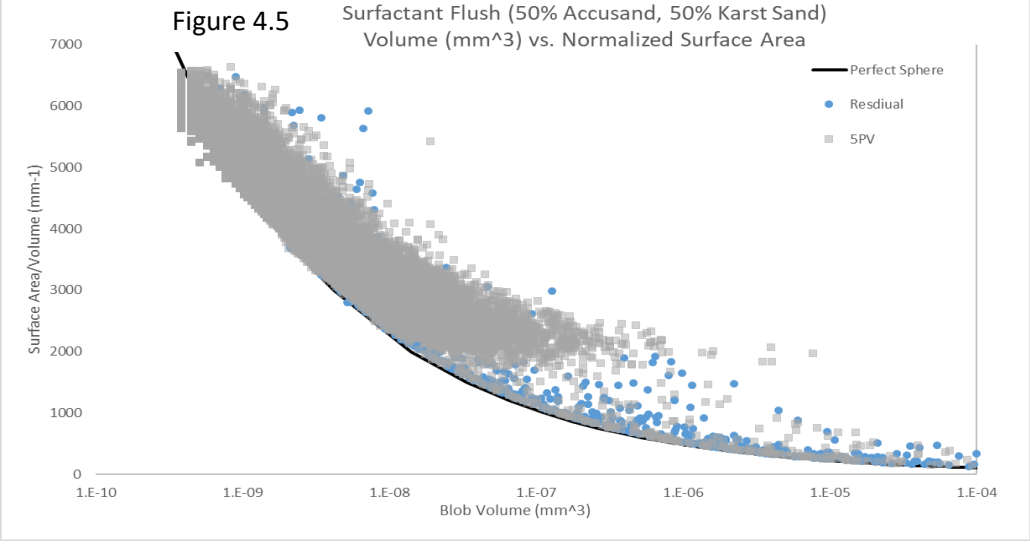

Figure 5.1-5.5 – Comparison of Blob Volume to the fraction of Blobs smaller. Shows the distribution of blobs, and the volume that has the greatest concentration of blobs. The figures are for each column and show residual, 2 PV and 5 PV distributions. Figure 4.1 is for Exp-1, Alkaline Flush in homogeneous sand. Figure 4.2 is for Exp-2, Surfactant Flush in homogeneous sand. Figure 4.3 is for Exp-3, Sequential Flush in homogeneous sand. Figure 4.4 is for Exp-4, Surfactant in slight heterogeneous sand (25% karst sand, 75% 40/50 Accusand). Figure 4.5 is for Exp-5, Surfactant flush with moderate heterogeneous sand (50% karst sand, 50% 40/50 Accusand).

Figure 5.1

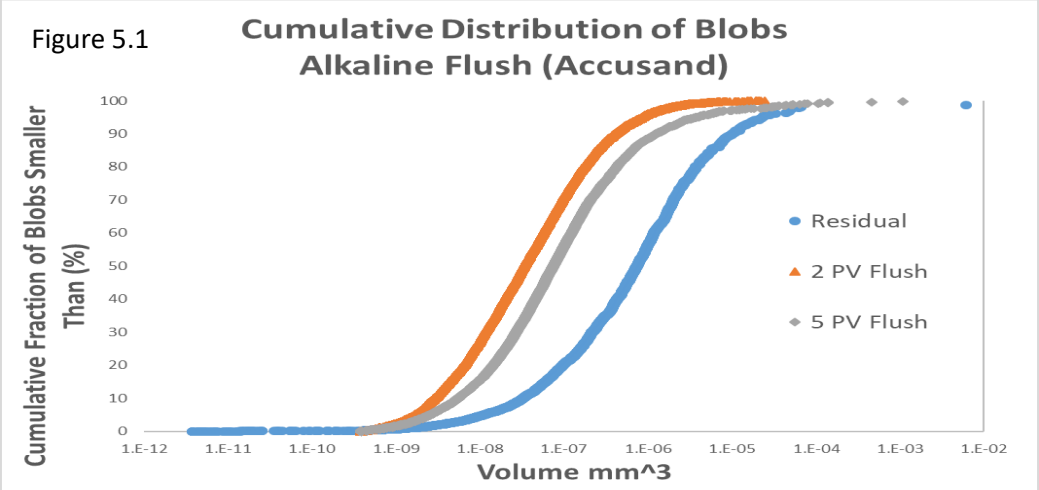

Figure 5.2

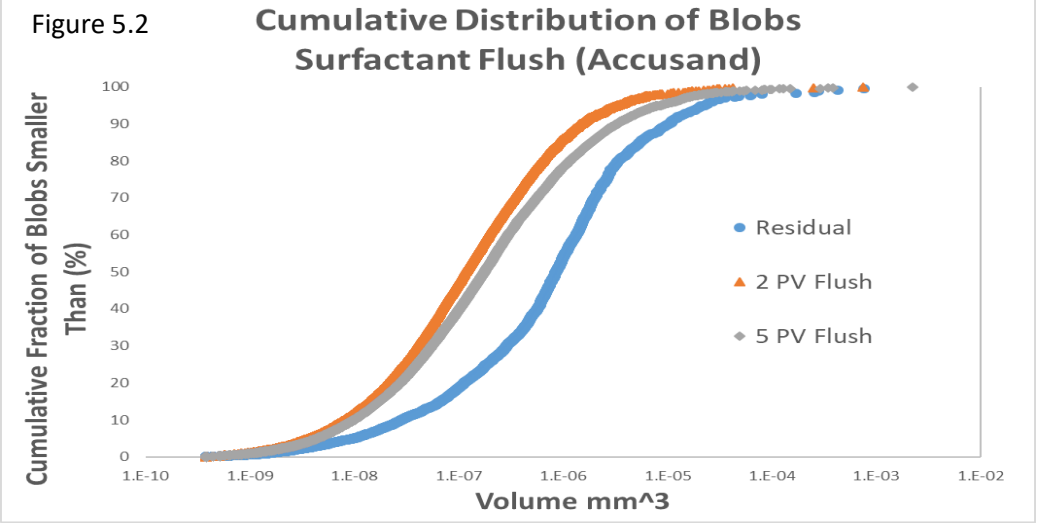

Figure 5.3

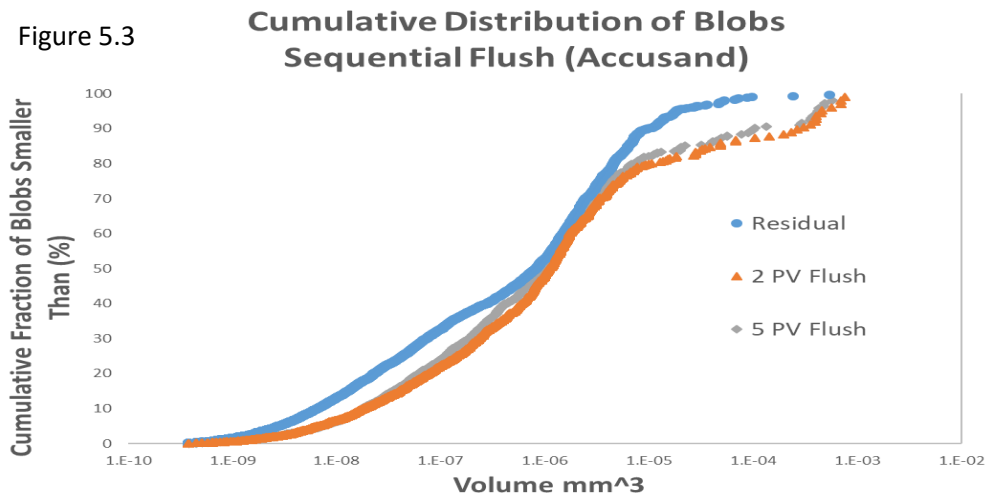

Figure 5.4

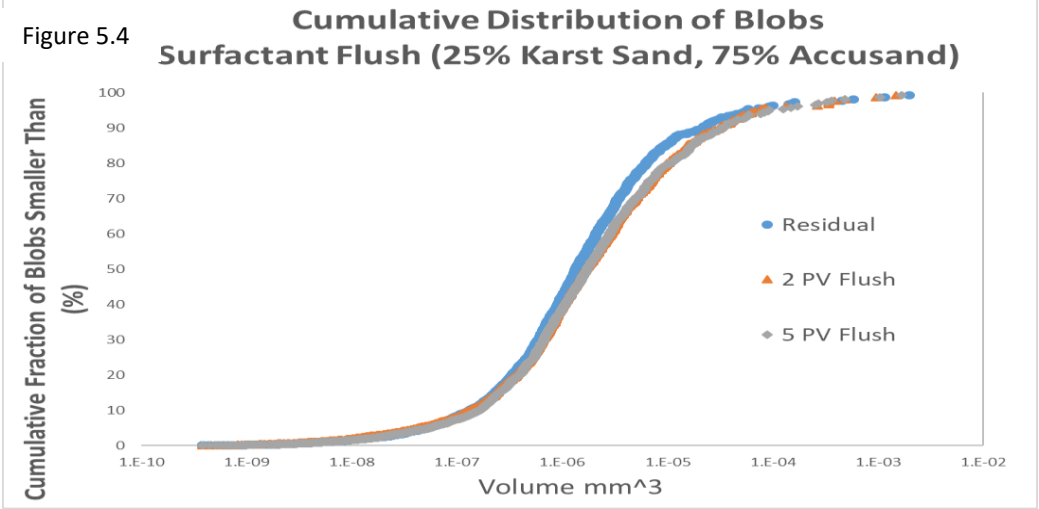

Figure 5.5

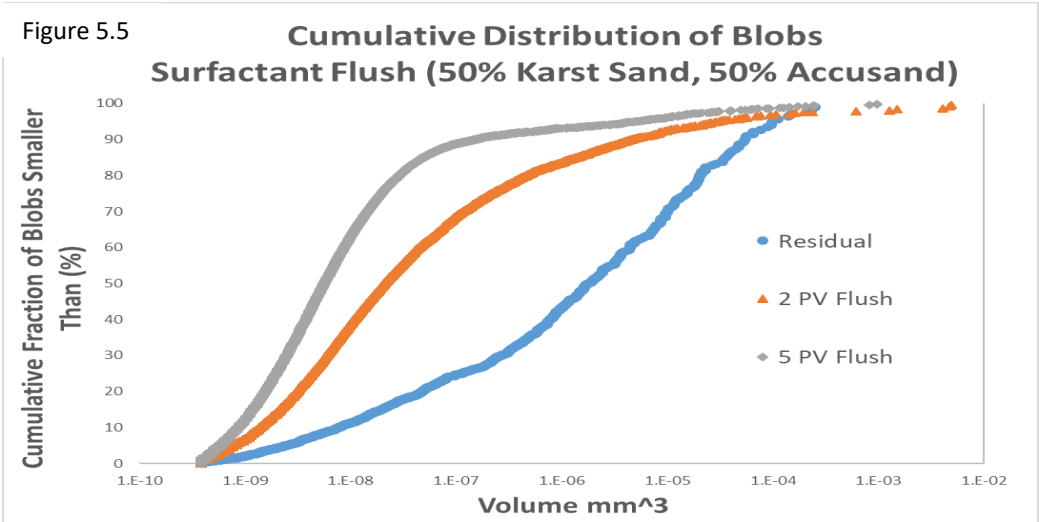

Figure 6 – Images taken by the KRUSS® DSA-1 drop shape analyzer. The images show the three different density oils in contact with a silica plate for varying pH NaOH solutions.

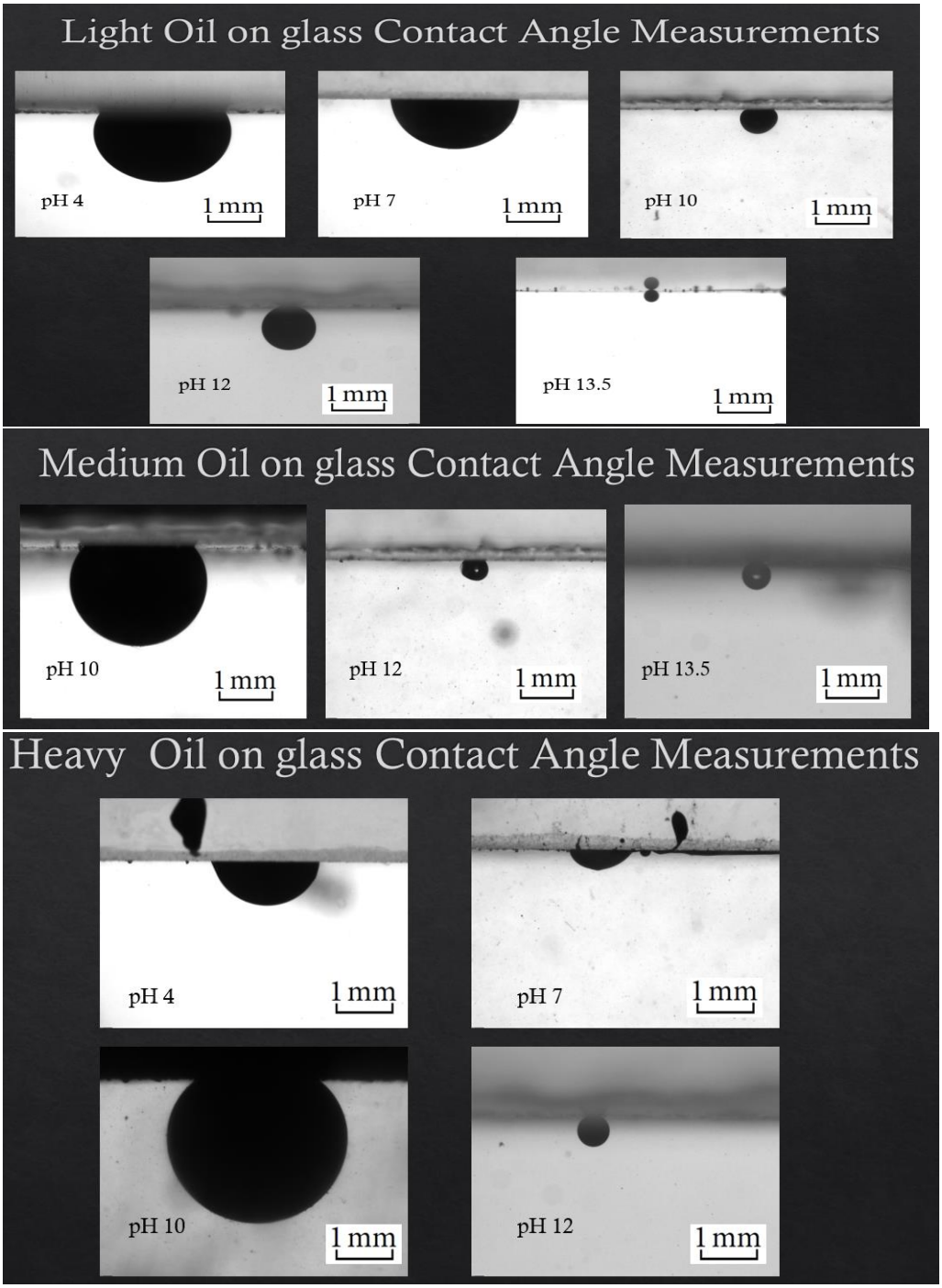

Figure 7 – Images taken by the KRUSS® DSA-1 drop shape analyzer. The images show the three different density oils in contact with a limestone plate for varying pH NaOH solutions.

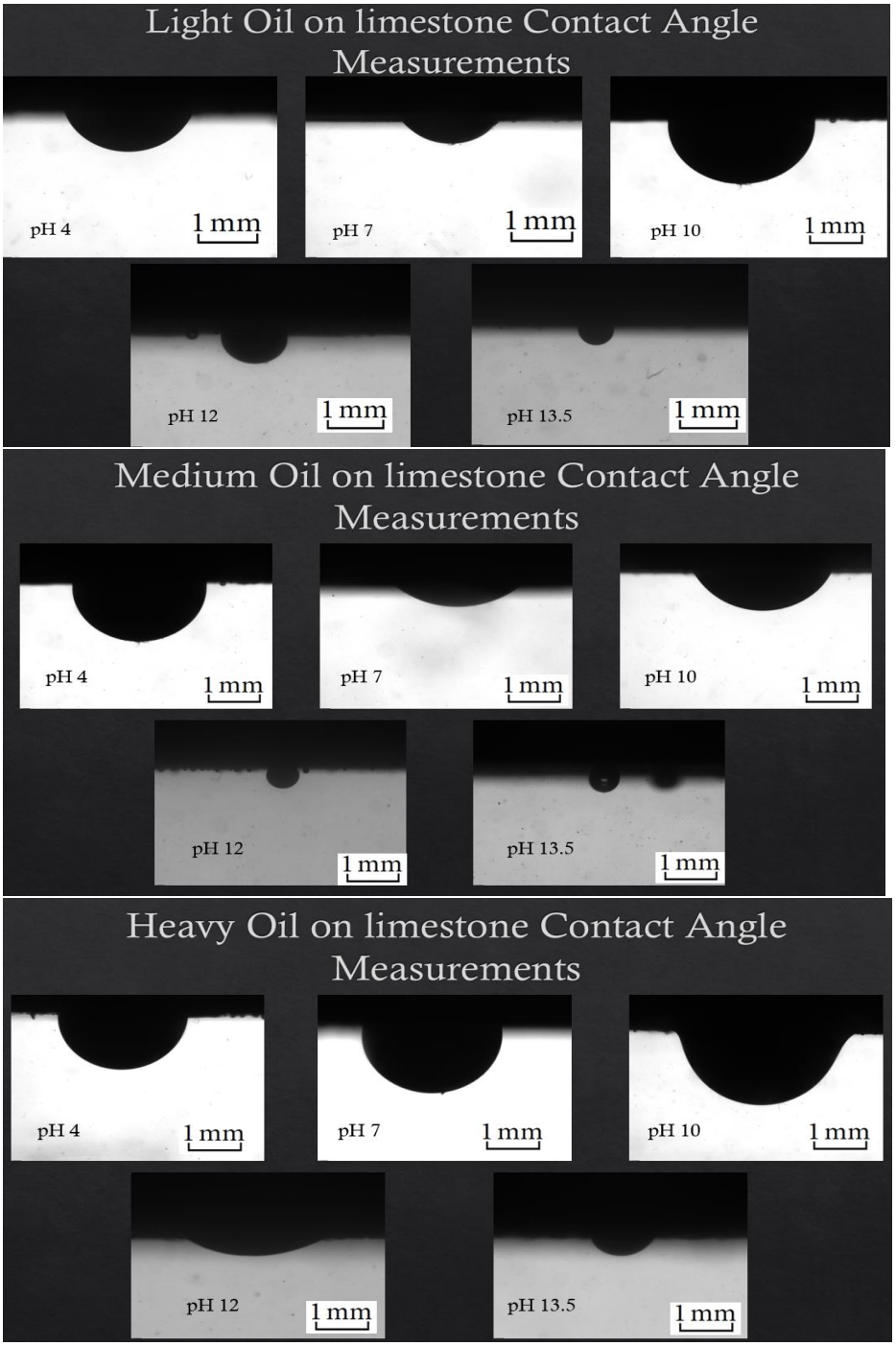

Figure 8.1-8.2 – A comparison of pH of the NaOH solution vs contact angle along the S-L-L junction. The top is for silica media, and the bottom calcium carbonate media.

Figure 8.1

Figure 8.2

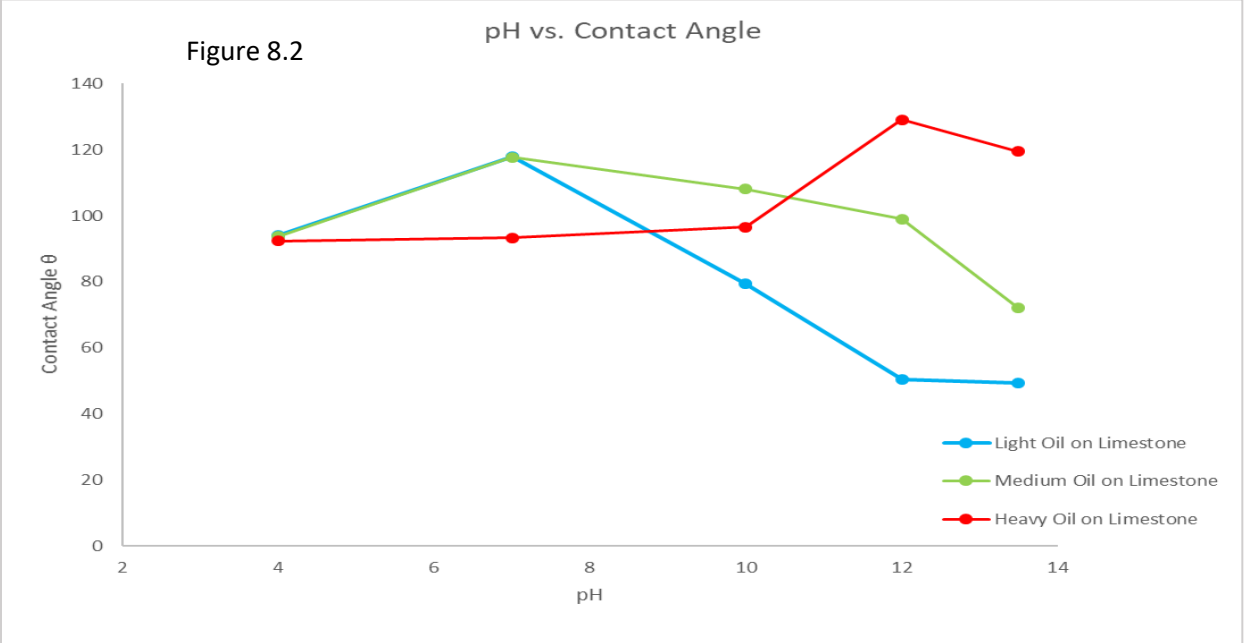

Figure 9 – A comparison of Interfacial Tension to different solutions with increasing pH values.

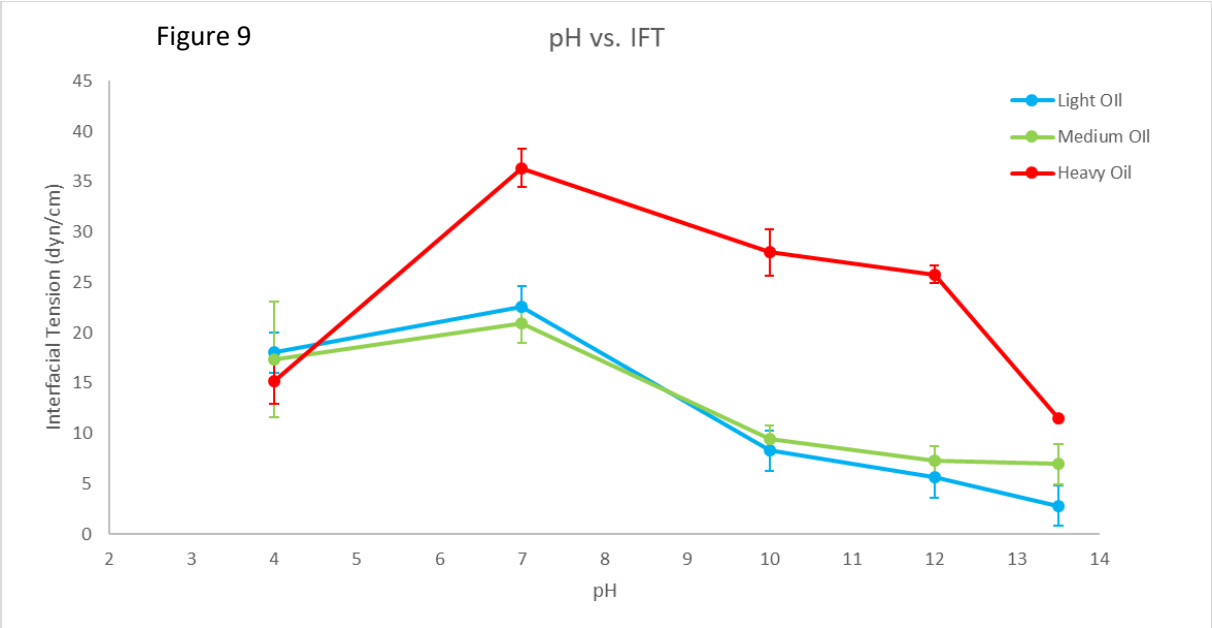

APPENDIX A – 3D IMAGES OF COLUMNS FROM SXM

Column 1 – Residual Saturation

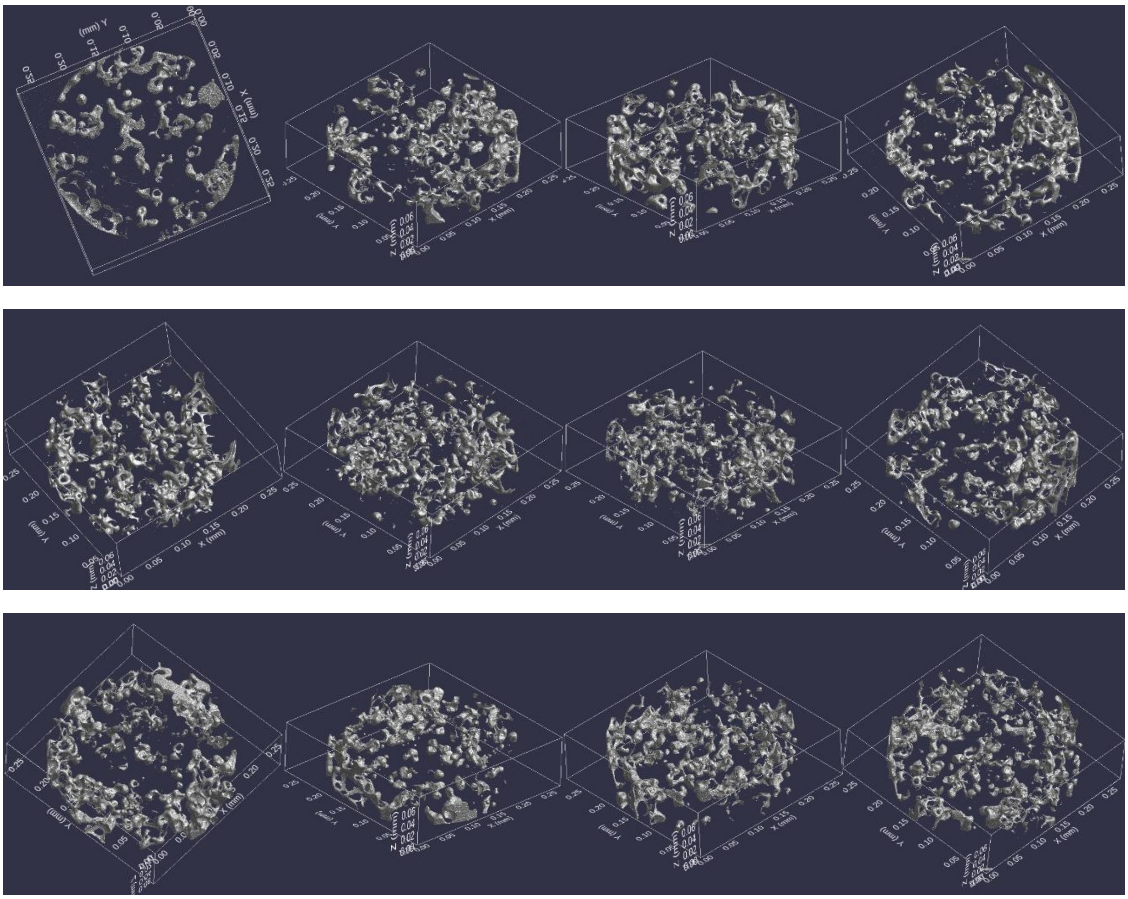

Column 1 – After 2 PV flush

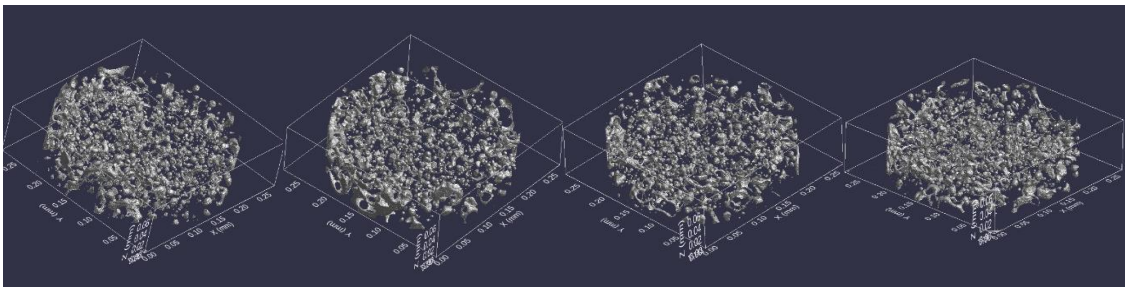

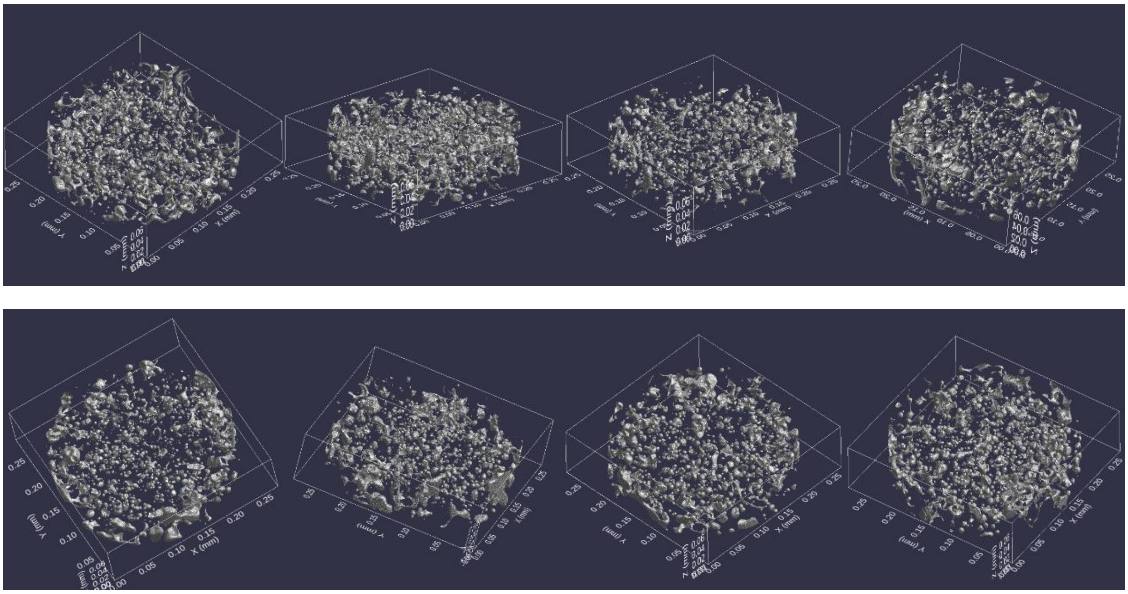

Column 1 – After 5 PV flush

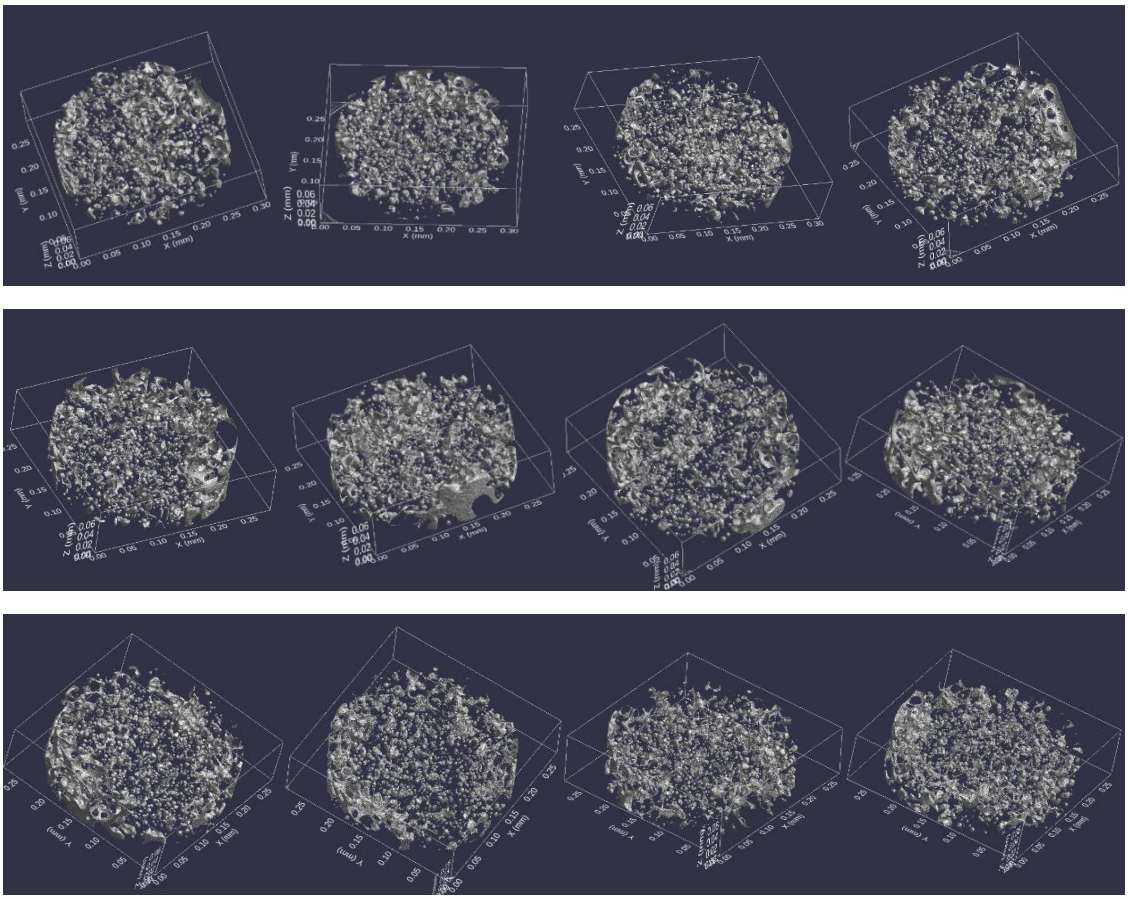

Column2 - Residual Saturation

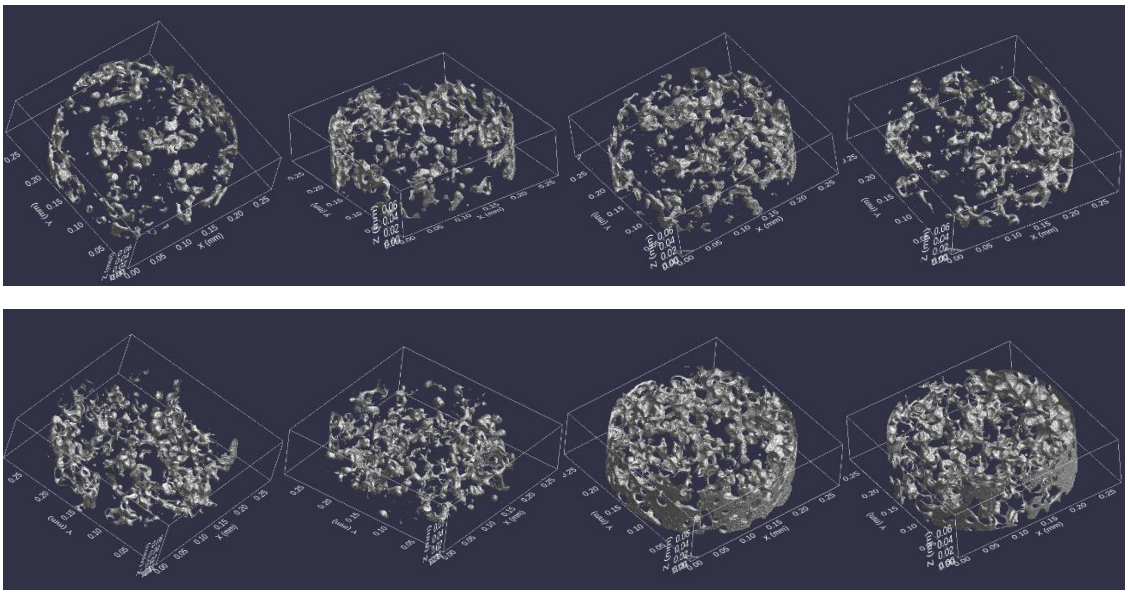

Column 2 – After 2 PV flush

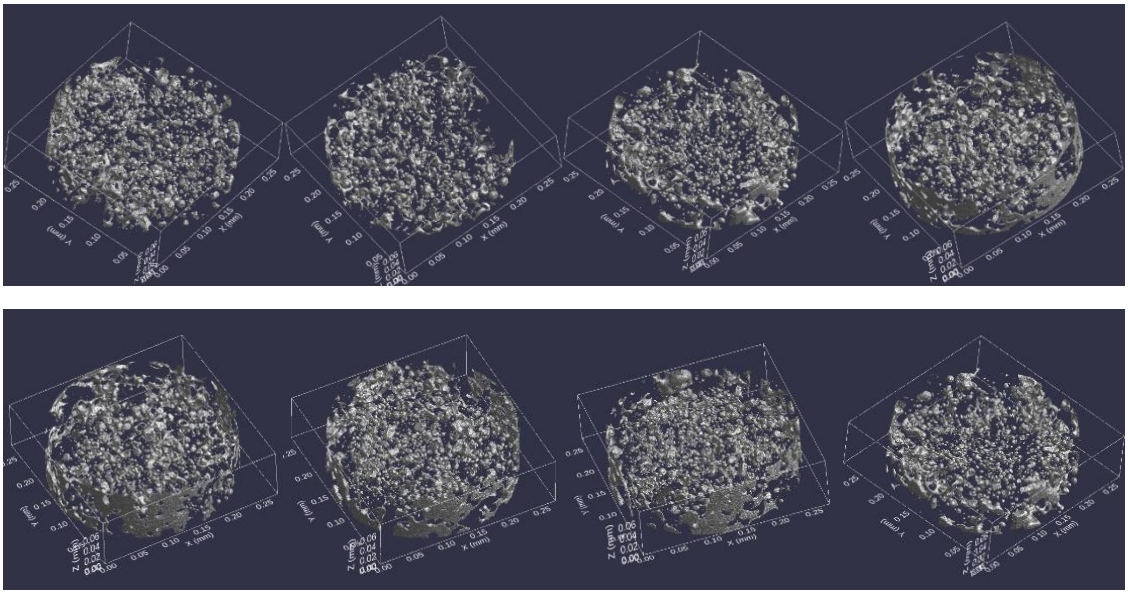

Column 2 – After 5 PV flush

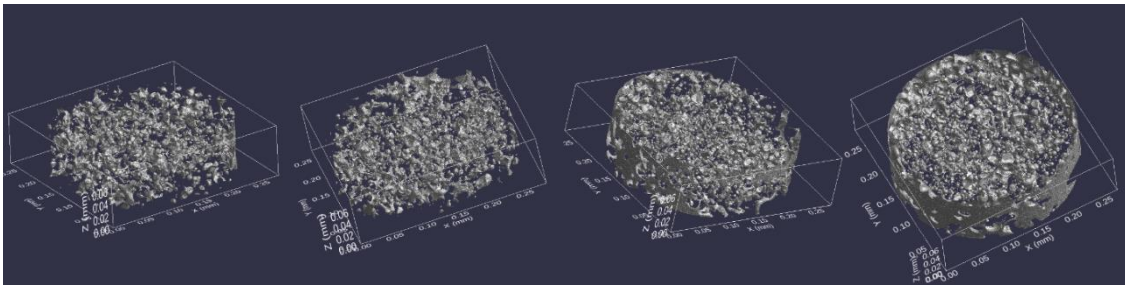

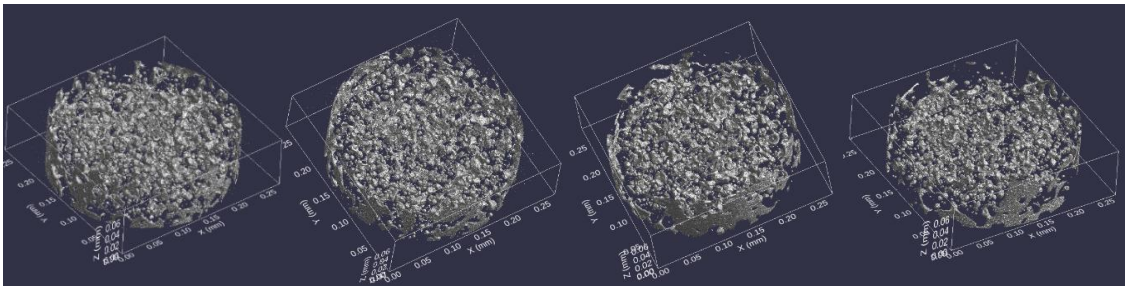

Column 3 – Residual Saturation

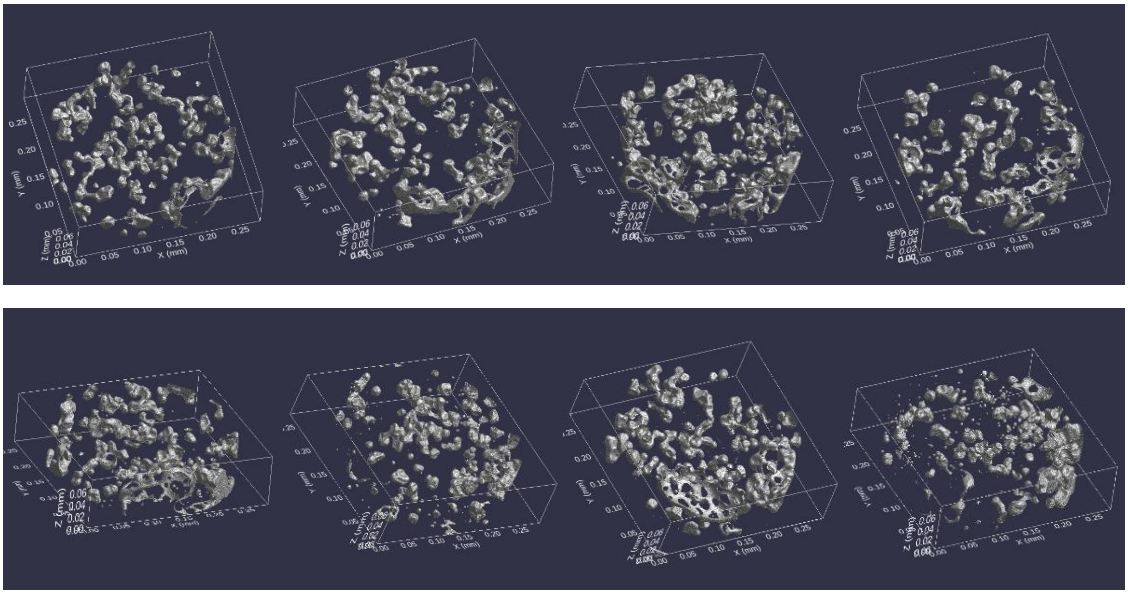

Column 3 – After 2/2 PV Flush

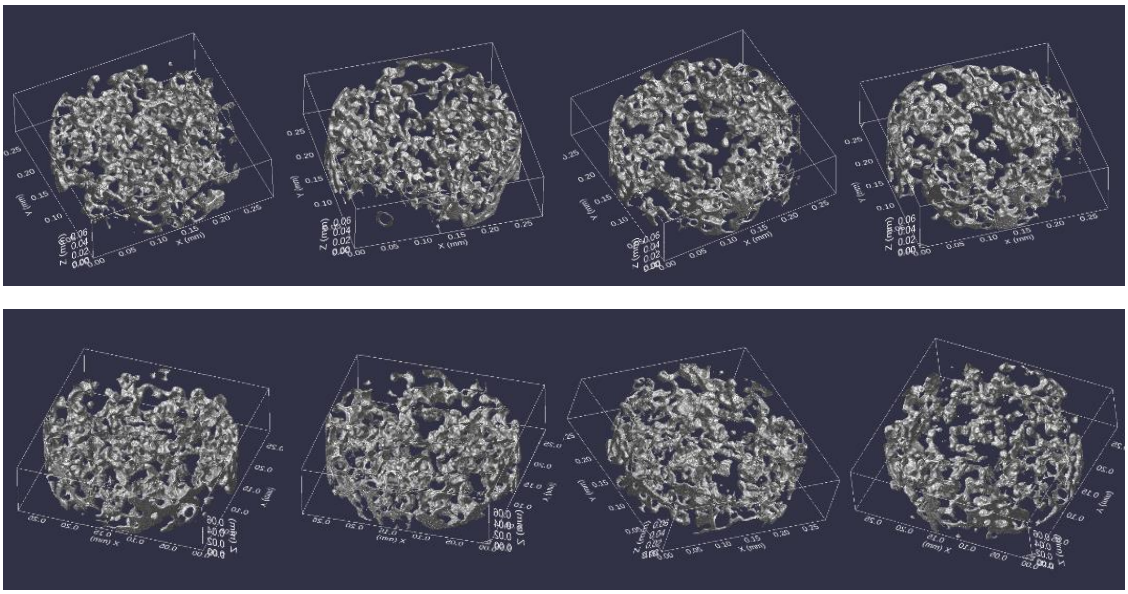

Column 3 – After 5/5 PV flush

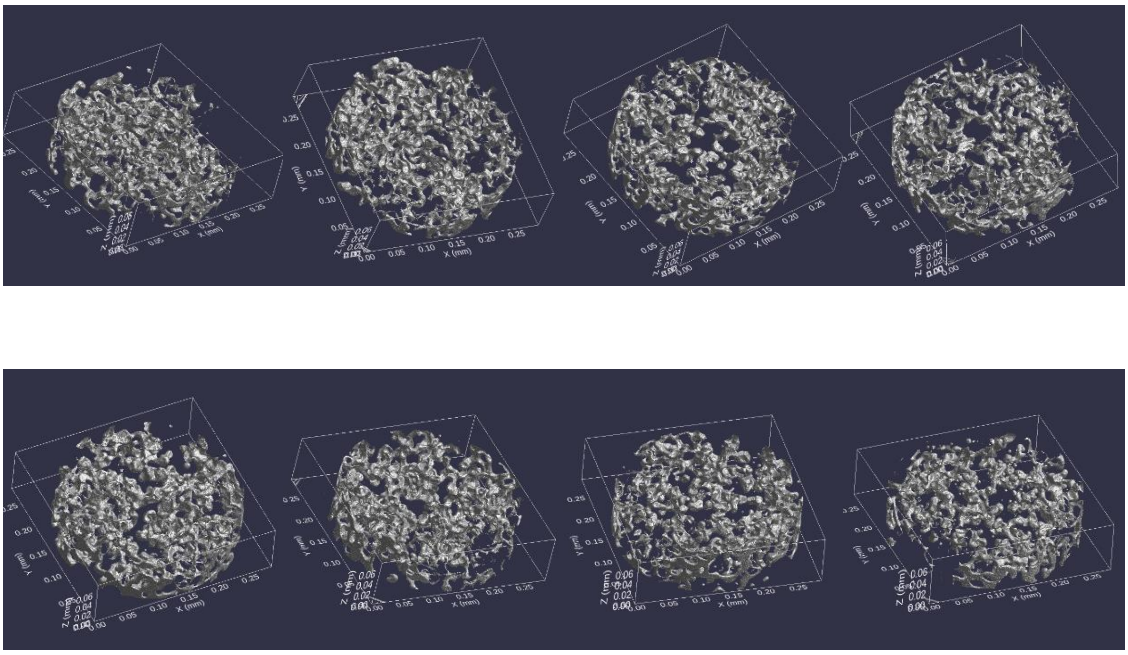

Column 4 – Residual Saturation

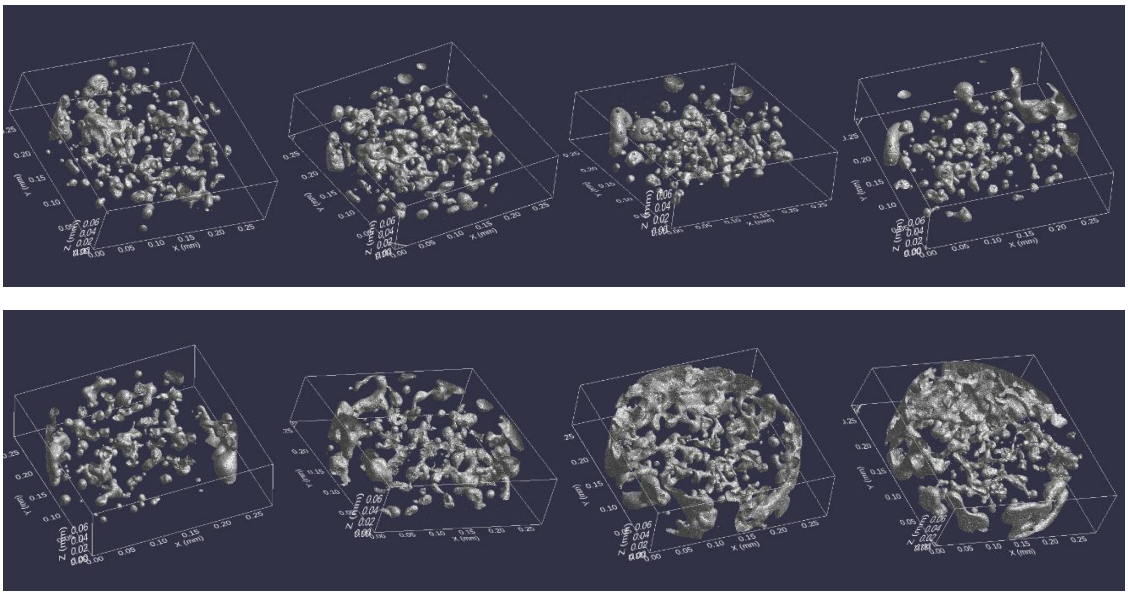

Column 4 – After 2 PV flush

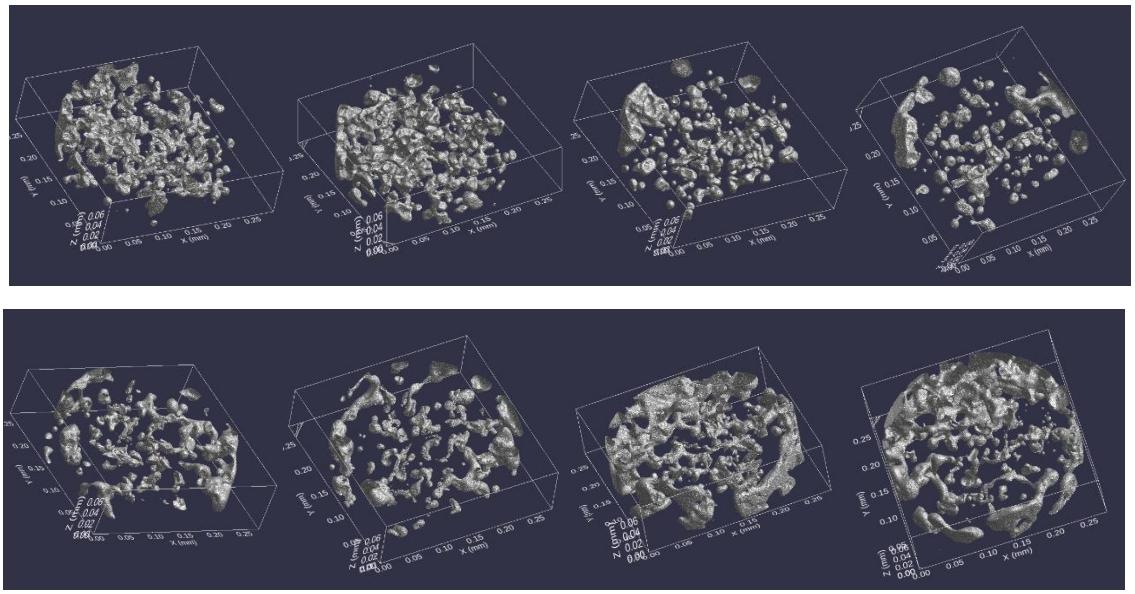

Column 4 – After 5 PV flush

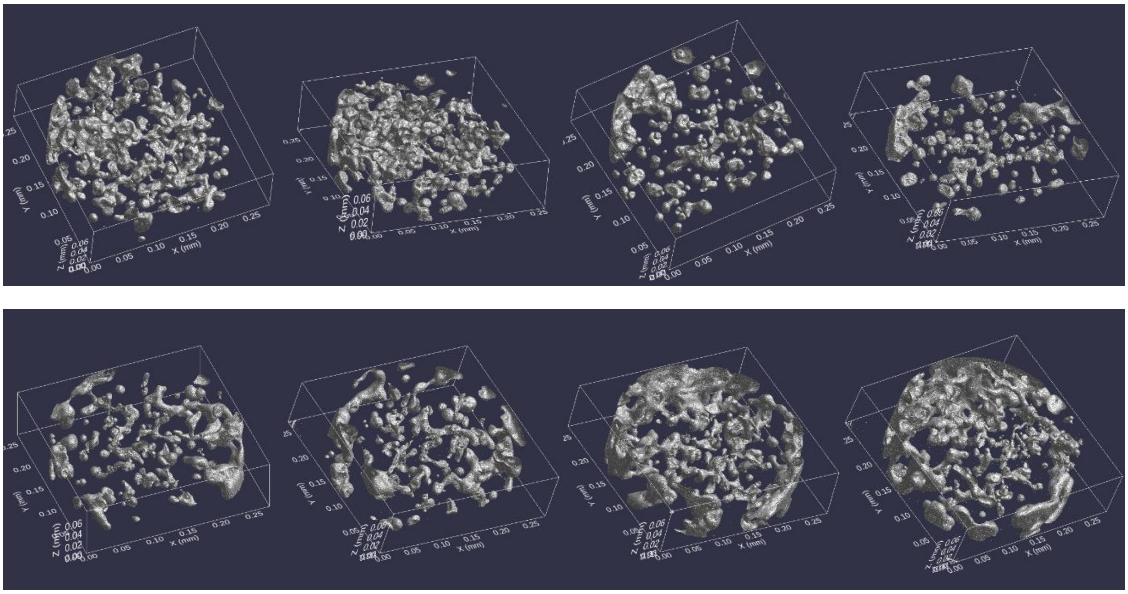

Column 5 – Residual Saturation

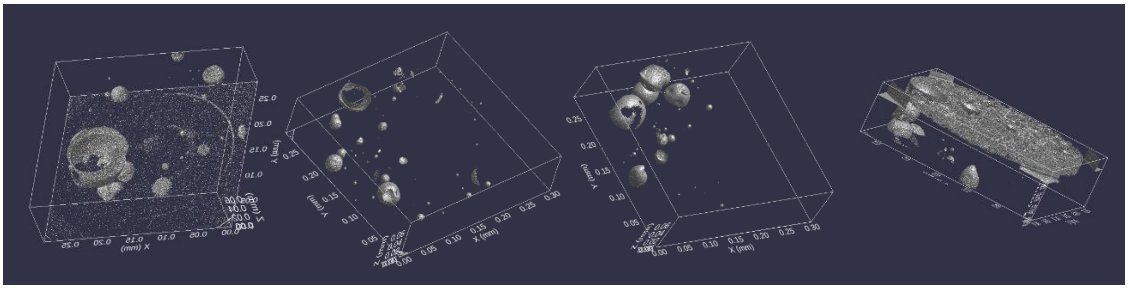

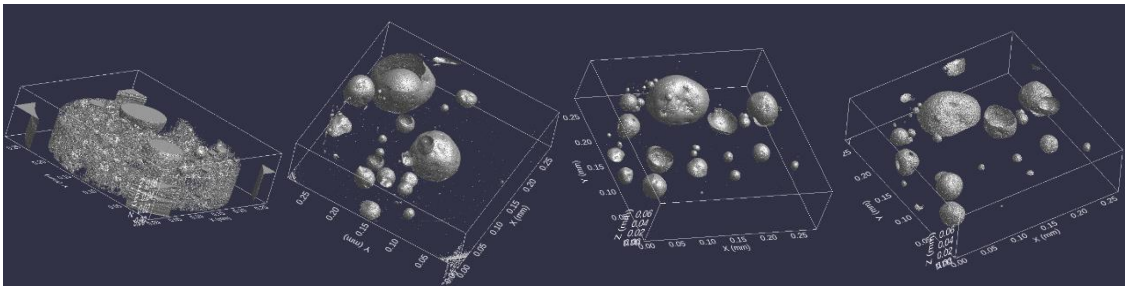

Column 5 – After 2 PV flush

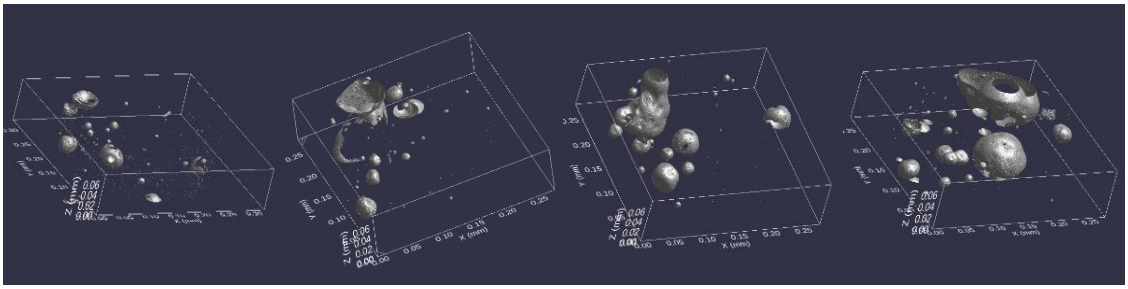

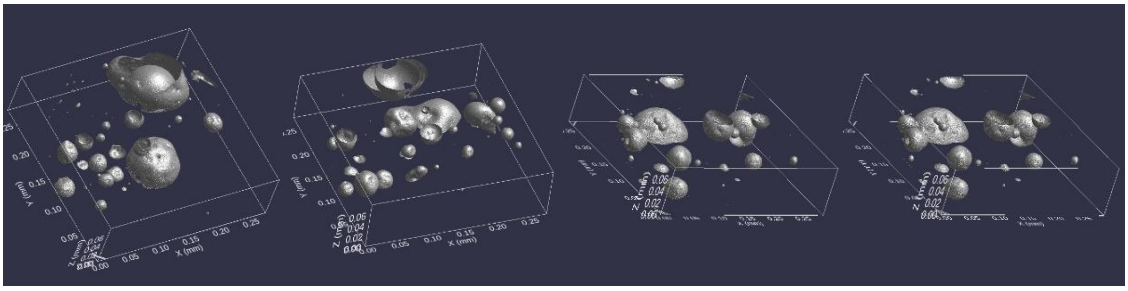

Column 5 – After 5 PV flush

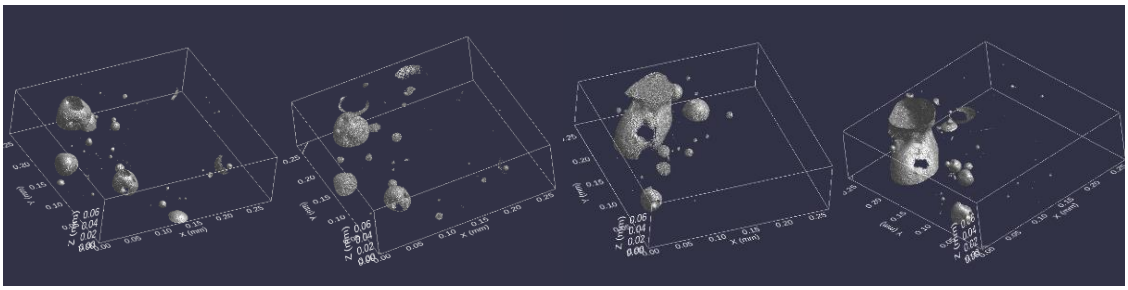

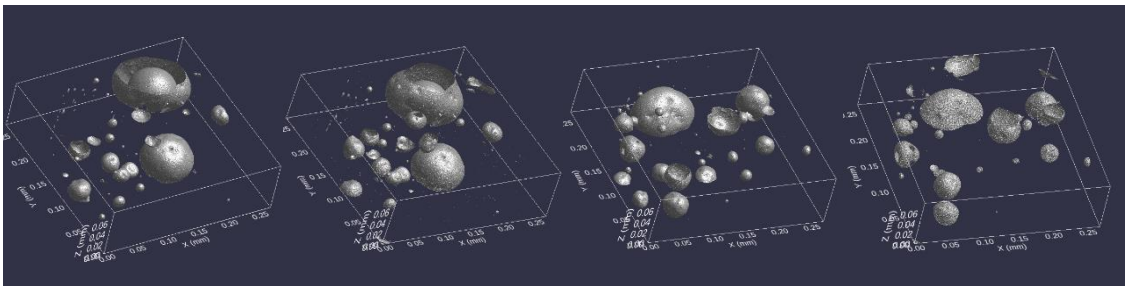

APPENDIX B – BLOB DISTRIBUTION AND HISTOGRAMS FOR COLUMNS DURING SXM

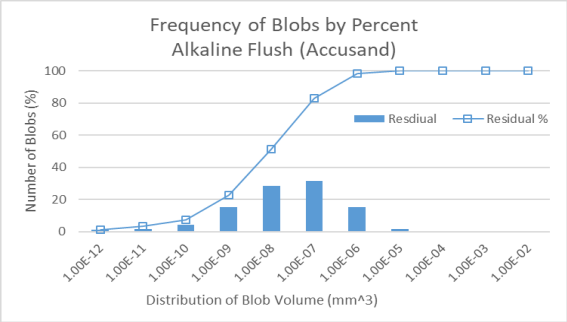

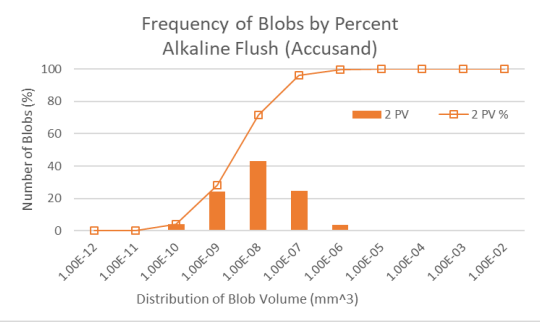

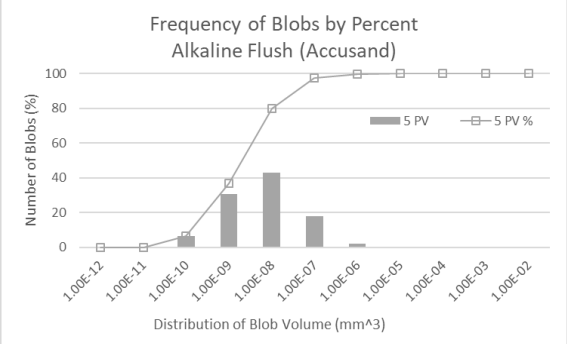

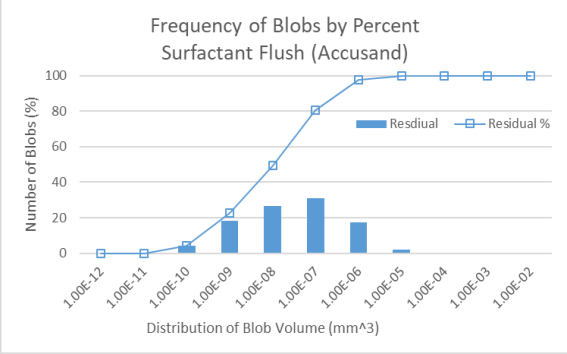

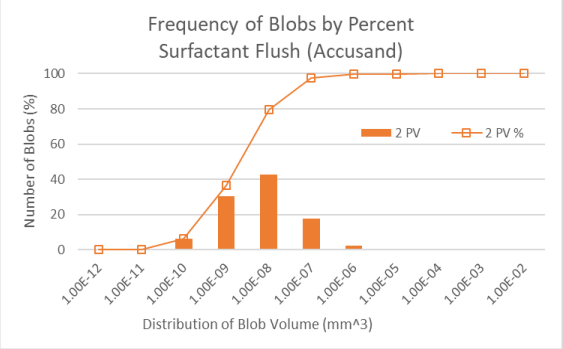

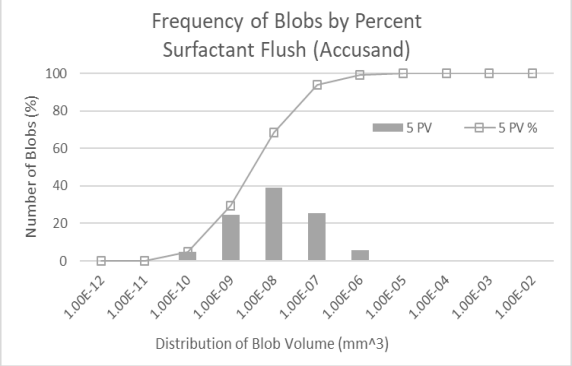

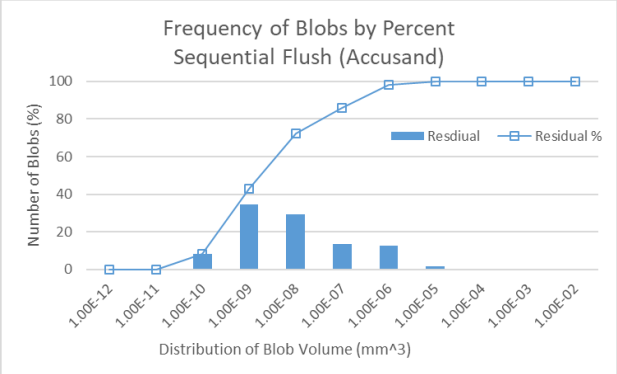
Frequency of Blobs by Percent
Sequential Flush (Accusand)
Number of Blobs (%)
Resdiual
Residual %
Distribution of Blob Volume (mm^3)

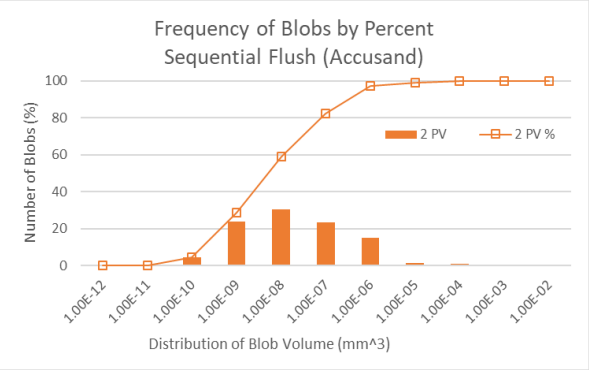
Frequency of Blobs by Percent
Sequential Flush (Accusand)
Number of Blobs (%)
2 PV
2 PV %
Distribution of Blob Volume (mm^3)

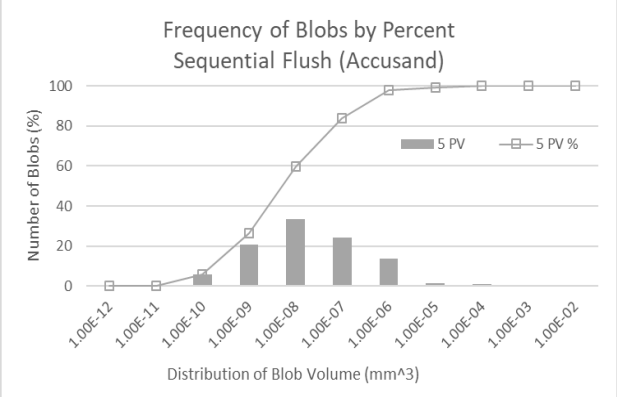
Frequency of Blobs by Percent
Sequential Flush (Accusand)
Number of Blobs (%)
5 PV
5 PV %
Distribution of Blob Volume (mm^3)

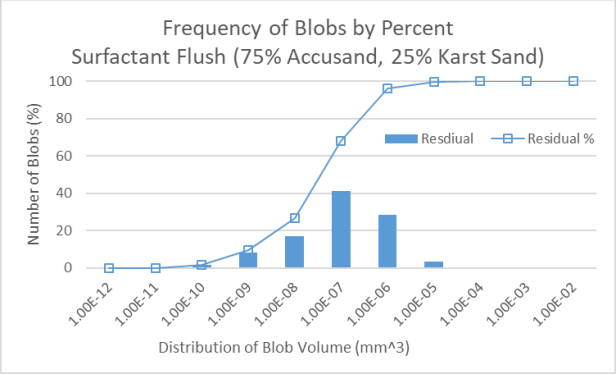
Frequency of Blobs by Percent
Surfactant Flush (75% Accusand, 25% Karst Sand)
Number of Blobs (%)
Resdiual
Residual %
Distribution of Blob Volume (mm^3)

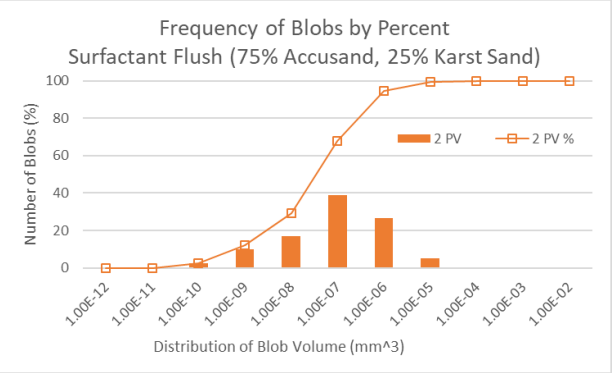
Frequency of Blobs by Percent
Surfactant Flush (75% Accusand, 25% Karst Sand)
Number of Blobs (%)
2 PV
2 PV %
Distribution of Blob Volume (mm^3)

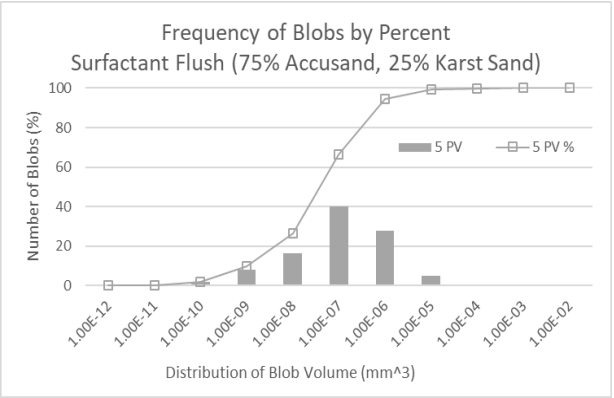
Frequency of Blobs by Percent
Surfactant Flush (75% Accusand, 25% Karst Sand)
Number of Blobs (%)
5 PV
5 PV %
Distribution of Blob Volume (mm^3)

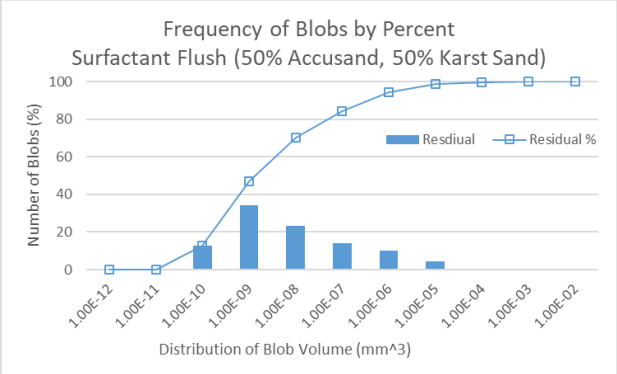
Frequency of Blobs by Percent
Surfactant Flush (50% Accusand, 50% Karst Sand)
Number of Blobs (%)
Resdiual
Residual %
Distribution of Blob Volume (mm^3)

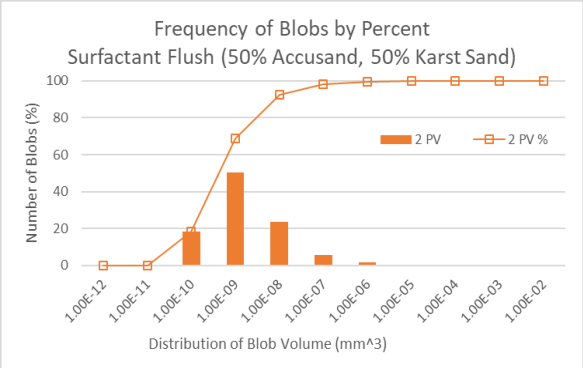
Frequency of Blobs by Percent
Surfactant Flush (50% Accusand, 50% Karst Sand)
Number of Blobs (%)
2 PV
2 PV %
Distribution of Blob Volume (mm^3)

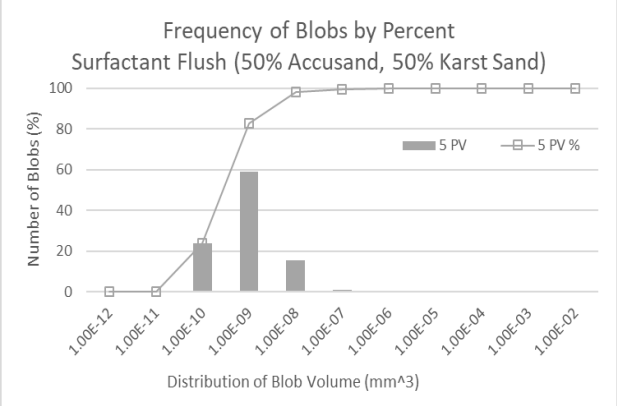
Frequency of Blobs by Percent
Surfactant Flush (50% Accusand, 50% Karst Sand)
Number of Blobs (%)
5 PV
5 PV %
Distribution of Blob Volume (mm^3)

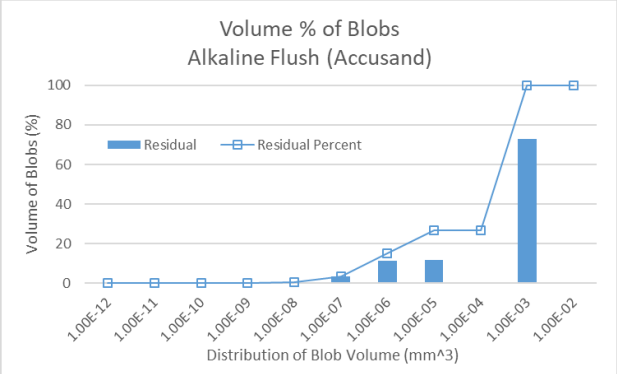
Volume % of Blobs
Alkaline Flush (Accusand)
Volume of Blobs (%)
Residual
Residual Percent
Distribution of Blob Volume (mm^3)

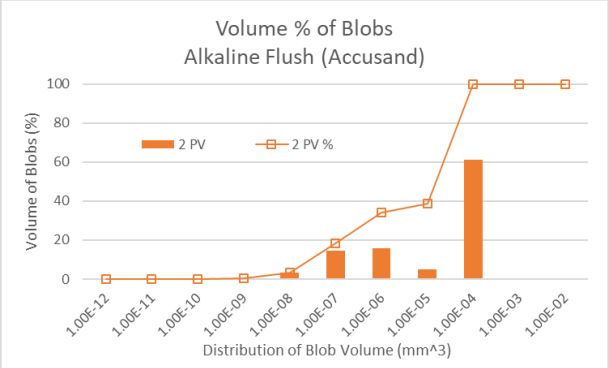
Volume % of Blobs
Alkaline Flush (Accusand)
Volume of Blobs (%)
2 PV
2 PV %
Distribution of Blob Volume (mm^3)

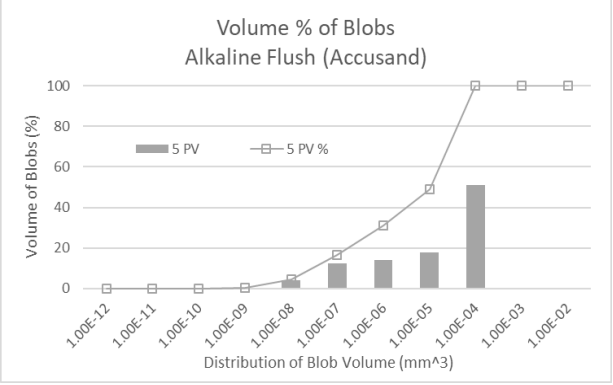
Volume % of Blobs
Alkaline Flush (Accusand)
Volume of Blobs (%)
5 PV
5 PV %
Distribution of Blob Volume (mm^3)

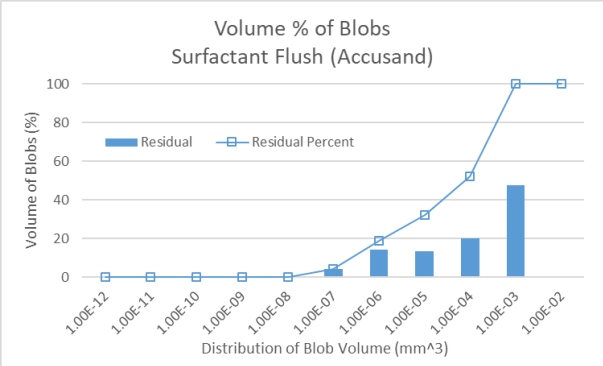
Volume % of Blobs
Surfactant Flush (Accusand)
Volume of Blobs (%)
Residual
Residual Percent
Distribution of Blob Volume (mm^3)

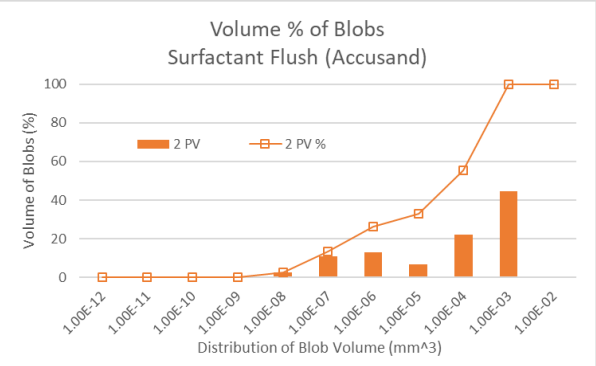
Volume % of Blobs
Surfactant Flush (Accusand)
Volume of Blobs (%)
2 PV
2 PV %
Distribution of Blob Volume (mm^3)

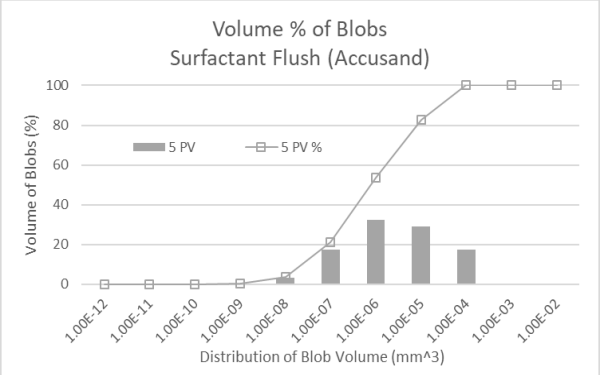
Volume % of Blobs
Surfactant Flush (Accusand)
Volume of Blobs (%)
5 PV
5 PV %
Distribution of Blob Volume (mm^3)

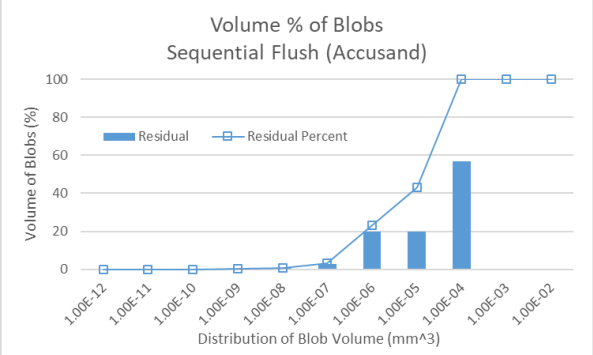
Volume % of Blobs
Sequential Flush (Accusand)
Volume of Blobs (%)
Residual
Residual Percent
Distribution of Blob Volume (mm^3)

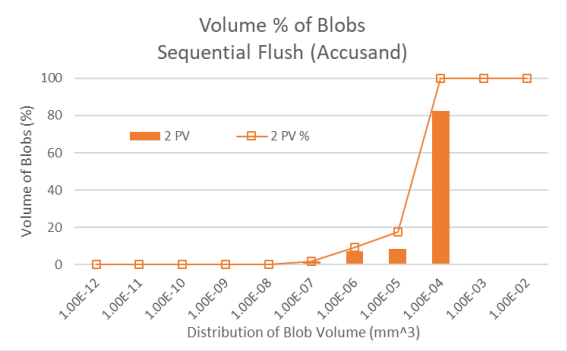
Volume % of Blobs
Sequential Flush (Accusand)
Volume of Blobs (%)
2 PV
2 PV %
Distribution of Blob Volume (mm^3)

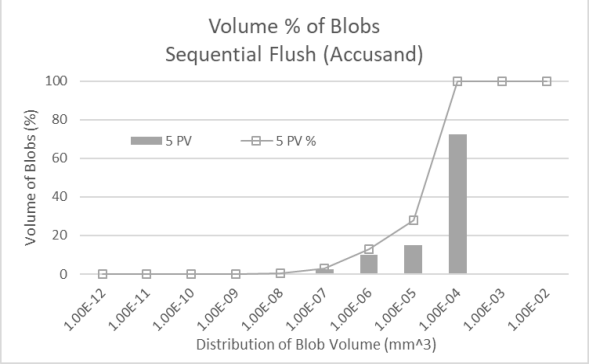
Volume % of Blobs
Sequential Flush (Accusand)
Volume of Blobs (%)
5 PV
5 PV %
Distribution of Blob Volume (mm^3)

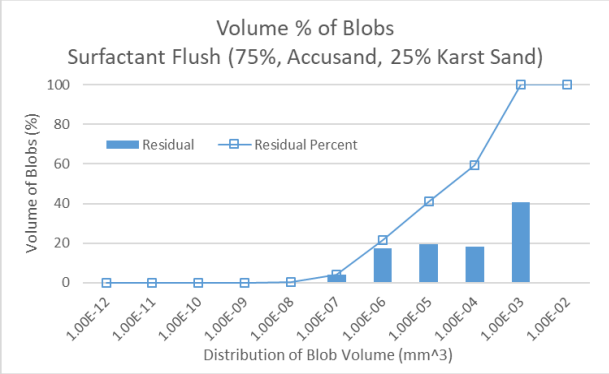
Volume % of Blobs
Surfactant Flush (75%, Accusand, 25% Karst Sand)
Volume of Blobs (%)
Residual
Residual Percent
Distribution of Blob Volume (mm^3)

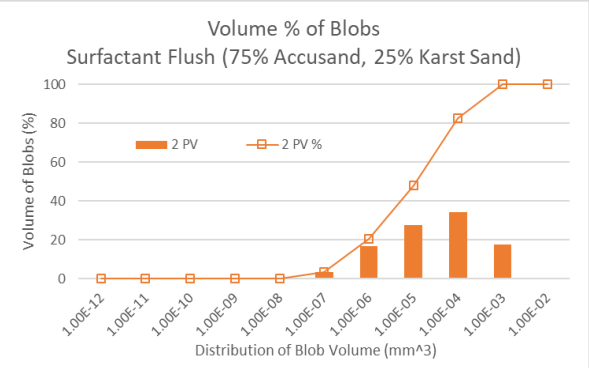
Volume % of Blobs
Surfactant Flush (75% Accusand, 25% Karst Sand)
Volume of Blobs (%)
2 PV
2 PV %
Distribution of Blob Volume (mm^3)

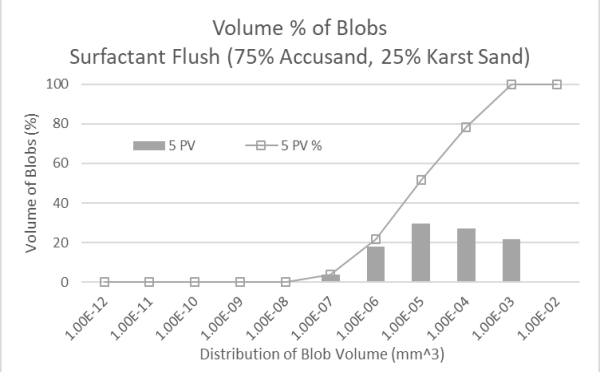
Volume % of Blobs
Surfactant Flush (75% Accusand, 25% Karst Sand)
Volume of Blobs (%)
5 PV
5 PV %
Distribution of Blob Volume (mm^3)

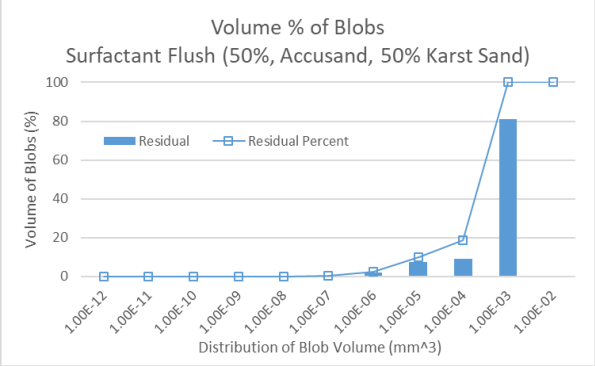
Volume % of Blobs
Surfactant Flush (50%, Accusand, 50% Karst Sand)
Volume of Blobs (%)
Residual
Residual Percent
Distribution of Blob Volume (mm^3)

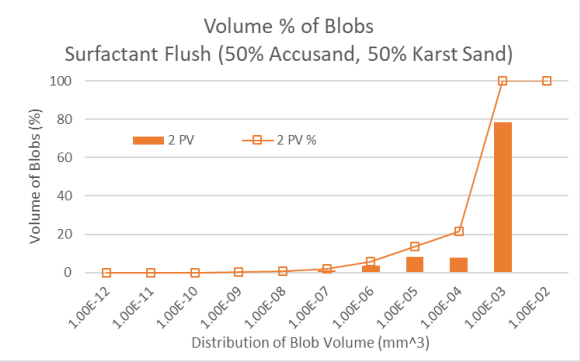
Volume % of Blobs
Surfactant Flush (50% Accusand, 50% Karst Sand)
Volume of Blobs (%)
2 PV
2 PV %
Distribution of Blob Volume (mm^3)

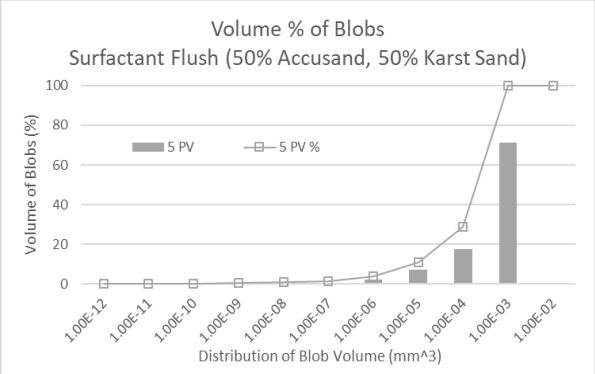
Volume % of Blobs
Surfactant Flush (50% Accusand, 50% Karst Sand)
Volume of Blobs (%)
5 PV
5 PV %
Distribution of Blob Volume (mm^3)

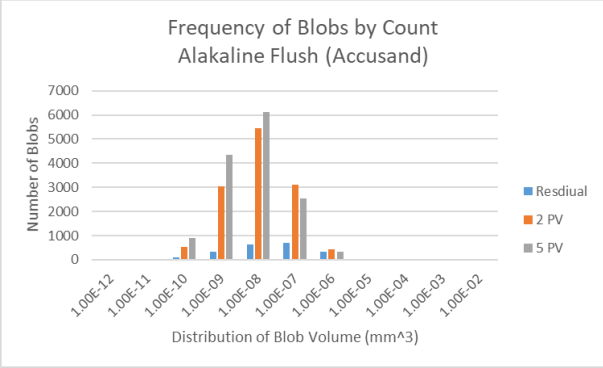
Frequency of Blobs by Count
Alakaline Flush (Accusand)
Number of Blobs
7000
6000
5000
4000
3000
2000
1000
0
1.00E-12
1.00E-11
1.00E-10
1.00E-09
1.00E-08
1.00E-07
1.00E-06
1.00E-05
1.00E-04
1.00E-03
1.00E-02
Distribution of Blob Volume (mm^3)
Resdiual
2 PV
5 PV

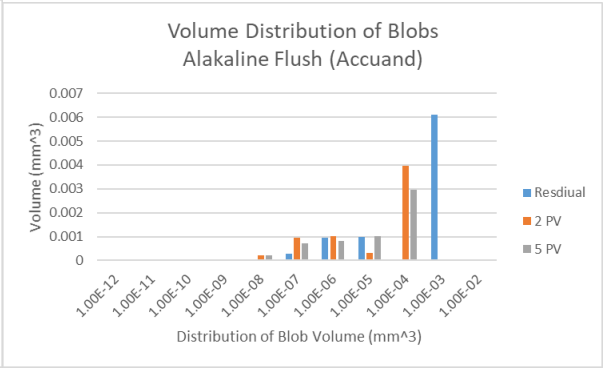
Volume Distribution of Blobs
Alakaline Flush (Accuand)
Volume (mm^3)
0.007
0.006
0.005
0.004
0.003
0.002
0.001
0
1.00E-12
1.00E-11
1.00E-10
1.00E-09
1.00E-08
1.00E-07
1.00E-06
1.00E-05
1.00E-04
1.00E-03
1.00E-02
Distribution of Blob Volume (mm^3)
Resdiual
2 PV
5 PV

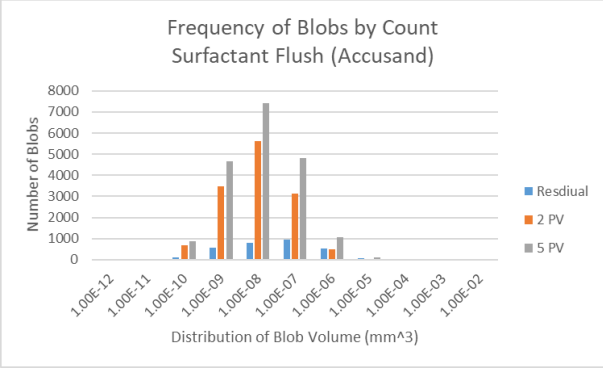
Frequency of Blobs by Count
Surfactant Flush (Accusand)
Number of Blobs
8000
7000
6000
5000
4000
3000
2000
1000
0
1.00E-12
1.00E-11
1.00E-10
1.00E-09
1.00E-08
1.00E-07
1.00E-06
1.00E-05
1.00E-04
1.00E-03
1.00E-02
Distribution of Blob Volume (mm^3)
Resdiual
2 PV
5 PV

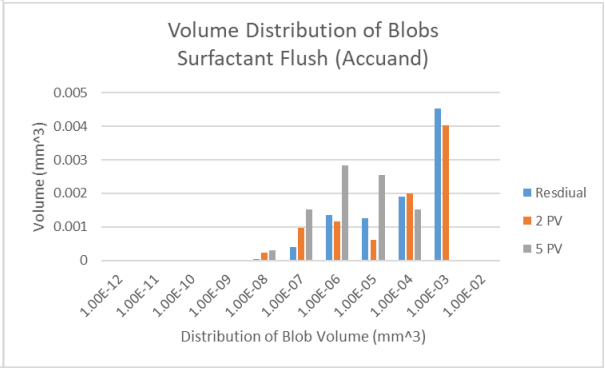
Volume Distribution of Blobs
Surfactant Flush (Accuand)
Volume (mm^3)
0.005
0.004
0.003
0.002
0.001
0
1.00E-12
1.00E-11
1.00E-10
1.00E-09
1.00E-08
1.00E-07
1.00E-06
1.00E-05
1.00E-04
1.00E-03
1.00E-02
Distribution of Blob Volume (mm^3)
Resdiual
2 PV
5 PV

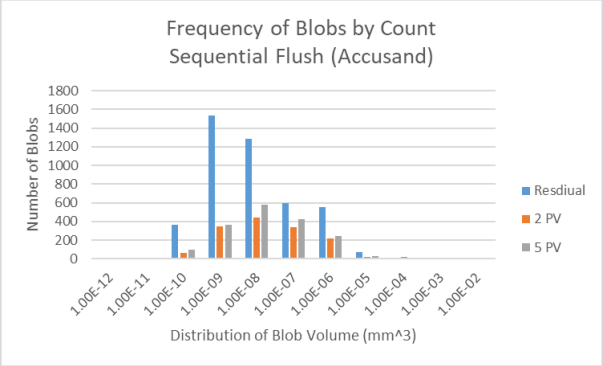
Frequency of Blobs by Count
Sequential Flush (Accusand)
Number of Blobs
1800
1600
1400
1200
1000
800
600
400
200
0
1.00E-12
1.00E-11
1.00E-10
1.00E-09
1.00E-08
1.00E-07
1.00E-06
1.00E-05
1.00E-04
1.00E-03
1.00E-02
Distribution of Blob Volume (mm^3)
Resdiual
2 PV
5 PV

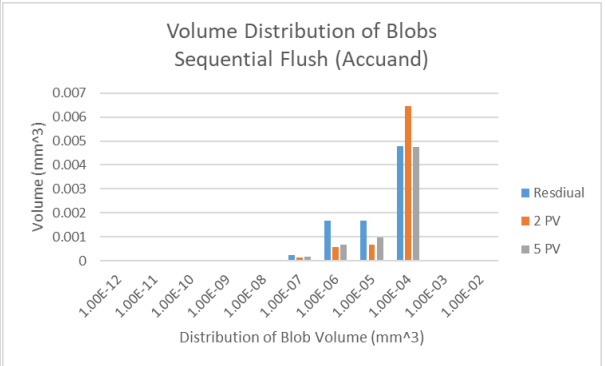
Volume Distribution of Blobs
Sequential Flush (Accuand)
Volume (mm^3)
0.007
0.006
0.005
0.004
0.003
0.002
0.001
0
1.00E-12
1.00E-11
1.00E-10
1.00E-09
1.00E-08
1.00E-07
1.00E-06
1.00E-05
1.00E-04
1.00E-03
1.00E-02
Distribution of Blob Volume (mm^3)
Resdiual
2 PV
5 PV

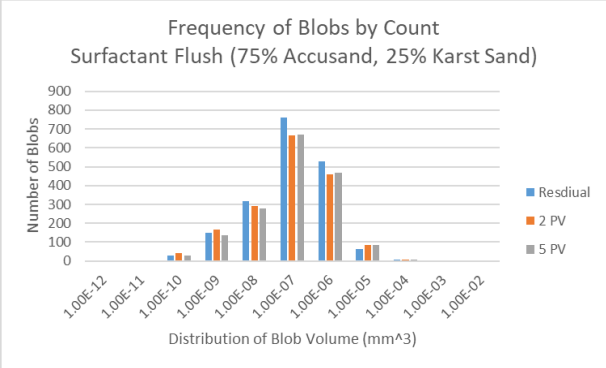
Frequency of Blobs by Count
Surfactant Flush (75% Accusand, 25% Karst Sand)
Number of Blobs
900
800
700
600
500
400
300
200
100
0
1.00E-12
1.00E-11
1.00E-10
1.00E-09
1.00E-08
1.00E-07
1.00E-06
1.00E-05
1.00E-04
1.00E-03
1.00E-02
Distribution of Blob Volume (mm^3)
Resdiual
2 PV
5 PV

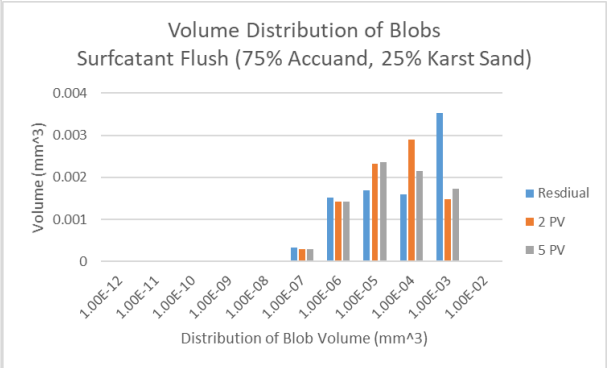
Volume Distribution of Blobs
Surfcatant Flush (75% Accuand, 25% Karst Sand)
Volume (mm^3)
0.004
0.003
0.002
0.001
0
1.00E-12
1.00E-11
1.00E-10
1.00E-09
1.00E-08
1.00E-07
1.00E-06
1.00E-05
1.00E-04
1.00E-03
1.00E-02
Distribution of Blob Volume (mm^3)
Resdiual
2 PV
5 PV

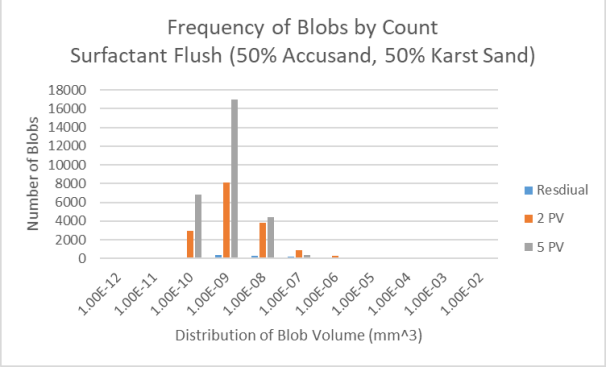
Frequency of Blobs by Count
Surfactant Flush (50% Accusand, 50% Karst Sand)
Number of Blobs
18000
16000
14000
12000
10000
8000
6000
4000
2000
0
1.00E-12
1.00E-11
1.00E-10
1.00E-09
1.00E-08
1.00E-07
1.00E-06
1.00E-05
1.00E-04
1.00E-03
1.00E-02
Distribution of Blob Volume (mm^3)
Resdiual
2 PV
5 PV

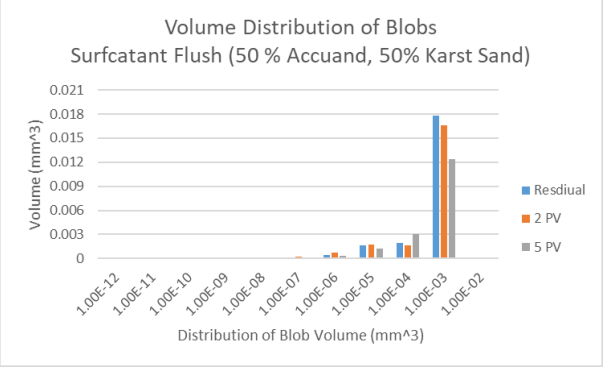
Volume Distribution of Blobs
Surfcatant Flush (50 % Accuand, 50% Karst Sand)
Volume (mm^3)
0.021
0.018
0.015
0.012
0.009
0.006
0.003
0
1.00E-12
1.00E-11
1.00E-10
1.00E-09
1.00E-08
1.00E-07
1.00E-06
1.00E-05
1.00E-04
1.00E-03
1.00E-02
Distribution of Blob Volume (mm^3)
Resdiual
2 PV
5 PV

APPENDIX C – CALCULATIONS OF BOND CAPILLARY AND TRAPPING NUMBERS FOR HETEROGENEOUS COLUMNS

	Surfactant Flush			
	Residual Saturation	75/25 sand	Residual Saturation	50/50 sand
	Medium	Medium	Medium	Medium
Interfacial Tension [dyn/cm]	20.9	11.8	20.9	11.8
Fluid API gravity	29.6	29.6	29.6	29.6
Fluid Density	0.87	0.87	0.87	0.87
Flushing Fluid Density	1.04	1.04	1.04	1.04
Δρ	0.17	0.17	0.17	0.17
Capillary Number	6.82E-07	3.18E-06 (+366%)	6.82E-07	3.18E-06 (+366%)
Bond Number	5.40E-06	9.56E-06 (+77%)	3.62E-06	6.41E-06 (+77%)
Trapping Number	6.08E-06	1.27E-05 (+109%)	4.30E-06	9.59E-06 (+123%)